THERMAL VACUUM CHAMBER MODIFICATION, TESTING, AND ANALYSIS

A Thesis

presented to

the Faculty of California Polytechnic State University,

San Luis Obispo

In Partial Fulfillment

of the Requirements for the Degree

Master of Science in Aerospace Engineering

by

Jared Lehmann

July 2021

COMMITTEE MEMBERSHIP

TITLE:	Thermal Vacuum Chamber Modification, Testing, and Analysis
AUTHOR:	Jared Lehmann
DATE SUBMITTED:	July 2021
COMMITTEE CHAIR:	Kira Abercromby, Ph.D. Professor of Aerospace Engineering
COMMITTEE MEMBER:	Pauline Faure, Ph.D. Assistant Professor of Aerospace Engineering
COMMITTEE MEMBER:	Jennifer Mott, Ph.D. Assistant Professor of Mechanical Engineering
COMMITTEE MEMBER:	Kim Shollenberger, Ph.D. Professor of Mechanical Engineering

ABSTRACT

Thermal Vacuum Chamber Modification, Testing, and Analysis

Jared Lehmann

This work dissusses the modification and analysis of the Blue Thermal Vacuum Chamber (TVAC) located at the Space Environments Lab at California Polytechnic State University, San Luis Obispo. The modified design has a cylindrical test section and can accommodate 6U Cubesats or larger for educational or research purposes.

The sizing process for the modified shroud cooling system and modular heating plates is discussed. The modified cooling system uses existing nitrogen plumbing into the chamber and control systems with a new copper shroud. The modified heating system uses modular heater plates, which utilize the existing three heater strips. The modified system includes high emissivity coatings for improved heat transfer performance, lower thermal mass materials to minimize thermal mass and liquid nitrogen consumption, and modular components for flexibility in operation.

Analysis presented shows correlation between experimental results and a steady state thermal model using SolidWorks and SolidWorks Flow Simulation. The results demonstrate a maximum absolute difference in modeled vs experimental temperatures at measured locations of 11°C in all cases, and 3°C for test article temperatures only.

Chamber performance is compared and characterized through a series of thermal vacuum tests and demonstrates capability exceeding ISO 19683 requirements for all thermal vacuum chamber testing categories except tolerance, with a tested temperature range of -145°C at the shroud to 95°C at the heater plates, >10 cycles between -15°C and 55°C, dwells in excess of 3 hours, ramp rates of 1-2°C/min, and chamber pressures under $<7.5\text{x}10^{-6}$ Torr after bakeout procedures.

ACKNOWLEDGMENTS

I would like to thank my parents for their support throughout my education and my life and my girlfriend, Brooke, who supported me through my thesis.

To Dr. Abercromby, you have taught me so much and have been such a great part of my college education, having taken at least 5 courses from you and having you be my thesis advisor. You always have great advice and I have learned so much from you.

To Dr. Faure, thank you for your guidance and support throughout classes, senior design, and my thesis.

To Cody Thompson, I cannot thank you enough for your assistance, advice, and knowledge about manufacturing. Without you this project would not have been possible.

Thank you to Dr. Shollenberger and Dr. Mott, for being apart of my thesis committee and for your support and feedback along the way.

TABLE OF CONTENTS

LIST OF TABLES

LIST OF FIGURES

Chapter 1

INTRODUCTION

1.1 Background

Spacecraft are exposed to a hostile and varied environment, including constant and cyclic bombardment of solar and electromagnetic radiation, neutral and charged particles, meteoroids, debris, and more [17]. Spacecraft must be designed to resist or manage the effects of exposure to these environments. The thermal environment plays a significant role in the design of spacecraft because the components and structures that make up the spacecraft have ranges of temperatures in which they can survive and operate [7]. In order to maintain these temperatures in a vacuum environment, care must be taken in the design of thermal control systems to ensure that these temperatures will be maintained throughout the mission. Mathematical analysis is used to predict the performance of a spacecraft's thermal control system in a particular environment, but verification methods are needed to ensure that the system meets design requirements.

A thermal vacuum (TVAC) chamber, used to conduct thermal vacuum testing, can be utilized to perform verification to ensure the system meets design requirements. To perform verification of the analytical models, the TVAC chamber must be able to precisely control the thermal and vacuum environment as needed to meet the requirements of the test and specification being followed. Typically, this includes pumping the chamber down to a specified vacuum level, ramping the temperature to a high temperature and holding for a period of time, then ramping down to a cold case condition and holding for a period of time [4]. The hold period is called a thermal soak or dwell. The intent of cycling between temperature extremes under high

vacuum is to verify the test article performs and meets requirements in a simulated space environment [4]. The number of cycles and duration of soaks is specific to requirements of each mission. However, the test levels are potentially limited by the capabilities of the TVAC chamber used.

This thesis explores methods of improving the performance of the existing and previously modified MDA US systems thermal vacuum chamber located in California Polytechnic State University, San Luis Obispo's space environments laboratory. Modifications will be made through cooling system and heater design improvements, the addition of surface coatings, updated control schemes, and defined processes. After modifications are made, the performance of the chamber will be analyzed through a series of tests and compared to a software based numerical model using SolidWorks and SolidWorks Flow Simulation.

1.2 The Thermal Space Environment

The thermal environment in space is dominated by radiative heat transfer because no significant particles exist in the vacuum of space for effective convection or conduction to the environment [17]. Any heat to or from the environment must be emitted or absorbed and can include a variety of sources and sinks including direct solar radiation, albedo, planetary radiation, and emitted radiation [17]. Direct solar radiation is from the sun, and the heat flux for a blackbody is proportional to the spacecraft's distance from the sun [17]. Albedo is reflected radiation from the nearby celestial body's surface to the spacecraft [17]. Planetary radiation is the radiation emitted by the celestial body due to the temperature of the body and is typically in the IR spectrum [17]. Emitted radiation from the spacecraft is the only method of transferring heat to the environment [17]. These sources of radiation must be considered when designing the thermal control systems for a spacecraft such that the incoming and

outgoing heat flux are generally balanced, depending on the specific requirements of the mission. Figure 1.1 summarizes the sources and sinks between a spacecraft and the environment.

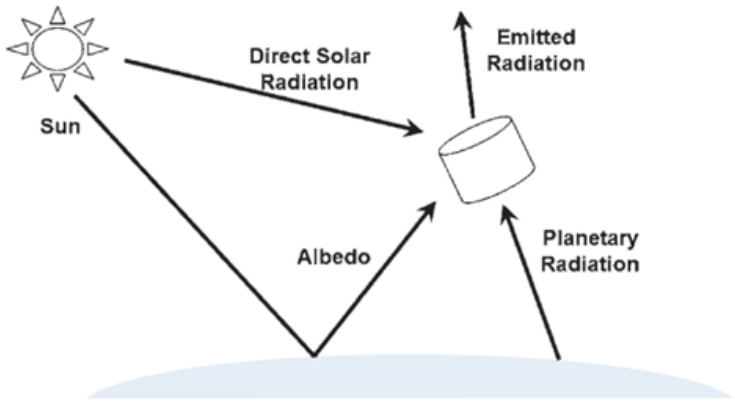

Figure 1.1: Spacecraft Energy Exchange Diagram [17]

When designing a spacecraft's thermal control systems, passive and active methods for thermal control can be used depending on the needs of the mission. Examples of passive methods are coatings, which affect the emissivity and absorptivity of surfaces, can be applied as needed to dissipate or absorb energy [17]. MLI blankets and thermal shields can be used to insulate interior faces from the external radiation environment [17]. Thermal storage like phase change materials or cryogenics can be used to regulate temperatures [17]. Heat pipes and radiators transfer and emit heat passively [17]. Active methods of thermal control include resistance heaters, heat pumps and pumped fluid loops to move heat around the spacecraft, thermoelectric coolers to pump heat typically from small components, and active radiators to emit heat selectively to the environment [17].

1.3 Thermal Testing and Standards

A thermal vacuum chamber can be used for a variety of test campaigns. Thermal vacuum tests, thermal vacuum cycling, thermal balance testing, burn-in tests, and thermal noise testing are among the types of tests that can be performed using a thermal vacuum chamber [4, 6]. Each test has a specific purpose, but the overall intent is to screen for environmental stress due to thermal expansion and cycling of hot to cold temperatures, test the ability for the test article or its components to turn on under specific thermal conditions, and to demonstrate that the test article can survive under specific thermal conditions [4, 11, 6]. Any of these test objectives can be evaluated or only some specific objectives can be evaluated, depending on the requirements of the test campaign. The test article can be anything from an individual component to a fully integrated satellite.

Thermal Vacuum Tests: This test verifies the performance and function of the test article under vacuum conditions and a specified number of hot and cold cycles [7]. Figure 1.2 shows a typical thermal vacuum test profile. The number of cycles, soak temperatures, margins, and ramp rates are all selected based on requirements, testing capabilities, and relevant specifications. For example, NASA's General Environmental Verification Standard (GEVS) requires prototype qualification test temperatures to be +10°C of the maximum expected flight temperature and -10°C from the minimum expected flight temperature [1].

Thermal Balance Test: This test simulates flight conditions at the steady state cold and hot conditions to verify thermal control systems and to correlate thermal analytic models [7]. Figure 1.3 shows a simple thermal balance test profile. This test is usually performed as part of the thermal vacuum testing for the system or satellite [7].

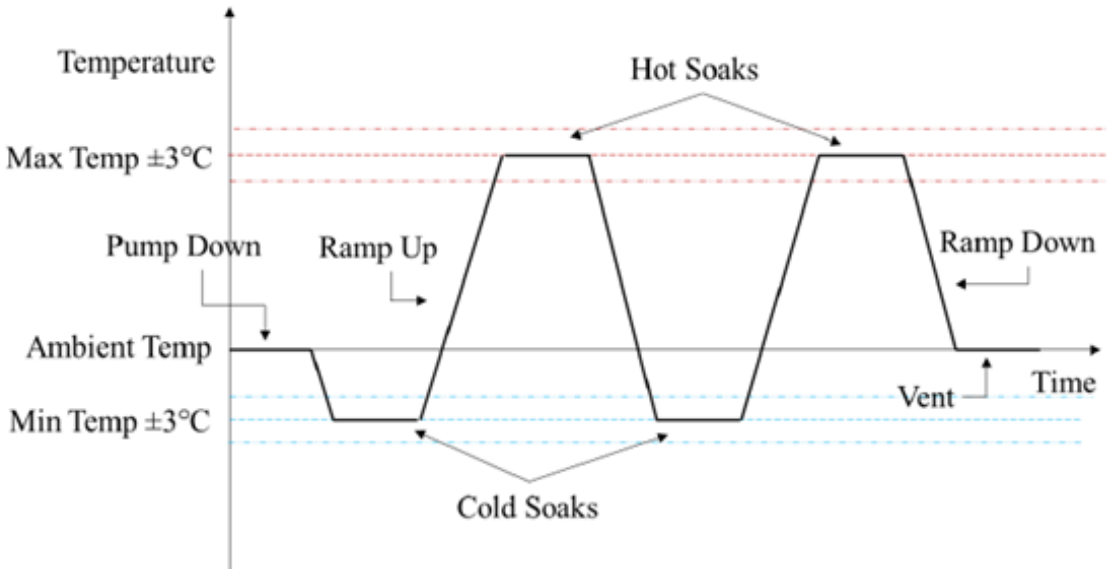

Figure 1.2: Typical thermal vacuum test profile [7]

Thermal Cycle Test: This test verifies performance of the test article under rapid cycling of hot and cold temperatures in an ambient or gaseous nitrogen environment, which screens primarily for environmental stresses [7]. It should be noted that thermal vacuum tests and thermal cycling tests typically use different test equipment due to the different ambient environment and difference in heat transfer modes.

Thermal Burn-In Test: Verifies the test article is operational at a set temperature or cycled for an added time as required. This test usually takes place as part of the thermal cycling test [7]. Thermal noise can also be evaluated during a burn in test, which is important for radiofrequency payloads [6].

1.4 Thermal Modeling

Thermal modeling is any mathematical tool used to predict temperatures, typically on a system scale with different components and structures interacting with each other and the environment [1]. This model is continuously developed and used to help design a satellite thermal control system and is continuously updated and modified as

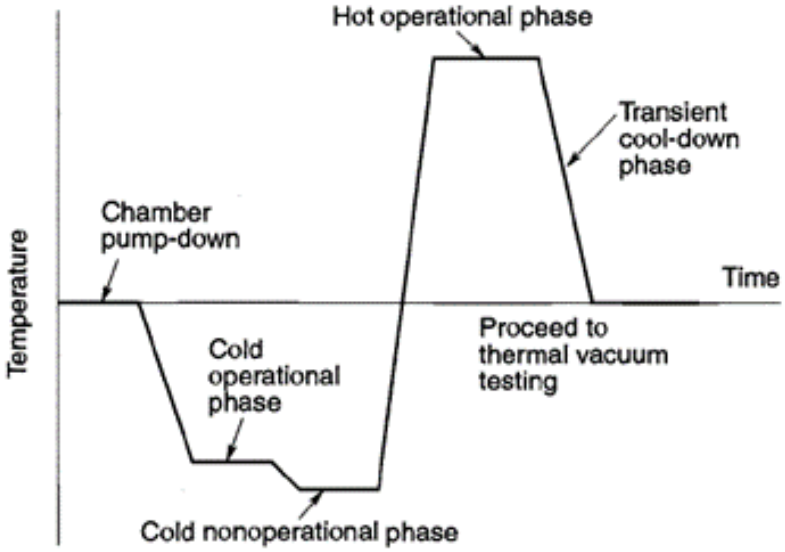

Figure 1.3: Thermal balance test profile [7]

a design progress. Eventually, the model can be used to evaluate the performance on orbit and can be helpful to investigate anomalies or perform specialized operations or maneuvers [12]. Software has made executing and analyzing thermal models simpler and allows for a variety of analysis that hand calculations do not, including numerical analysis. However, it is important to note that hand calculations are often helpful before jumping into thermal modeling as a first pass analysis before more detailed analysis can take place.

1.4.1 Fundamental Equations

Depending on the specific question, basic equations like those used for conduction, convection, and radiation are below in equations 1.1,1.2, and 1.3 respectively. In these equations, $\dot{q}$ represents heat flux, typically measured in Watts per meter squared. In equation 1.1, k refers to thermal conductivity and is typically measured in Watts per meter-Kelvin, and ∇T refers to the temperature gradient in Kelvin per meter. This

equation can be used to model heat flowing through solids as well as between liquids and gases via conduction.

$$\dot{q} = -k\nabla T[17] \tag{1.1}$$

Equation 1.2 is similar to conduction except the coefficient h relates to the convection coefficient in Watts per meter squared-Kelvin, and this equation refers to heat flowing due to fluid flow past a solid surface [17].

$$\dot{q} = -h\Delta T[17] \tag{1.2}$$

Equation 1.3 represents radiative heat transfer, where ϵ_{eq} is the emissivity, σ is the Stefan-Boltzmann constant, and $|{T_i}^4 - {T_o}^4|$ is the absolute difference of the cube of the inner surface temperature minus the cube of the inner surface temperature. This equation is refers to radiative heat transfer between inner and outer surfaces, and is directly proportional to emissivity.

$$\dot{q} = \epsilon_{eq}\sigma|{T_i}^4 - {T_o}^4|[17] \tag{1.3}$$

1.4.2 SolidWorks vs Thermal Desktop

For the analysis in this thesis, SolidWorks Simulation and SolidWorks Flow Simulation was selected over continuing to use Thermal Desktop, used by Williams and

Jensma for their thermal modeling [11, 22]. The primary reason this change was made was because of ease of use for Cal Poly students. As this chamber will be used primarily by Cal Poly students, who learn computer aided design (CAD) in classes using SolidWorks and have access to the software on their own computer or virtual/-physical lab computers, using SolidWorks for the modeling and analysis reduces the learning curve for users vs Thermal Desktop, which is generally unfamiliar to most students.

The previous thermal models by Williams and Jensma used Thermal Desktop, which uses SINDA/FLUENT [11, 22]. These software packages are generally more flexible in that the user has more variety of models and solution methods to use, and generally more options when it comes to setup and calculation. However, SolidWorks as well as SolidWorks Flow Simulation has all of the same general capabilities and is more than capable of analysis for this thesis, including flow simulation capabilities for nitrogen through the coolant tubing as well as radiation ray tracing and conduction finite element analysis. Thermal desktop is particularly useful in that it includes specialized tools to determine thermal loads in specific orbits, where SolidWorks does not. This is useful in some cases but for the purpose of thermal modeling of the vacuum chamber, these thermal loads are not needed to be calculated and could be manually imported into Solidworks based on a Thermal Desktop model or other calculations to simulate specific heat loads. Additionally, in general SolidWorks is more user friendly and more widely used, therefore documentation and online tutorials are readily available which is not always the case for thermal desktop.

SolidWorks thermal and flow simulation uses a general-purpose thermal/fluid solver which utilizes a finite volume method to solve partial differential equations relating to fluid mechanics and heat transfer for convection and conduction [12, 20]. Starting from a solid model, the mesher prepares for analysis by breaking the assembly into finite elements, like tetrahedrons. Governing thermodynamic equations

are used and integrated over each element. Each element has specific defined thermal properties and initial conditions and contains multiple nodes, which are typically located at the vertices of the finite element [12]. The equations are then solved numerically for each element given the specific thermal properties and state of the node and surrounding nodes [12]. For radiative heat transfer, SolidWorks utilizes a ray tracing algorithm that creates paths from node surfaces to other node surfaces in order to determine the view factors between all surfaces in the model [20]. This method can be done forwards from source to sink or backwards from sink to source and is called forward and backward ray tracing, respectively [20]. For steady state analysis, each node is solved iteratively until the solution converges to a steady state within a specified tolerance. In SolidWorks flow simulation, the results are able to be viewed with the solid model and changed to allow for rapid iteration during the designing, testing, and analysis process.

The intent of the thermal model is to predict how the chamber will perform so that the response of the test article can be known or approximated before the test. When the thermal test is conducted, the experimental data is used to validate the model results, within a certain thermal uncertainty margin. NASA GEVS requires a 10°C margin for qualification/protoflight testing [1] and The European Cooperation for Space Standardization (ECSS) requires a 15°C [1, 11] margin for the same testing. These margins are for thermal test levels above or below the predicted flight levels, so they are not exactly analogous to comparing the thermal model of the chamber to the response of the chamber. However, they show that the worst case prediction should have an error less than 10-15°C.

1.5 Experimental Apparatus Background and Previous Capabilities

The MDA US systems thermal vacuum chamber, referred to as the "Blue" TVAC was donated by MDA Corporation and was originally used in the development of the Mars exploration rover's robotic arm [11]. Since it was donated, significant refurbishment, analysis, and testing has been performed by multiple graduate and undergraduate students to improve the functionality and capabilities of the system. Figure 1.4 from Jensma's thesis shows the Blue TVAC in its state before any work in this thesis was performed [11]. When the previous state is referenced, this refers to the state of the chamber before any modifications for this thesis.

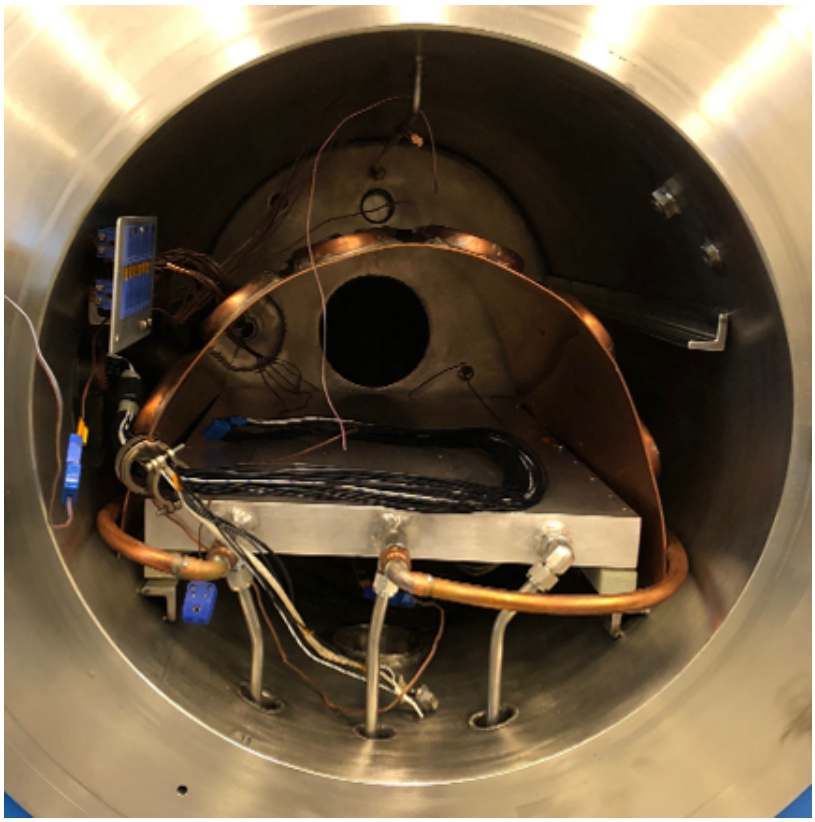

Figure 1.4: Blue TVAC Chamber [11]

The Blue TVAC consists of three primary systems: the vacuum system, the thermal control system, and the data collection and control systems. The vacuum system

consists of pressure gauges and two pumps: one turbomolecular pump, and one mechanical pump. The thermal control system consists of a platen with heaters and coolant lines, a shroud with coolant lines, a door shroud, and nitrogen management systems including valves and a dewar. The data collection system includes feedthroughs for thermocouples, a temperature controller to manage heaters and nitrogen flow, and a DAQ system with 12 thermocouple channels. A system level block diagram from Jenmsa's thesis is shown in Figure 1.5 [11].

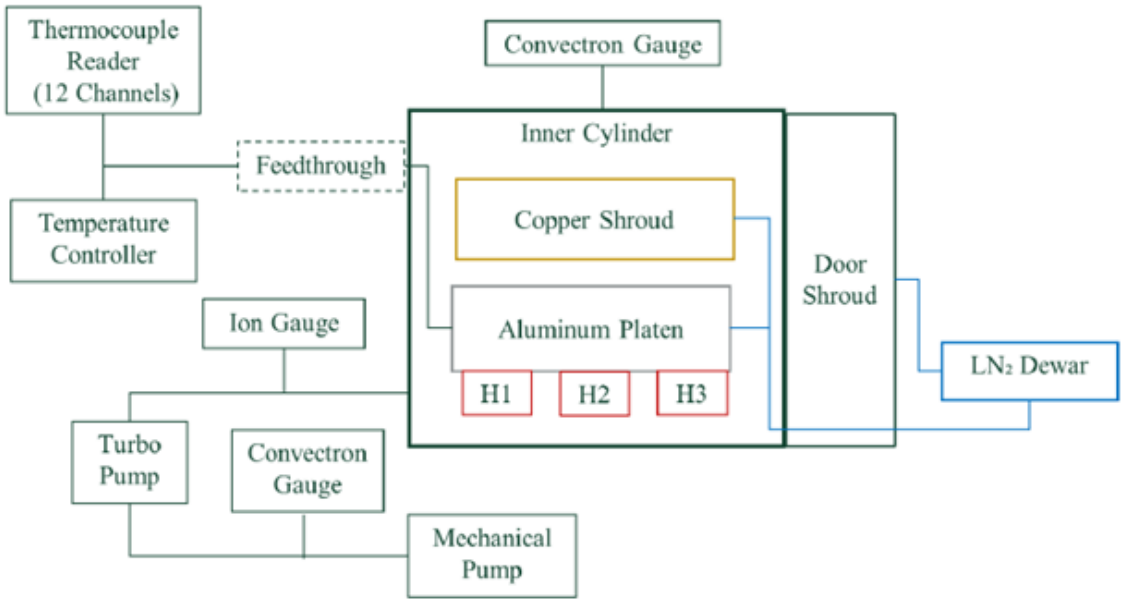

Figure 1.5: Blue TVAC systems block diagram [11]

The previous capabilities of the Blue TVAC as of June 2020 are adequate for up to two full thermal vacuum cycles with the mass model according to ISO Standard 19683 at a minimum vacuum pressure of $<2.0e^{-4}$ Torr [11]. The previous minimum vacuum pressure was not compliant with ISO Standard 19683 for thermal vacuum testing but was assumed adequate for the assumption that convective heat transfer is negligible [11]. The previous lowest and highest achievable temperatures during thermal vacuum testing were approximately -30°C and 50°C for the shroud, and -20°C to 65°C for the platen [11]. The existing DAQ has 12 thermocouple inputs

for measuring shroud, platen, and test article temperatures throughout a test along with data logging capability [11]. Table 1.1 summarizes the Blue TVAC's previous capabilities compared to ISO 19683. Note that tolerance limit is the minimum and maximum difference of the test article from the set point during thermal dwells. It is difficult to precisely compare this value between different experimental setups due to a difference in where temperatures are recorded and the limitations of only logging temperature at certain locations along with varying definitions of steady state.

	ISO 19683 Requirement [9]	**Previous Capability [11]**	**Description**
Temperature Range	-15°C to +50°C	-15°C to +50°C	For cold soaks, only capable of a couple cycles due to liquid nitrogen tank size and consumption rate [11].
Chamber Pressure	$<7.5e^{-6}$ Torr	$<2.0e^{-4}$ Torr	Further leak investigations could improve this.
Number of Cycles	2 or More	4	Greater is better, modifications should increase this.
Thermal Dwell	1 hour or longer	1 hour or longer	Modifications should increase this.
Temperature Ramp Rate	$\pm 5°C$ or slower	$\pm 5°C$ or slower	Greater is better, modifications should increase this.
Tolerance Limit	3°C	Not Specified	Modifications should allow this to be met.

Table 1.1: Previous Capability vs ISO 19683 Requirements for TVAC Testing

Table 1.2 shows a further breakdown of the various levels, margins, and tolerances for thermal vacuum testing from various rules and standards. Note that the average tolerance is +/-3°C and a chamber pressure requirement is $<10^{-4}$ Torr for all standards shown.

The thermal control system consists of the shroud, platen, and door shroud. All these components are plumbed such that nitrogen can flow through them for cooling and the flow can be controlled using a PID controller and solenoid actuated valves.

The platen has electric resistance heaters mounted underneath it that are controlled using a PID controller. The shroud is made up of copper sheeting with soldered on copper tubing and is uncoated. The platen has built in coolant channels and heaters installed underneath and is made of uncoated aluminum. The door shroud is likely aluminum with coolant channels and is coated with a flat black coating on the inside face. Liquid nitrogen is fed from an external 35 L Dewar and the outlets from the chamber through tubing to the atmosphere outside of the lab.

1.6 Limitations and Modifications

The major limitations with the Blue TVAC in its previous state were maximum potential test article size, minimum pressures, maximum and minimum temperature ranges, and cold hold duration. These were persistent limitations with the chamber since it was donated and as it was upgraded, and extensive testing and characterization of the chamber has been performed by previous students to model and improve the performance and consistency of the chamber. Caudill and Diamond implemented the cooling system, and they demonstrated the shroud cools more rapidly than the platen, likely due to thermal mass and plumbing differences [3]. It was also noted that times to reach thermal equilibrium for a 3U CubeSat mass simulator were on the order of hours [3]. This is likely due to poor heat transfer between the shroud, platen, and test article. The shroud is bare copper, which has an emissivity of less than 0.1 depending on the surface roughness and presence of oxidation [11]. The platen is bare aluminum, which also has an emissivity of typically less than 0.1 [11]. This reduces the rate of radiative heat transfer to the test article compared to a higher emissivity surface, as the shroud and platen emissivity is directly proportional to the amount of heat it can absorb or emit.

Both maximum and minimum temperature capabilities and ramp rates can be improved by decreasing the shroud and platen thermal mass and adding high emissivity coatings to the interior faces of the shroud and platen. High emissivity coatings in this thesis are regarded as those with an emissivity of greater than 0.8, which is typical of aerospace grade black coatings [8]. Research by Jayaram and Gonzalez has demonstrated a low cost, small thermal vacuum chamber can be constructed using common materials with comparable performance to existing commercially available chambers [10]. They utilize copper sheeting and copper refrigeration tubing to construct a cylindrical shroud, with a small platform to accommodate test articles. This is similar to the previous configuration, except with a lower thermal mass relative to the size of the chamber and a larger maximum test article size relative the pressure vessel size. Based on the results from Jayaram and Gonzalez, the reduction in thermal mass of the Blue TVAC shroud and platen will offer performance improvements due to the lower thermal mass, which will reduce time to equilibrium temperatures and use less nitrogen to achieve a given set temperature. The shroud plumbing will need to be resized with thinner materials and tubing to achieve the lowest temperatures possible with a backpressure of 27,579-48,263 Pa (4-7 psi) [11, 3], 35 L storage capacity, and evaporation rate of 0.22 L/day [10]. Additionally, improving the insulation around the dewar feed lines to reduce thermal losses based on the losses noted by Jensma, Caudill, and Diamond during testing. The existing platen heaters must be repurposed as heater plates such that they can be arranged around the test article as needed to simulate an IR source like the Earth or other planetary bodies, or an approximation of the sun's heat input. This can be achieved by setting the heaters such that they provide the equivalent heat flux that would be seen in flight from the sun [1].

In addition to reducing the thermal mass of the heating/cooling system, coatings can be utilized to improve the performance and efficiency of the system. By applying

high emissivity coatings to the interior faces of the shroud and heater plate surfaces, equilibrium temperatures for the test article are expected to be achieved in less time, and as a result less heater power and nitrogen is needed to achieve a given test article temperature. Extensive testing of thermal control materials has been conducted at the International Space Station on the Long Duration Exposure Facility to evaluate the performance of commonly used coatings for thermal control. Specifically, low outgassing polyurethane thermal control coatings like Aeroglaze Z306 were resistant to the space environment and even increased in emissivity likely due to roughening by erosion from Micrometeorites and orbital debris (MMOD) and atomic oxygen (AO) [10]. While the TVAC chamber will be free of AO and MMOD, this polyurethane coating will likely be able to survive the extreme temperatures, thermal cycling, and vacuum environment in the chamber with minimal degradation and outgassing/contamination risk.

Since the likely leak noted previously is persistent and increasing, it is important that the leak is investigated thoroughly, and resolutions are made as appropriate. The space environments lab is equipped with a helium leak detector, which was used to attempt to locate the major leak sources as part of the work performed for thesis. It was not documented by Williams or Jensma that the helium leak detector has been used with the Blue TVAC before to help determine the root cause, and Jensma recommended its use to find leaks in the system [22, 11].

1.7 Thesis Motivation and Work

After hardware changes and leak testing discussed in the previous section were made to the Blue TVAC, TVAC testing and thermal modeling was needed to confirm the changes made improved performance and capabilities. A new thermal model using SolidWorks and SolidWorks Flow Simulation was updated to match the current con-

figuration and compared to testing results such that a predictive analytical model can be made. This testing involved measuring the temperature response of different components of the system as well as test articles during thermal vacuum testing. Test articles include a CubeSat mass model and a coated and bare aluminum plate, which are geometrically simple and well characterized in terms of surface and material properties.

The goal and motivation of this thesis is to improve the performance of the system and re-calibrate the models and control systems to the new configuration such that it meets the ISO 19683 test level requirements for thermal vacuum testing. This work builds off the efforts of previous students so that the chamber can be used as an educational and research tool for projects within and outside of Cal Poly. In general, the chamber in its current state meets ISO 19683 requirements except for vacuum level and tolerance. However, the capabilities can be extended with the modifications which should increase test volume, reduce the leak rate and therefore minimize chamber pressure, improve thermal mass such that the nitrogen consumption rate is decreased which enables longer dwells and more cycles, and improve the radiation efficiency of the heaters and shroud with coatings which will enable and faster equilibrium times and more efficient heat transfer to test articles. These improvements, while not strictly based on any requirements beyond ISO 19863, are important because they offer more flexible test capabilities. These more flexible capabilities are able to accommodate full scale, extended tests in the case of larger CubeSats, for example.

Table 1.2: Rules and standards for thermal vacuum cycling tests from Chisabas et al. [4]

		Rules & Standards				
		GSFC-STD-7000.[6]	MIL-HDBK-340A.[8]	ECSS-E-ST-10-03C.[1]	TR-2004 (8583)-1 Rev.A.[9]	NASA LSP-REQ-317.01 Rev.B.[11]
Qualification	Chamber pressure	1.33×10^{-3}Pa (10^{-5} torr)	13.3×10^{-3}Pa (10^{-4} torr)	10^{-3} Pa (7×10^{-6} torr)	13.3×10^{-3}Pa (10^{-4} torr)	13.3×10^{-3}Pa (10^{-4} torr)
	Temperature margins*	10°C	No info.	See [f]	10°C	10°C
	Number of cycles	4	13[a] or 3[b]	4	8	8
	Dwell time	24h	8h[c] or 4h[d]	No info.	8h[c] or 4h[d]	1h
Acceptance	Chamber pressure	No info.	13.3×10^{-3}Pa (10^{-4} torr)	10^{-3} Pa (7×10^{-6} torr)	13.3×10^{-3}Pa (10^{-4} torr)	13.3×10^{-3}Pa (10^{-4} torr)
	Temperature margins*	5°C	No info.	See [g]	0°C	5°C
	Number of cycles	No info.	13[a] or 3[b]	3[e]	4	2
	Dwell time	No info.	8h[c] or 4h[d]	No info.	8h[c] or 4h[d]	1h
Protoqualification	Chamber pressure	No info.	No info.	10^{-3} Pa (7×10^{-6} torr)	13.3×10^{-3}Pa (10^{-4} torr)	13.3×10^{-3}Pa (10^{-4} torr)
	Temperature margins*	No info.	No info.	See [f]	5°C	10°C
	Number of cycles	No info.	No info.	3[e]	4	4
	Dwell time	No info.	No info.	No info.	8h[c] or 4h[d]	1h
Tolerances	Pressure	±80%	±80%	±80%	+0/-80%	No info.
	Temperature	±2°C	±3°C (-54°C to +100°C)	Tmin +0/-4°C Tmax -0/+4°C (T>-193.15°C)	±3°C (-54°C to +100°C)	No info.

* This temperature margins are with respect to the worst expected temperatures

[a] If no thermal cycling test was performed before

[b] If thermal cycling test was performed before

[c] First and last thermal cycles

[d] Intermediate cycles

[e] Plus 1 more back up cycle that can be decided to be performed during tests

[f] Qualification and protoqualification temperature limits are reached when any equipment reaches its qualification temperature limits. Its qualification limits represents the maximum and minimum acceptance temperatures and a 5°C margin.

[g] Acceptance temperature limits are reached when any equipment reaches its qualification temperature limits. Its qualification limits represents the maximum and minimum design temperatures and a 5°C margin.

Chapter 2

MODIFICATION DESIGN DEVELOPMENT

The changes to the Blue TVAC heating and cooling system were motivated by the efforts of previous students and build off their work and incorporate the future work specified in previous theses by Williams and Jensma [22, 11]. The focus of this chapter is on sizing and optimizing the cooling shroud, as well as designing for modularity and manufacturability using vacuum compatible materials.

2.1 Goals and Design Criteria

In order to improve the performance of the heating and cooling systems, the entire existing platen and shroud assemblies required design from the ground up. The modified design was developed with funding and manufacturing limitations in mind. In general, parts are reused and modified where possible, and manufacturing is limited by student capabilities and the tools available in the Aerospace Engineering shop and other shared work spaces on campus. The goals of the modifications are to:

- Expand the available space for test articles by incorporating a larger shroud and modular components
- Improve the temperature distribution across the shroud and platen such that test articles are evenly heated/cooled
- Reduce the thermal mass of the chamber to improve response time of the chamber and require less energy to heat and cool by using thinner materials where appropriate, allowing for greater numbers of thermal cycles and/or greater temperature range per unit of liquid nitrogen consumed

- Improve the heat transfer rate between the test article and the chamber systems through the use of high emissivity coatings
- Improve the minimum pressure achieved using vacuum compatible materials and a leak tight cooling system
- Allow the thermal response to be more predictable through the creation of a validated thermal model using SolidWorks

The modification goals would be considered successful if there was a noted improvement in all the mentioned criteria above while also maintaining and exceeding ISO 19683 requirements for thermal vacuum testing.

2.2 Cooling Shroud Sizing

It was determined that a cylindrical cooling shroud would make the most efficient use of space in the chamber because the existing pressure vessel is cylindrical in shape. Additionally, fabricating a cylinder shape allows for simple tooling compared to other geometries. After an initial shape was determined, a detailed study was performed to determine how to direct the nitrogen coolant throughout the shroud such that it allows for an even temperature distribution across the interior surface.

2.2.1 Initial Configuration Comparisons

It was determined that using commercially available copper tubing, common for refrigeration, HVAC, and water distribution applications would be best suited for this application. This tubing is generally high purity copper, which is desirable for outgassing properties, corrosion resistance, thermal conductivity, and workability. After a base material was selected, different configurations were conceptualized and mod-

eled using SolidWorks. Figure 2.1 shows the four main options considered for the tubing configuration.

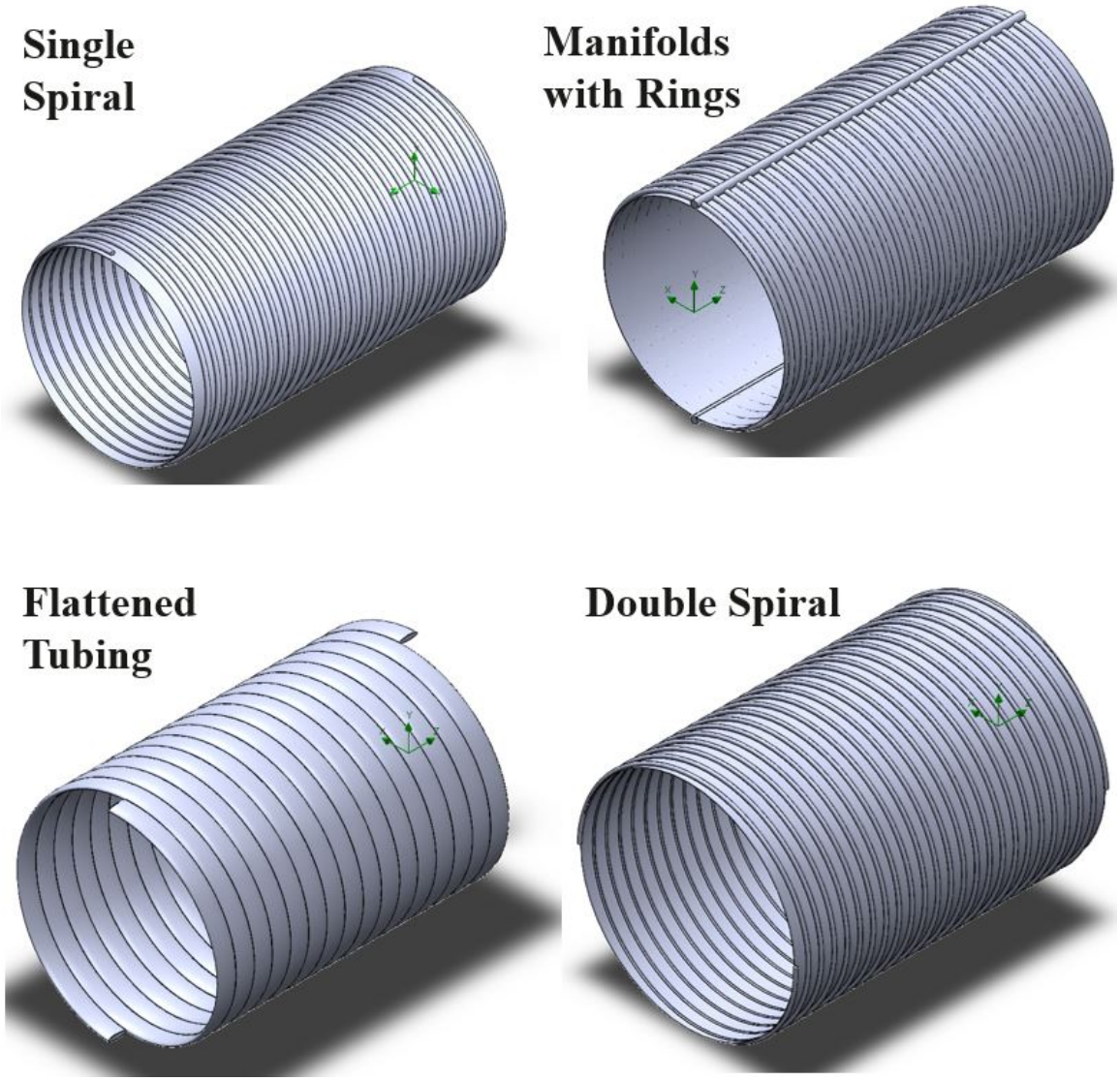

Figure 2.1: Concept shroud cooling tubing configurations

The single spiral configuration consists of continuous tubing from one end of the shroud cylinder to the other, wrapping around the outside of a thin sheet of copper. This is the simplest configuration because there is only one inlet and outlet, one continuous shape, and commercial tubing can be used directly with little modification. The double spiral consists of interwoven spirals, where one outlet and one inlet exists on each end of the shroud cylinder. The concept behind the double spiral was that a

more even temperature distribution could be achieved with inlets and outlets on both sides, but at the cost of using the coolant less efficiently since the warmer nitrogen exiting the shroud would be in close proximity to the incoming nitrogen from the other spiral segment. The flattened tubing configuration is a single spiral without any underlying sheet of copper to act as the shroud cylinder. Large tubing would be flattened such that the tubing is wide along the axis of the cylinder, and thin in the axis normal to the cylinder. This configuration requires tubing that can be easily formed into this shape without damaging the tubing such that it would leak or fail to hold pressure. The flattened tubing configuration is shown as a double spiral, but could be a single spiral as well. Finally, the manifolds with rings configuration consists of an inlet manifold on the top of the cylinder and an outlet manifold at the bottom of the cylinder. These manifolds run along the walls of the cylinder and carry nitrogen coolant to the semi-circumferential tubing that runs from the inlet to the outlet manifolds along the walls of the shroud.

Further research into available materials lead to the elimination of the flattened tubing configuration. This is because the available tubing sizes that would be able to be flattened as shown in Figure 2.1 have wall thicknesses that would result in excessive mass compared to other configurations, which is undesirable because the thermal mass of the cooling system would significantly increase.

The manifolds with rings configuration requires many tens of joints that must be entirely leak tight, or the chamber will have nitrogen leaking into it, which the pumps would likely not be able to keep up with. Additionally, the number of precise holes in the manifold and subsequent joints means the configuration is more complex in terms of manufacturability than the spiral and double spiral configurations. Because of this, the manifolds with rings configuration was eliminated as well.

2.2.2 Detailed Configuration Comparison

After the configurations were narrowed down to the single and double spiral configurations,study was performed using SolidWorks Flow simulation to compare and optimize the spiral configurations, focusing on even temperature distributions across the shroud while seeking to minimize material used and manufacturing complexity.

2.2.2.1 Numerical Model Setup

SolidWorks Flow Simulation was used for the configuration comparisons and consisted of a simplified chamber geometry to simulate heat moving from the environment to the chamber as well as the shroud and test article to examine temperature distributions across the various surfaces in the cold, steady state case.

An 18" outer diameter 304 stainless steel cylinder was used to approximate the vacuum chamber, with a polished interior face. 0.75" of fiberglass insulation around the chamber cylinder section was included to approximate the insulation installed on the chamber. All exposed chamber and insulation surfaces were assumed to be at a constant temperature boundary condition of 20°C. This is an approximation of the average temperature in the lab based on day/night cycles where the chamber is located. Because there are multiple buffer zones between the outside and the test article, like the building walls, air gap, chamber insulation, chamber walls, vacuum gap between the shroud and chamber, external temperature variation is not expected to play a significant role in measured thermal response. Additionally, the chamber is actively controlled which will further damp variation in experimental results. The emissivity used for polished stainless steel was 0.074 and is from the SolidWorks standard material library for polished stainless steel [20].

The coolant used is nitrogen and is assumed to be gaseous at 100 K when it enters the tubing (77 K boiling point + arbitrary losses). The nitrogen flow rate was estimated to be 49 g/min [11]. This is based on estimates of the duty cycle and endurance of the 35 L dewar used in Jensma's testing. The backpressure for the cooling system outlet is assumed to be 0.6 m of water, which is based on previous test configuration [11].

The copper sheet used to support the tubing and absorb energy from the test articles was defined as 0.005" copper sheeting with a diameter of 16.5" and a length of 30". The shroud tubing consisted of standard 1/4" OD copper refrigeration tubing. A tubing spacing of 2" for the spirals was selected for the initial single and double spiral comparison. The sheet and tubing are bonded with no contact resistance and the interface completely connects the thickness of the shroud to the base of the tube. The emissivity used for polished copper was 0.025 at 300 K and is a function of temperature. The emissivity is from the SolidWorks standard material library for polished copper [20].

The test article simulator used was a simplified 3U CubeSat mass model made of black painted aluminum with 1/8" wall thickness and a heat dissipation of 5 W throughout its volume. An emissivty of 0.91 was assumed for the coated surfaces including the inside walls of the shroud and CubeSat.

There is no contact between the CubeSat and shroud or shroud and chamber interior to simplify losses through supports so that radiation is the only means of heat transfer between the surfaces.

2.2.2.2 Single and Double Spiral Comparison

Because this model compares temperature distributions and the only parameter being changed is the tubing configurations, direct comparisons can be made between the

results at steady state. The actual temperatures in this simulation are not intended to be compared to the experimental results since the coolant flow rate was approximated, but the intent is that the temperatures will be representative and comparable between different configurations. In Chapter 4 and 5, the thermal model used for experimental results comparison is discussed. Because the temperature distributions do not vary by more than 1°C across the surface, contour plot results are not shown.

Figure 2.2 shows the temperature distribution across the shroud for the double spiral configuration. Note that the middle region has the smallest difference in temperatures, around -144°C to -150°C, and the edges farthest from the tubing tend to have the greatest difference in temperatures compared to the average, around -136°C to -156°C. The maximum temperature difference across the shroud is 29°C, but the majority of the shroud is between -145°C to -155°C. The test article surface temperature is maintained to within 0.13°C.

Figure 2.3 shows the temperature distribution across the shroud for the single spiral configuration. Note that the middle region has the smallest difference in temperatures, around -180°C to -184°C, and the edges farthest from the tubing tend to have the greatest difference in temperatures compared to the average, around -162°C to -175°C. The maximum temperature difference across the shroud is 22°C, but the majority of the shroud is between -180°C to -184°C. The test article surface temperature is maintained to within 0.13°C.

It is clear that the minimum temperature for the majority of the shroud is lower for the single spiral, and this because the double spiral is less efficient at cooling because of the proximity of different spiral tubing, where the inlet side of one spiral is close to the outlet side of the other spiral. There was no improvement in test article surface temperature difference between the single and double spiral cases, and the minimum temperature was lower for the single spiral. The single spiral also had less

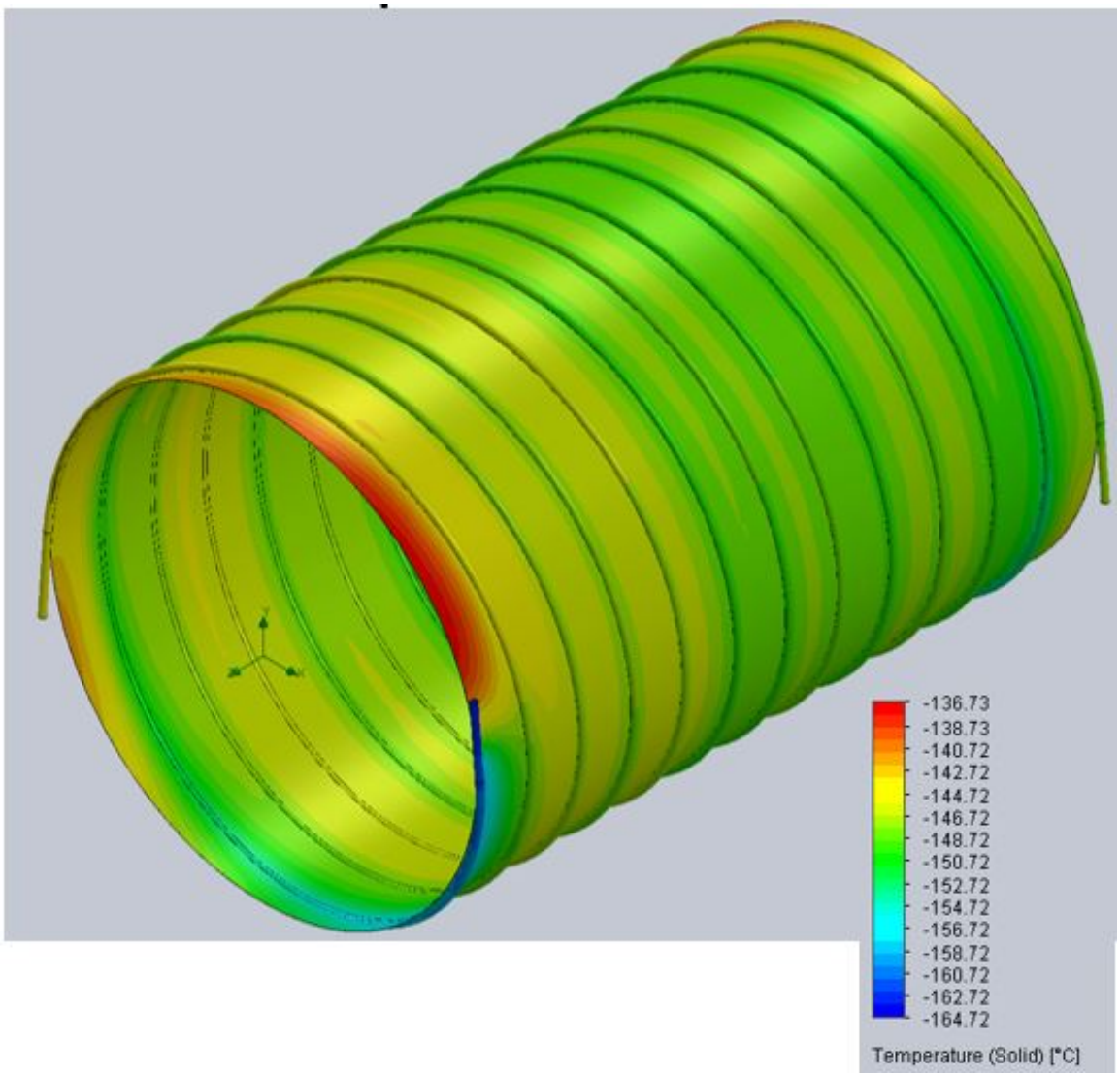

Figure 2.2: Double spiral temperature contour plot for the shroud with 2" spacing

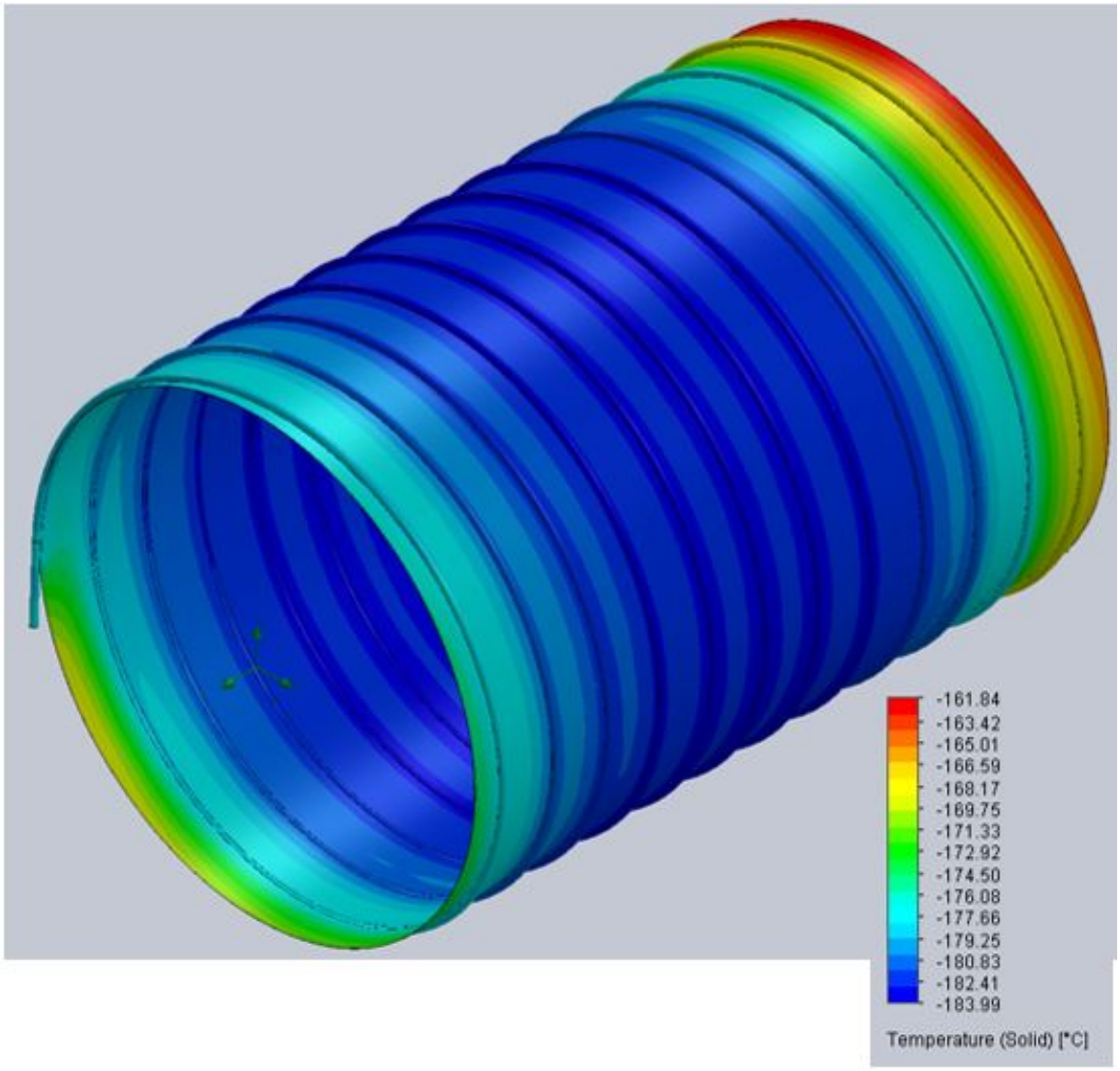

Figure 2.3: Single spiral temperature contour plot for the shroud with 2" spacing

variation in temperature across it, which is clear from the contour plots. Overall, the single spiral offers similar or better performance with less complexity, and will be further optimized in the next section.

2.2.3 Single Spiral Optimization

Following a similar methodology for model setup from the previous section, the single spiral configuration was compared with various changing parameters including the spiral spacing, the tube size, and the shroud sheet thickness. First, the tubing spacing was compared at 1", 2", and 3" between spirals to determine the sensitivity of spacing on temperature distribution and minimum temperatures. Figures 2.4 and 2.5 show the temperature distributions at the 1" and 3" spacing, with 2" being the same as 2.3 from the previous section.

The different configurations shows smaller spacing leads to more consistent temperature distributions, with a minimum temperature of -190°C at 1" compared to -184°C at 2" and 3". All cases showed test article surface temperature is maintained to within 0.14°C. Because the single spiral requires over 100 feet of tubing and has a negligible affect on test article surface temperatures in this case, it was determined that a spacing between 2" and 3" would be selected.

In addition to tubing spacing, shroud thickness and tubing size was varied. Figure 2.6 shows the effect of increasing the tubing OD from 1/4" to 3/8". The minimum and maximum range increases and the minimum temperature is higher compared to the 1/4" tubing case, so the 3/8" tubing was not used. Sizes smaller than 1/4" OD were not studied in detail because there are not standard, commonly available sizes below 1/4".

The effect of thicker shroud sheet was studied by increasing the shroud sheet from 0.005" to 0.008" thickness. Figure 2.7 shows the effect on temperatures across

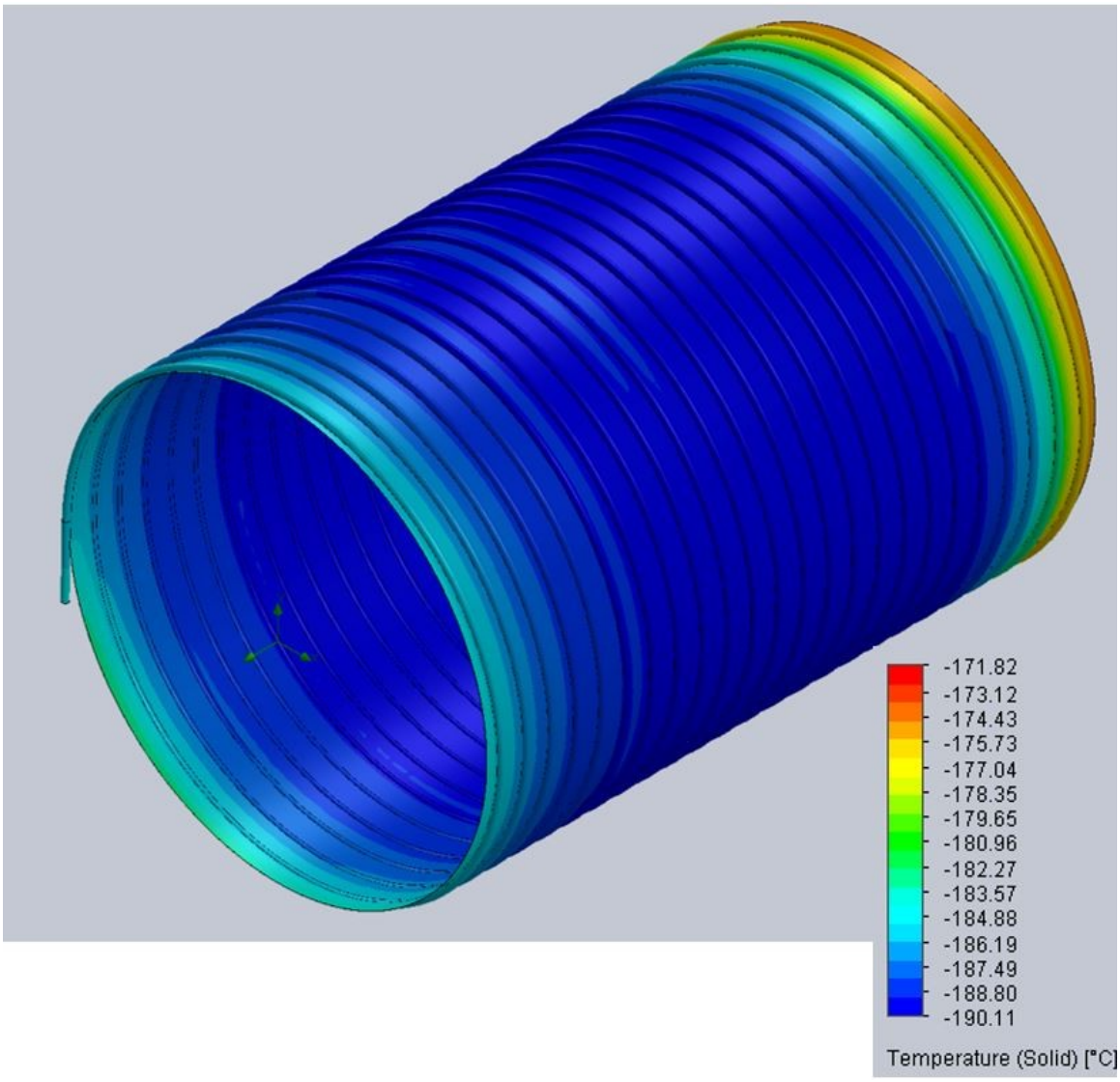

Figure 2.4: Single spiral temperature contour plot for the shroud with 1" spacing

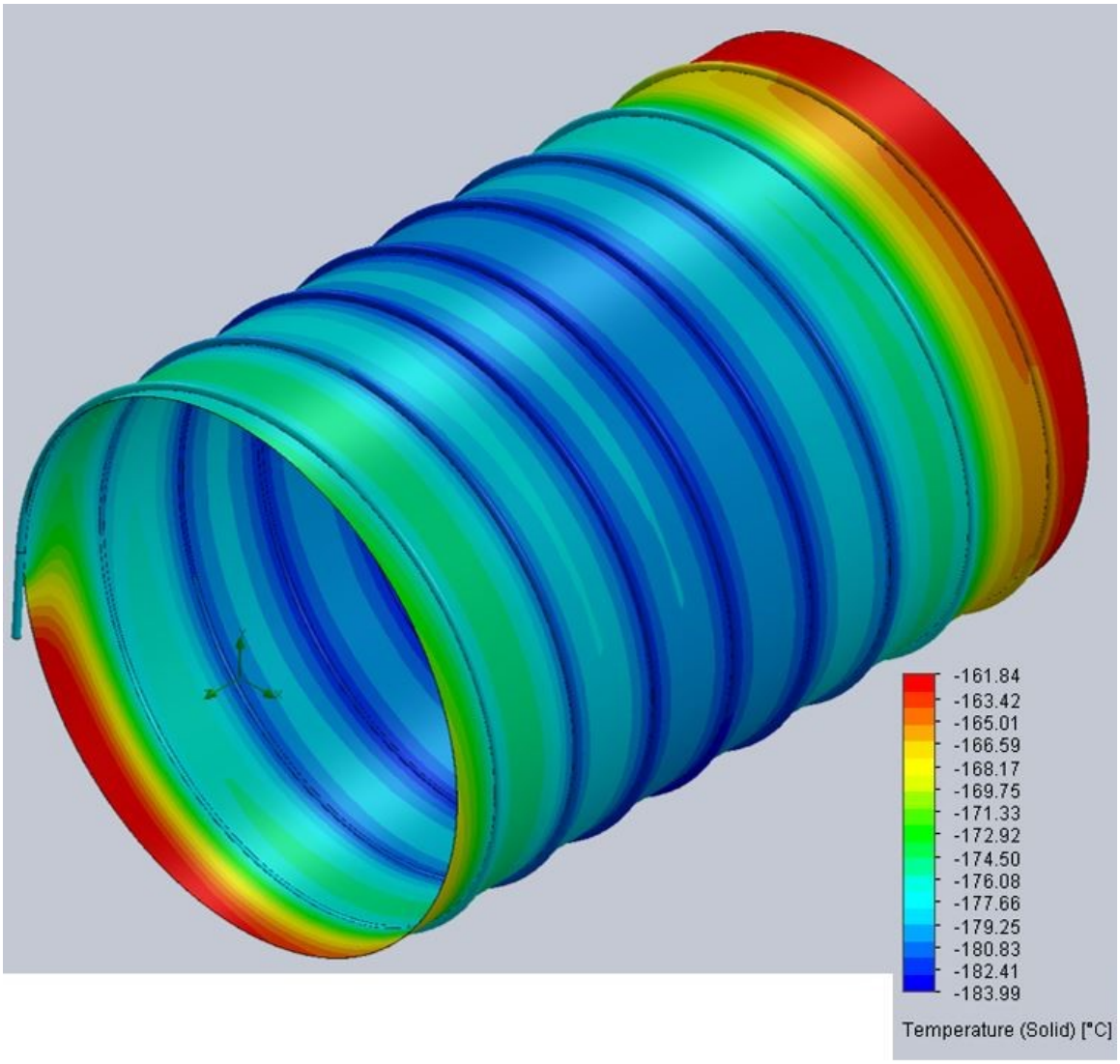

Figure 2.5: Single spiral temperature contour plot for the shroud with 3" spacing

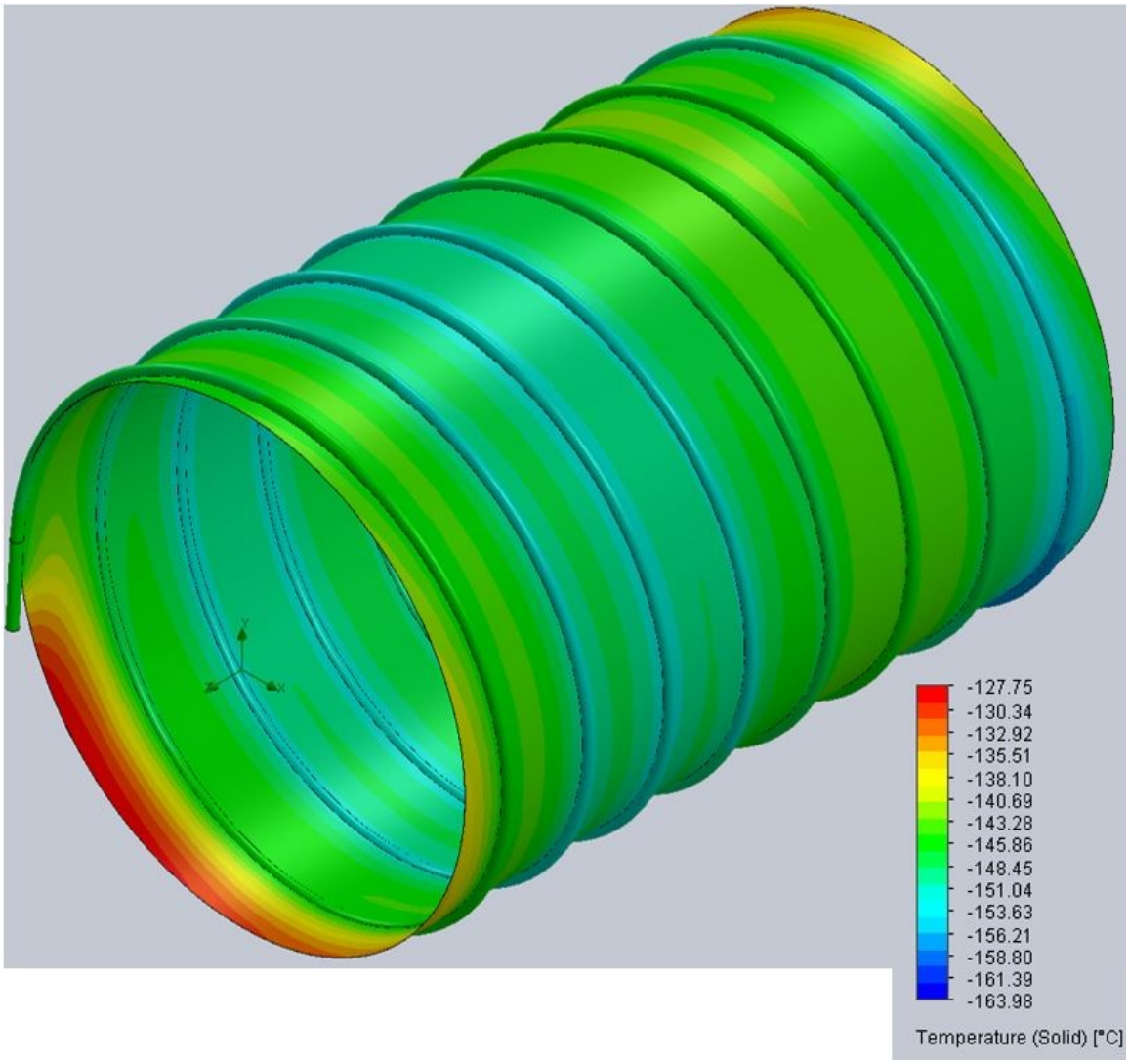

Figure 2.6: Single spiral temperature contour plot for the shroud with 3" spacing and 3/8" OD tubing

the shroud and platen. The effect is insignificant because the minimum temperature changes by 0.19°C and the maximum and minimum temperatures are less than 2°C different. Because of this, the 0.005" shroud sheet was selected due the lower thermal mass and easier formability.

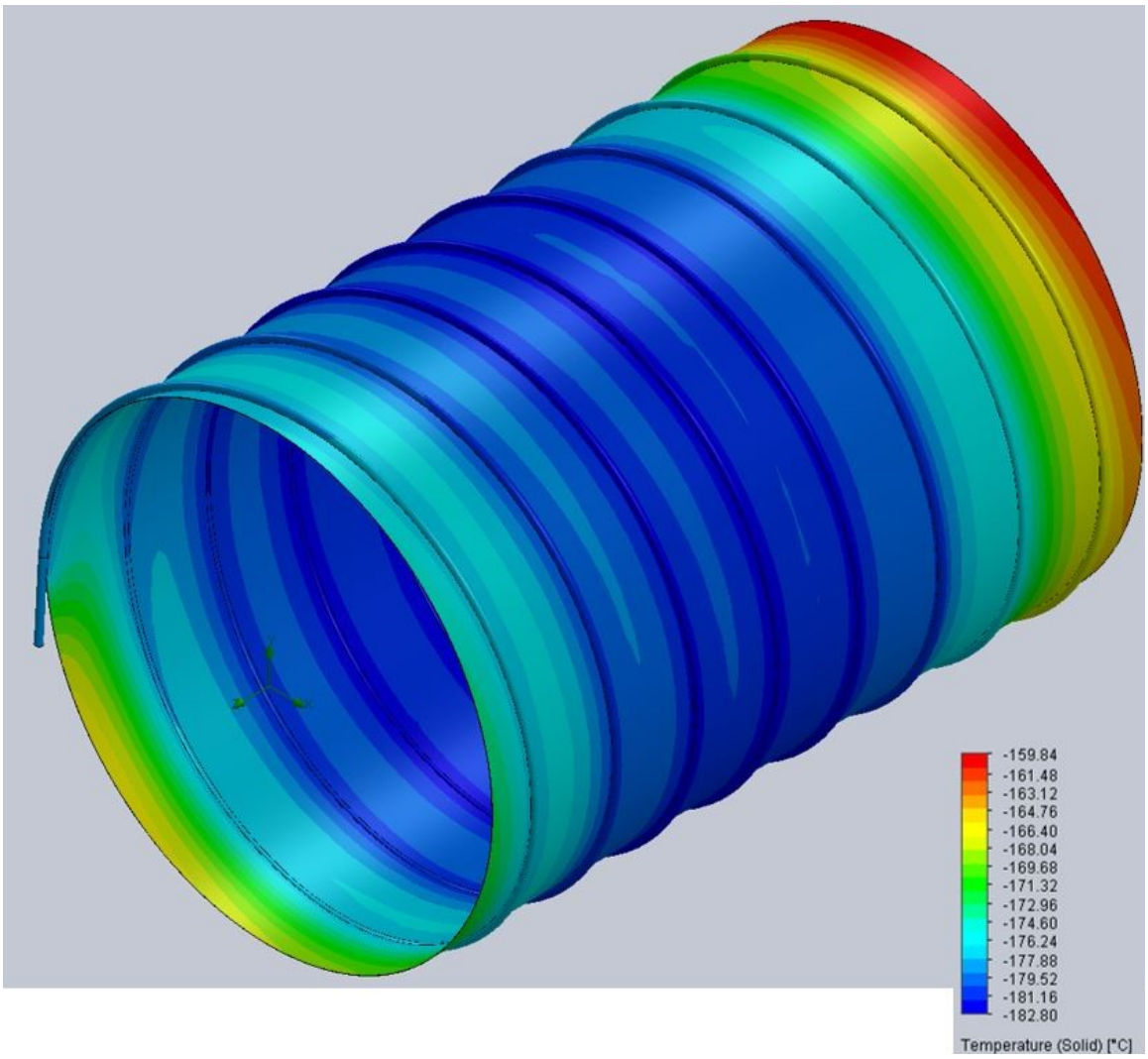

Figure 2.7: Single spiral temperature contour plot for the shroud with 3" spacing and 0.008" thick sheet

2.2.4 Configuration Selection

Shroud configuration was selected based on comparisons and rankings of different factors shown in Table 2.1. The shroud maximum temperature difference is the

difference in maximum and minimum temperatures across the entire shroud surface. Temperature distribution rank is a ranking from 1 to 6, where 1 is the best, of how even the temperature is across the majority of the shroud surface. Minimum temperature rank is the lowest achieved temperature for a given configuration, where 1 is the best or lowest temperature. Manufacturability rank considers how difficult it is to manufacture a given configuration, considering length of tubing, geometrical complexity of configuration, and material thickness.

Table 2.1: Cooling sizing analysis summary table, best configurations highlighted in green

Shroud Configuration	Shroud Max. Temp. Diff. [°C]	Temp. Distrib. Rank [1-6]	Min. Temp. Rank [1-6]	Manufactur-ability Rank [1-6]
Double spiral, 2" spacing	27.99	3	5	5
Single spiral, 2" spacing	22.15	2	2	4
Single spiral, 1" spacing	16.98	1	1	6
Single spiral, 3" spacing	22.15	6	3	1
Single spiral, 3" spacing & 3/8" OD tubing	36.23	4	6	3
Single spiral, 3" spacing & 0.008" sheet	22.96	5	4	2

The final configuration was selected with 1/4" OD tubing and a 0.005" shroud sheet thickness was selected based on the above results. The spacing ultimately used for manufacturing was 2.75", because the tubing came in a roll at a fixed length and 2.75" allowed for it to be fully consumed without increasing the copper tubing length required to be purchased. The final length of the shroud cylinder was 24" to allow for 4" at the front of the chamber for the thermocouple input board as well as plumbing connections for nitrogen. The mass of this modified shroud is less than 3 kg, compared to the previous shroud with a measured mass of over 11 kg.

2.3 Heater Plate Sizing

The heater plates were sized to minimize thermal mass while still maintaining rigidity and allowing for an even temperature distribution across the plate under expected conditions with the heater element operating. It was determined that three heater plates were to be cut from the existing platen, and were sized to be capable of surrounding a 3U CubeSat on three of the largest faces. The existing platen material was used to save cost and minimize the risk of damage to the strip heaters integrated in the platen, as they were press fit into slots in the platen.

The final dimensions for the heater plates were 6" by 12" with a 0.14" wall thickness and 0.25" wide slots to mount the heater strips. The heating elements are 10" x 0.25" x 1.5" and cover over 20% of the back surface area. The mass of the modified heater plates was approximately 0.5 kg each or 1.5 kg total, compared to the previous platen which weighed in excess of 20 kg. These are not directly comparable since the platen also provided a cooling function that is replaced by the cylindrical shroud, but give an idea of the difference in thermal mass of the system.

2.3.1 Heater Plate Thermal Model

To verify the temperature distribution across the front face of the plates would be even with these dimensions, a simple thermal analysis using SolidWorks simulation was performed. The analysis assumes the heater strip acts as an 85°C constant temperature boundary condition for the slot where the strip is pressed into. The faces except for the slot for the heater strip is painted black with an emissivity of 0.91 and is assumed to have a view factor to the ambient environment of 1 with an environment temperature of 65°C. These conditions are intended to represent a worst case where the test article and surrounding shroud are 20°C colder than the heater

strip temperature. The resulting front face temperature distribution contour plot is shown in Figure 2.8. Because the surface temperature varied by less than 1°C, the modified heater plates approximate a constant radiating surface temperature that a test article will be exposed to.

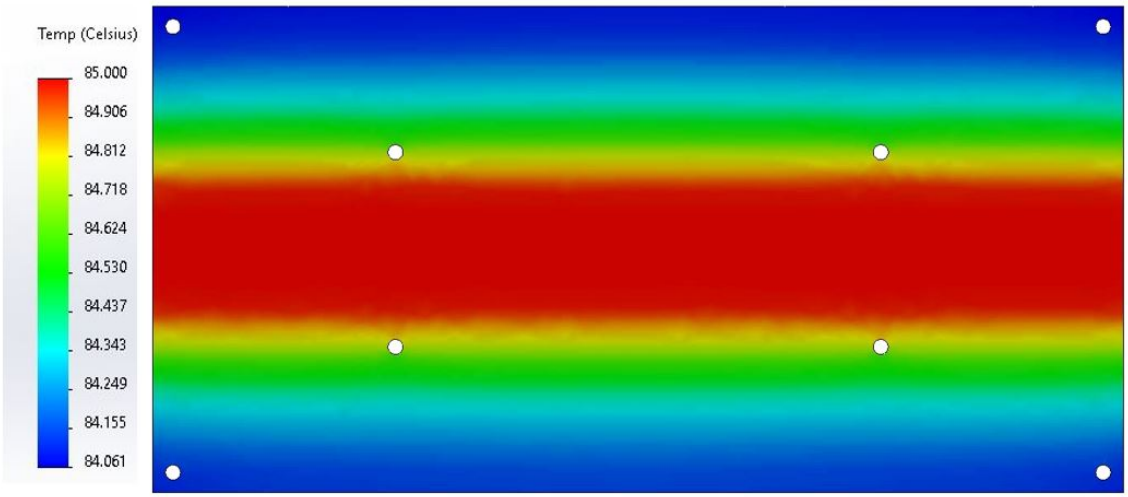

Figure 2.8: Contour plot of heater plate front face temperature distribution

It was determined that placing the heater plates at the bottom of the chamber as shown in Figure 2.9 allows for an even temperature distribution in the chamber and keeps the modular platen free to be used exclusively for test articles. Placing them at the bottom of the chamber means that they are able to radiate to a test article from underneath as well as to the sides and bottom of the shroud, which conducts the heat around the shroud and allows for an even temperature distribution across the shroud. This configuration can be modified since the heater plates are modular and not permanently mounted.

2.4 High Emissivity Coatings

For this thesis, one gallon of Aeroglaze Z306 was donated by Socomore and other supporting materials including primer and thinner were also purchased or donated

from Socomore. Aeroglaze Z306 has extensive flight heritage and has been extensively studied and used for spaceflight applications [8]. The coating has a typical emissivity of 0.91, an ASTM E 595-77 TML of 1.0% and CVCM of 0.02%, and an operating temperature range of -150°C to 130°C [19]. The high emissivity improves heat transfer via radiation between the shroud, heater plates, and test articles to allow for more even temperatures and faster equilibrium time.

2.5 Platen, Modular Mounting System

The platen selected based on commercially available oven racks or cooling racks. Oven racks are typically constructed from polished stainless steel, which is vacuum compatible. For this thesis, two 10"x15" oven cooling racks were selected and modified to remove unnecessary parts. The open area of the platen wire mesh is approximately 71%, and is made up primarily of 1/16" 302 stainless steel wires in a square pattern, with larger wires around the perimeter and in the middle for support. The open area, in combination with the reflective surface, means that heat can transfer via radiation between the bottom of the chamber to the test article on top of the platen. The spacing between the mesh is approximately 3/8" with wire diameters of approximately 1/16th of an inch. Mounting bolts with washers are recommended to secure test articles to the platen.

The modular mounting system consists of modified, commercially available aluminum rails. The rails selected are modified low profile T slotted framing rails. They have a width of 1" and depth of 0.5" and span the entire 24" length of the chamber with 4 rails spaced 90° apart. These allow for platen mounting as well as flexibility for test article and heater plate mounting depending on the requirements of a given test. For example, the platen could be removed entirely and a test article could be hung from the top mounting rail using a custom bracket or brackets to allow for larger test

article. The aluminum rails can accommodate any nuts compatible with 1" 80/20 t-slotted framing.

2.6 Aluminum Foil Reflectors

High vacuum compatible aluminum foil was utilized in the back of the shroud, over the door shroud, and at the front of the shroud to act as a radiative barrier between the test article, shroud interior, and the outer chamber. This saves energy or nitrogen and allows for more even temperature distributions on the shroud and test articles. The reflectors are shown in the final modification design section.

2.7 Final Modification Design

The final modification design is shown in Figure 2.9. It incorporates the findings from the cooling system sizing and includes a 3U CubeSat mass model test article for scale.

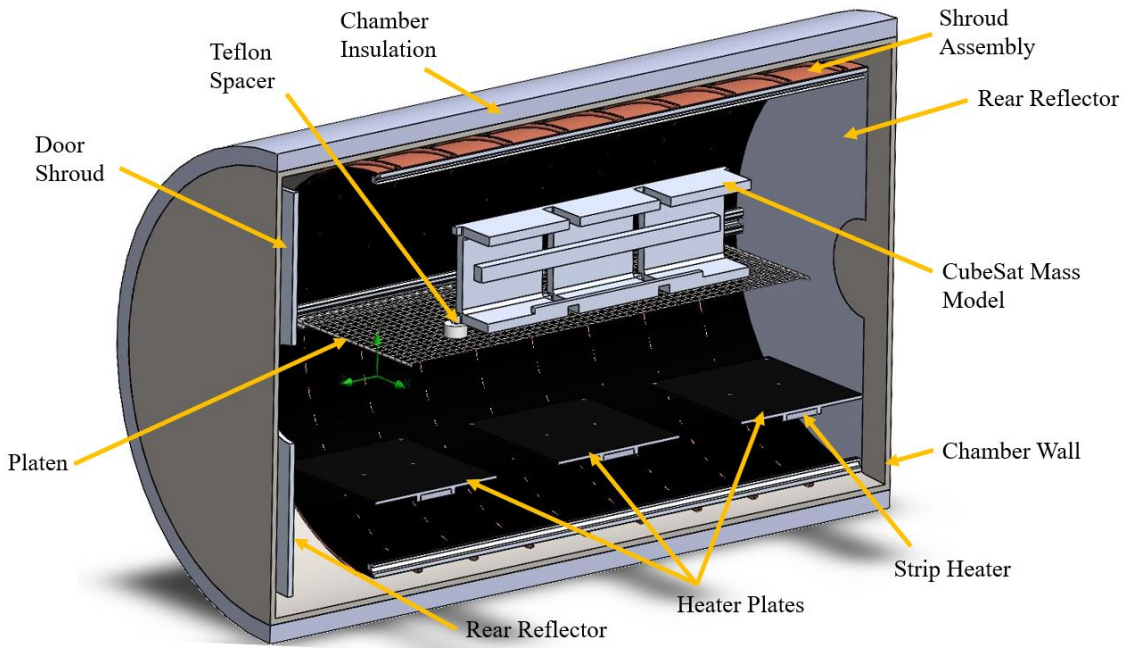

Figure 2.9: Final modification design section view with labeled components and a CubeSat mass model test article shown

2.8 Liquid Nitrogen Tank Upgrade

For this thesis, an R-IDC grant was secured by Dr. Abercromby for the purpose of upgrading the existing 35 L liquid nitrogen dewar, which cost $1,925 with freight shipping. The funding allowed for the purchase of a 180 L liquid nitrogen tank and supporting hardware, including a scale and a dolly. This represents a stored liquid nitrogen capacity increase of over 400% which offers greater flexibility and capabilities for extended duration testing, including lower temperature dwells, extended dwell periods, and/or greater thermal cycles.

The tank is a Dura-Cyl LC180-22, and comes with ports, gauges, and safety features required for operation. The existing cryogenic liquid hose used with the 35 L dewar can be directly connected to the liquid withdraw outlet on the 180 L dewar and feed into the chamber plumbing. The 180 L tank comes with a relief valve and a burst disk to prevent over-pressure. The tank automatically maintains a pressure of approximately 21-22 psi by venting gaseous nitrogen through the relief valve as the liquid slowly evaporates. The tank has an evaporation rate of 1.5% which corresponds to a loss of approximately 2.7 L/day. This means that liquid nitrogen can be stored without significant losses for days while it is in use. The cost to refill the tank from Praxair was approximately $86 as of June 2021. There is 1 week lead time on the refills from Praxair, as they pick up the tank on Thursdays and return it filled the following Thursday. It is possible other gas suppliers like Airgas could be used if shorter lead time is required, but this was not investigated in detail.

Chapter 3

MANUFACTURING PROCESS

As mentioned in the previous section, manufacturability played a significant role in the design of the updated cooling and heating systems, as well as re-usability of existing parts and materials due to budget limitations. Despite this, margin in both manufacturing timelines and budgets should always be included and were needed for this work. The greatest challenge in the manufacturing process was the shroud assembly, specifically the brazing process, which will be outlined along with other major parts of the manufacturing process.

3.1 Shroud Assembly

3.1.1 Copper Tubing and Sheet Properties

The copper tubing was purchased in coil form from McMaster Carr, and is typically used in refrigeration, water, and oil and gas industries [14]. The tubing is soft 122 copper with a purity of 99.9% with trace amounts of phosphorous to displace oxygen [14]. Outer diameter is 1/4 inch with a 0.003" wall thickness, and is rated for 1,400 psi at room temperature [14], and given the maximum operating pressure of approximately 14.7 psi, no additional analysis was performed to verify it would hold pressure, as copper becomes stronger and more ductile at lower temperatures [5].

The copper sheet was made from A110 copper, which has 99.9% purity, and was purchased from basiccopper.com in a 24" x 6' x 0.005" roll [2]. It could be formed by hand to the previous dimensions and cut using metal shears or a foot shear due to its thickness.

3.1.2 Tubing Forming

It was desirable to increase the contact area with the shroud copper sheet to improve heat transfer from the nitrogen flowing through the tubing to the copper tubing. To accomplish this, an electric roller was used to deform the tubing to have two flat faces and constant radius, semicircular edges, similar to a slot. The final dimensions for the formed tubing are a height of 0.17" with a flat width of 0.15" and a semicircular radius of 0.08". A labeled section of sample tubing is shown in Figure 3.1.

Figure 3.1: Tubing cross section after rolling process

After the tubing was rolled to the desired cross section, a ring roller was used to roughly form the tubing such that it has a 16.5" inner diameter and is spiral in shape so that it can be brazed to the outside of the copper sheet. Final forming takes place when the tubing is tacked and brazed to the shroud sheet. Since the tubing is soft copper, it can be formed by hand to meet final required radius of 16.5" and spacing of 2.75".

3.1.3 Shroud Assembly Brazing

The brazing of the shroud tubing to the copper sheet was the most involved and time consuming part of the manufacturing process. This process required the brazing of over 40 feet of tubing in a single spiral around the 16.5" diameter, 24" long sheet. The brazing alloy used for this process was an alloy of 45% silver, 30% copper, and 25% zinc in strip form 1/2" wide by 0.005" thick. An oxyacetylene torch was used to heat the tubing and sheet for brazing, and appropriate white brazing flux was used to prevent oxides from forming and inhibiting the connection during the brazing process.

Ideally, the shroud surfaces to be brazed would be cleaned and abraded with Scotchbrite or similar abrasion, however, it was found with coupon testing that for this application cleaning was not required as the raw materials were clean enough that flux alone allowed for an adequate bond. Bonds were periodically checked during the brazing process by visual inspection and physically pulling on the joint to ensure it does not separate by hand forces on the order of 10-20 lbf. This is required because when the flux melts, it forms a dark, glassy substance that can obscure the joint visually and physically joins the brazed parts, so the parts can appear joined when in reality only flux holds them together. An adequate bond has a consistent, visible, and polished looking fillet indicating that the brazing material has joined the two parts cleanly and evenly.

To become familiar with the brazing process using these specific materials, test coupons were created first using scrap copper sheet and tubing, then using cutoffs of actual materials used for the project, to verify the methods used will not damage the final materials and to practice brazing technique. It was noted that during brazing, heat should be focused on the tubing and not the sheet. This is because the tubing is more massive and takes heat away from the brazing area. Moreover, directly heating the sheet can cause overheating and melt the copper, burning a hole through the sheet.

It was determined that a copper sheet patch could be brazed on to burned through areas if repairs were needed. It was also noted that brazing circular tubing to the sheet required more brazing material vs a flattened tube with a smaller radius fillet. Figures 3.2 and 3.3 show the brazing coupons. In Figure 3.2, the joint is consistent, even, and reflective but is relatively large because the tubing is not flattened, while in Figure 3.3 the bottom quarter of brazed joint has a relatively smaller fillet because of the flattened tubing. The fillet is not visible past the bottom quarter and that section would be considered inadequate since a fillet is not fully visible.

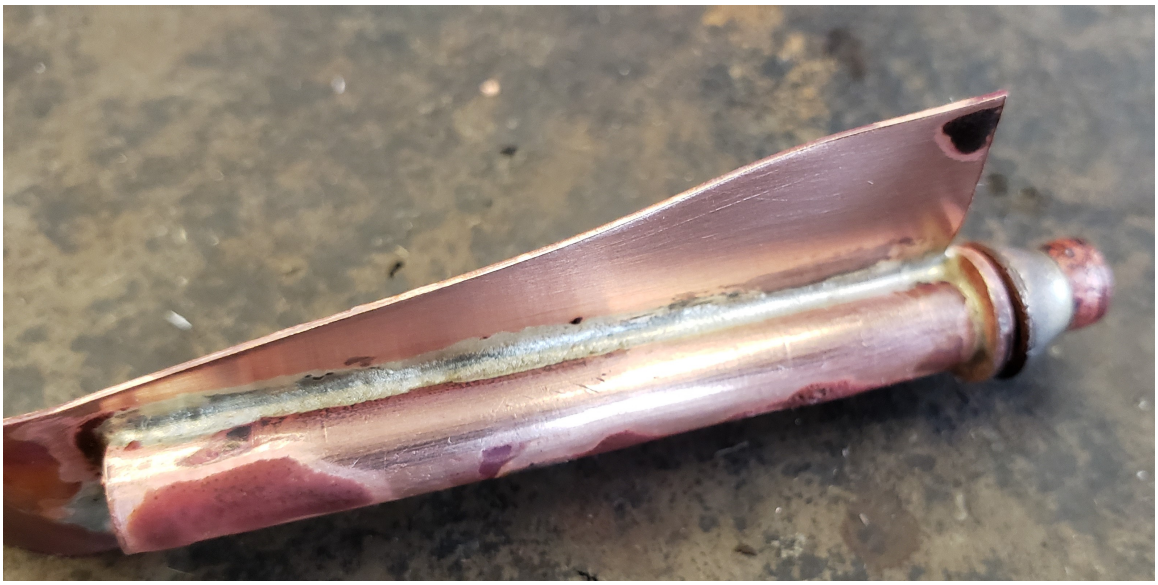

Figure 3.2: 1st brazing coupon with round tubing and thicker copper sheet

Note that in the 2nd brazing coupon, the fillet is not fully formed in some locations due to the technique used. Later during brazing, the technique changed, as discussed later, allowing for the fillet to be maintained along the majority of the interface.

To begin final brazing, the copper sheet was trimmed to the desired circumference such that the diameter is 16.5 inches and overlapped by approximately 1/4" and clamped on its ends, then brazed together from the center outwards. Figure 3.4 shows the sheet during seam brazing. Note that because of the thin nature of the sheet, it does not hold its shape without the supporting copper tubing.

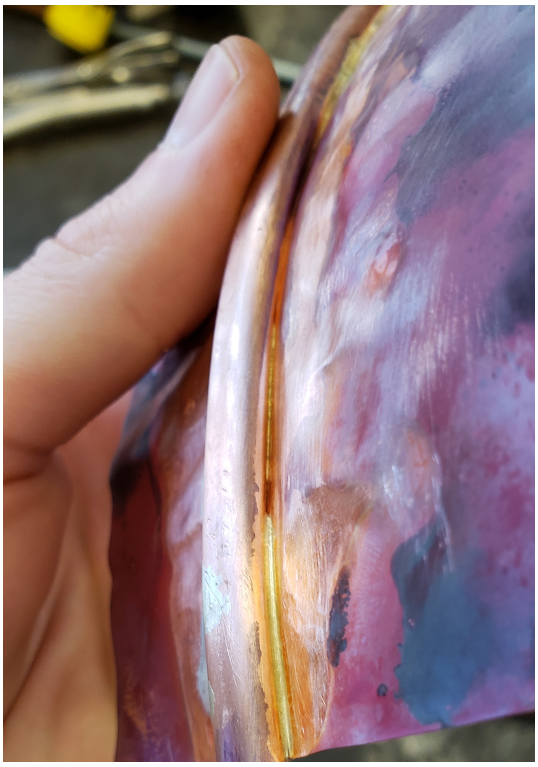

Figure 3.3: 2nd brazing coupon with flattened tubing and 0.005” copper sheet

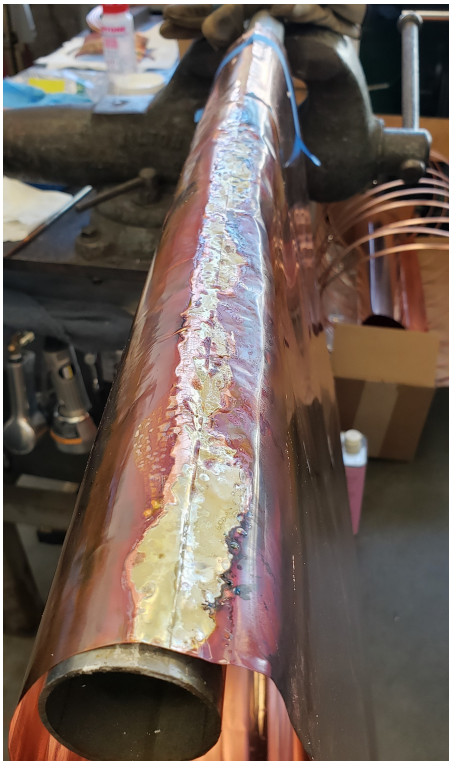

Figure 3.4: Copper sheet during brazing process for cylinder forming

After the sheet was joined, the diameter was checked, and the formed tubing was roughly fit onto the sheet. The tubing provides reinforcement and allows the rough shape of the shroud to be seen. This is illustrated in Figure 3.5.

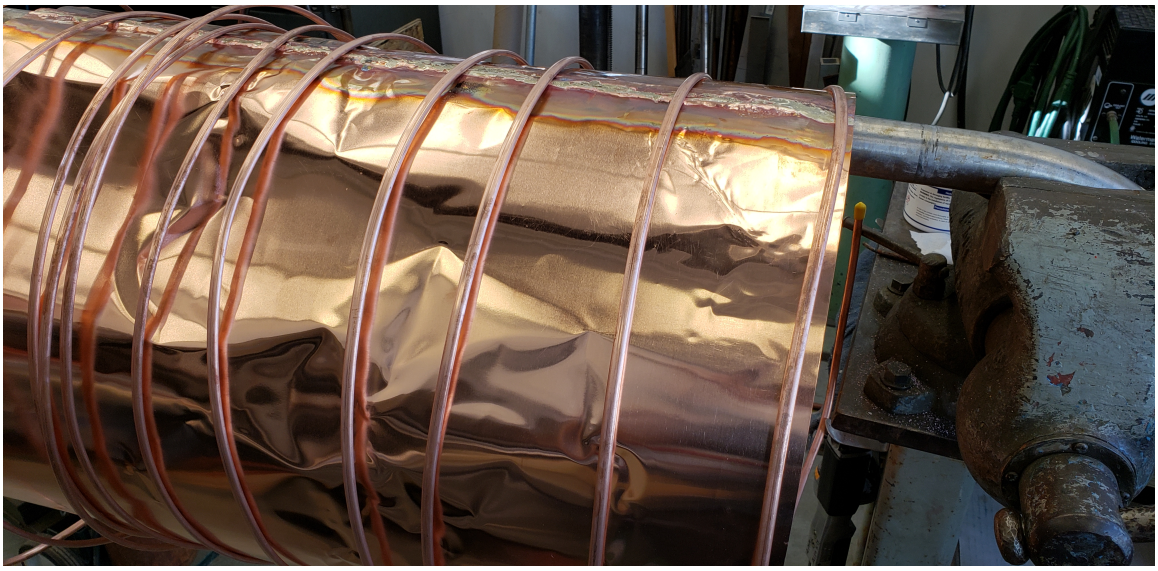

Figure 3.5: Copper coil roughly fit onto brazed sheet

After the initial connection of the copper tubing to the shroud sheet was made, different methods of brazing the sheet and tubing were compared so that the brazing process would use the least amount of brazing material possible and provide a seamless connection between the tube and shroud. The best method in this case involved tack brazing the coil every 1/4 to 1/3 rotation using a spacer gauge to maintain the 2.75" tube spacing. After tacking, the space between tacks was filled by placing 0.005" thick brazing rod sheet between the coil and sheet, and heating the joint until the brazing material liquefied. Then, using a ball peen hammer on the inside sheet and the torch on the outside to keep the joint liquid, the joint was hammered together along the space between tacks. Because the shroud sheet is thin and malleable, it forms around the bottom of the tube and squeezes out excess brazing material, creating a thin joint and allowing for consistent contact along the length of the interface. Figure 3.6 shows the state of the shroud about halfway through the brazing process.

Figure 3.6: Shroud during brazing process

Note that the brazing process causes oxidation of the shroud interior and can be seen by the darkening of the chamber interior. Additionally, the outside of the chamber shows oxidation and flux residue on and near the tubes length that has been brazed. The tubing was purged with constant flow of gaseous nitrogen during brazing to prevent oxide formation inside of the tubing, which would be difficult to remove. After brazing, a thorough cleaning method was needed to remove brazing fluxes and oxides on the exterior faces. These had to be removed because brazing fluxes are known to outgas significantly, oxides are known to absorb water vapor, and the impact of contamination on primer and paint adhesion was unknown [13]. A solution of hot dilute citric acid and water was used to remove brazing flux and oxidation. Citric acid is the safest acid recommended for use by the flux manufacturer for thorough flux removal. The citric acid solution consisted of approximately 1 lb of citric acid and 6 gallons of water. The shroud was placed in the solution and scrubbed

with a stainless steel wire brush. Figures 3.7 and 3.8 show the shroud during cleaning, and after cleaning, respectively.

Figure 3.7: Shroud in plastic tub during cleaning with dilute hot citric acid

Before shroud painting, the modular mounting rails used to support the heaters, platen, and test articles were fit and mounting holes in the shroud were made. The rails are attached to the shroud using six stainless steel 10-32 machine screws and stainless steel washers. Each rail position was measured, then holes were made in the shroud and rails for the bolts. Each bolt was test fit and marked to be trimmed so that it did not protrude into the interior slot of the rail, where it could interfere with anything being mounted to the rails through the slots. Figure 3.9 shows one rail with protruding bolts in the slot. Before the rails were test fit, the anodize coating was removed using oven cleaner, which contains sodium hydroxide. This method was used because it is common practice, utilizes commonly available cleaning products, and is safe to use with proper personal protective equipment [16]. The coating was

Figure 3.8: Shroud after cleaning process with dilute hot citric acid

removed to reduce outgassing of adsorbed water vapor, and the profile was machined to reduce the thermal mass while maintaining functionality.

3.1.4 Shroud Assembly Painting Coupon Testing

After citric acid cleaning, the shroud was ready for paint preparation. The nominal application method utilizes thin coats of primer and paint using an HVLP (high velocity, low pressure) paint sprayer to apply thin coats of primer and paint [19, 18]. Coupon tests were performed to determine the best method to apply the Aeroglaze 9947 wash primer and Aeroglaze Z306 flat black polyurethane coating. During coupon tests of primer application using an HVLP paint sprayer, significant fisheyes or pinholes were visible on the surface, causing uneven application of primer to the surface. This are seen in Figure 3.10. In addition to the fisheyes and pinholes, the primer was applied thicker than specified, since the substrate should be visible through the primer, and should only leave a slight orange tinge to the surface. The opacity of

Figure 3.9: One mounting rail test fit and bolted in place to determine bolt lengths

the coating indicates it is applied thicker than specified, which could lead to poor adhesion of the topcoat.

In order to determine the source of the contamination, the manufacturer was consulted and provided recommendations for cleaning methods and possible contamination sources. Initially, when applying primer, acetone and IPA was used to clean the surface in preparation for painting. The manufacturer recommended performing a water break test after cleaning to approximate how clean the surface is. Using copper sheet coupons, one coupon was cleaned thoroughly using acetone, IPA, then using HET Grease, Wax, and Silicone Remover, then a final clean with IPA, and the other coupon was not cleaned for control comparison. Figure 3.11 shows the water break test before and after cleaning. The surface after cleaning was not fully water break free despite the thorough cleaning.

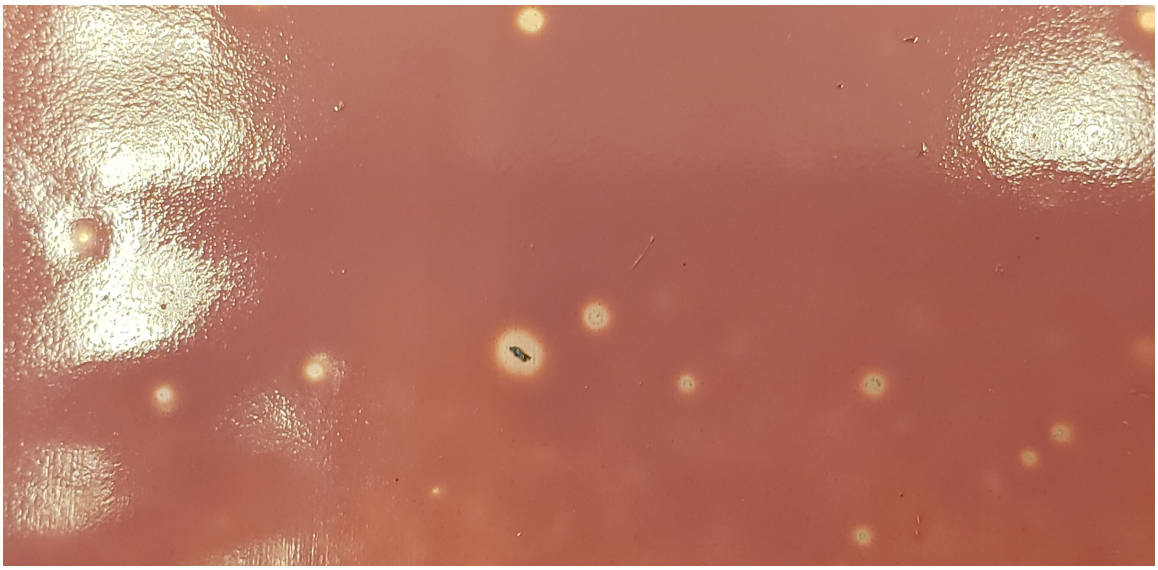

Figure 3.10: First primer coupon primer application with fisheyes and excessive coating thickness

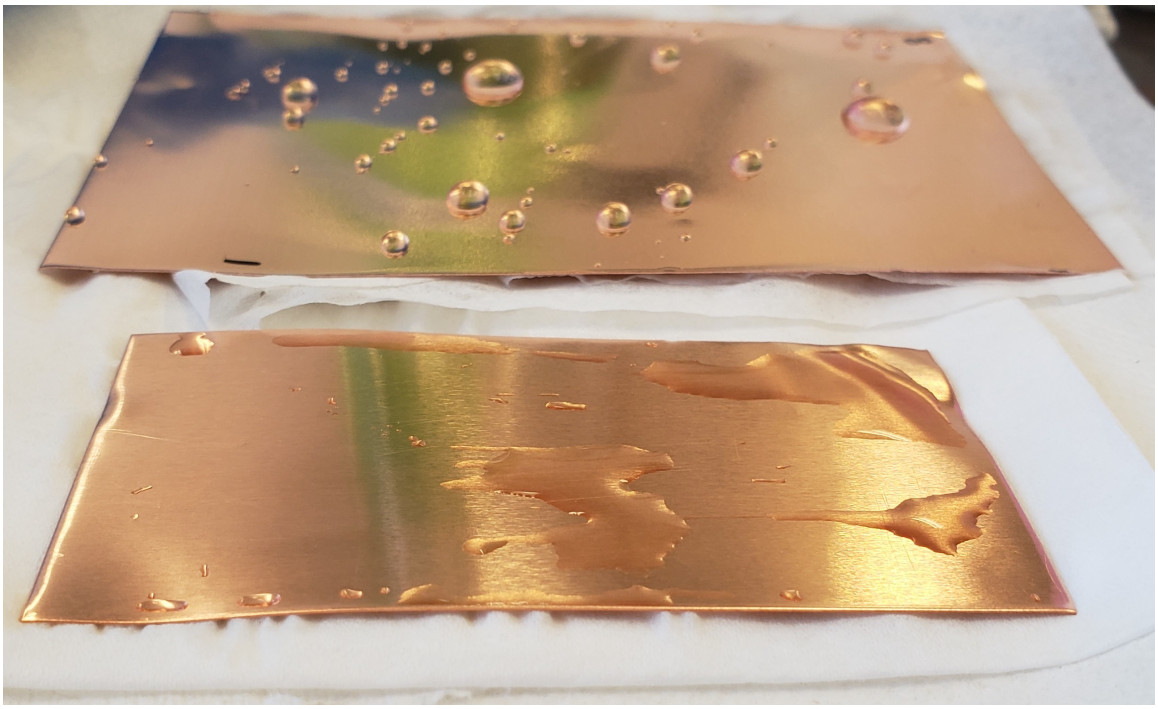

Figure 3.11: Copper sheet coupon water break test before cleaning (upper) and after cleaning (lower)

There are a variety of potential causes of this residual contamination indicated by the water break test, including but not limited to:

- Residual, hard to remove silicone contamination embedded in copper sheet surface from unknown factory contamination source
- Contamination in one of the cleaning solvents, like residual silicone or oil
- Contamination from environment around cleaning area (cleaning and painting took place in a machine shop and outdoors)

Additionally, contamination from residual paint in the paint sprayer itself as well as oil or other contaminants in the air lines were possible sources during spraying. Cleaning issues were not further investigated because after the thorough cleaning method above and wiping off excess primer after spray application, an acceptable surface quality was achieved. For shroud painting an additional final cleaning using Aeroglaze 9958 paint thinner was performed after the 2nd IPA cleaning step. A second primer coupon was prepared using the new cleaning method as well as wiping off excess primer, and the results are shown in Figure 3.12

The 2nd primer coupon was then painted with two brushed coats of Aeroglaze Z306. The resulting finish can be seen in Figure 3.13. After curing, this coupon was subjected to a variety of tests to ensure the coating was well adhered to the copper substrate. First, it was bent in the middle along its long and short axis multiple times to see if the paint would flake off or crack. Then, it was pumped down in the vacuum chamber overnight to see if there was any significant offgassing or if the vacuum would cause the paint to flake off. After both of these tests, no visible damage to the coating was present and no significant outgassing was detected, where outgassing would be indicated by higher than expected pressures and pump down times. Therefore, it

Figure 3.12: Second primer coupon with minimal fisheyes and even, thinner application

was determined that this methodology would be adequate for the full size shroud and heater plates.

3.1.5 Shroud Assembly Painting

After the shroud was brazed and cleaned with citric acid to remove flux and oxides, the shroud exterior was masked off using blue painter's tape and a black trash bag. Because of the known issues with the sprayer causing defects and spraying in a more speckled pattern instead of an even coating, the primer was diluted before spraying using thinner as much as allowed per the technical data sheet (TDS). Primer was then applied using the HVLP sprayer on the inside of the shroud. Finally, a lint free wipe was used to spread and remove excess primer for an even coating with minimal fisheyes or other defects. The primer is intended to be applied such that when it dries it has a dull, matte, see-through appearance [18]. Figure 3.14 shows the shroud interior after the primer dried, with the masking visible on the outside.

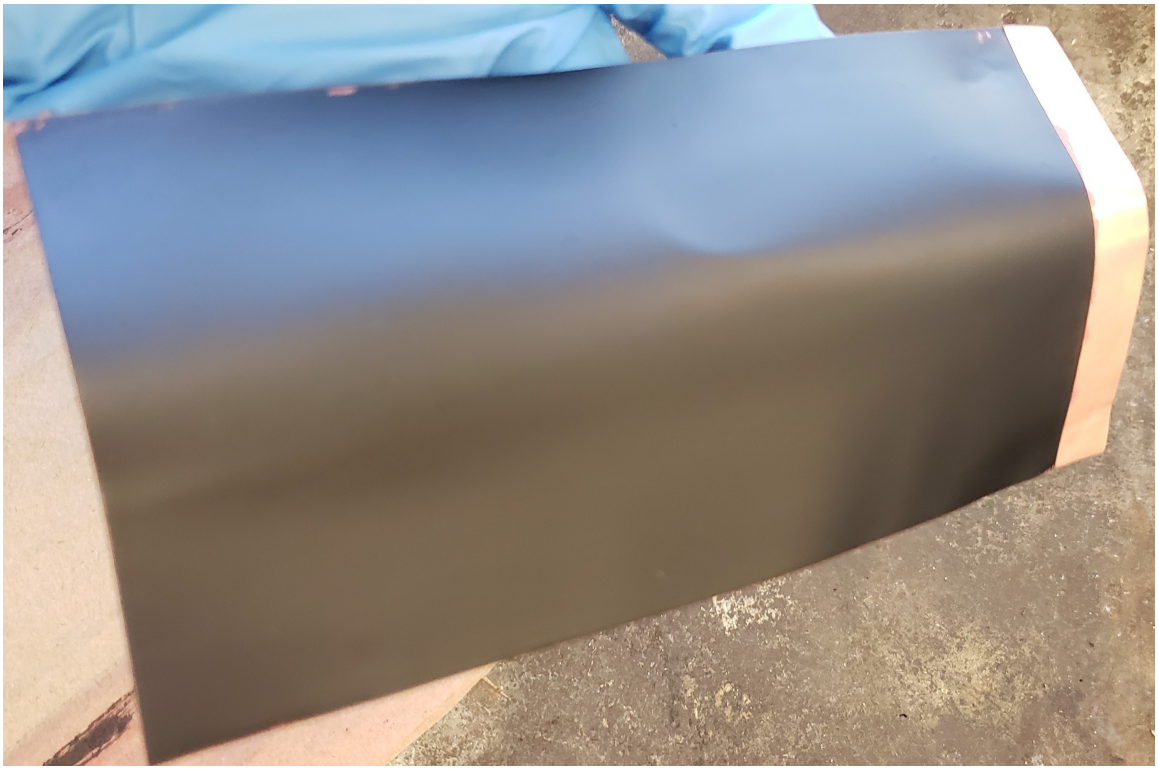

Figure 3.13: Paint test coupon after 2 coats of Aeroglaze Z306 on top of primer

Figure 3.14: Masked shroud after primer application

After the primer fully dried, the topcoat of Aeroglaze Z306 was applied with the HVLP per the TDS with the maximum dilution allowed, again to aid in preventing a more speckled pattern during application. To maintain even and consistent coverage, some areas were touched up with the HVLP sprayer after the initial passes. After drying, but within 24 hours of the initial coating, touching up painting using undiluted Aeroglaze Z306 was performed using a paintbrush to fix minor defects and light spots. The dried shroud interior after painting can be seen in Figure 3.15. Overall the coating was consistent with some dust or other debris visible upon close inspection in some areas. This contamination was not expected to cause any issues with the function of the coating because it appears the coating envelops the debris, so the function of the coating is maintained because the surface is still fully coated.

Figure 3.15: Shroud interior after Aeroglaze Z306 application

3.2 Heater Plate Machining

The existing heater strips were tightly fit into the existing slots in the platen and could not easily be removed without risking damage. Because of this and to save on

material cost, the heater plates were made from the existing platen. This required extensive material removal in order to reduce the thermal mass of the heater plates compared to the original platen. To begin, the platen was cut into three large plates, approximately 8”x14”, using a large vertical bandsaw. After rough cutting, the plates were then cut in half along their thickness and the side without the heaters installed was not used. Figure 3.16 shows one of three heater plates being cut along its thickness using a horizontal bandsaw.

Figure 3.16: Heater plate in the horizontal bandsaw to cut along the thickness

After the thickness was reduced using the bandsaw, the plates were then milled to their final dimensions using a shell mill to face the remaining thickness and provide

a smooth and flat surface for painting. Figure 3.17 shows the sectioned heater plate with the original cooling pipe cuts visible.

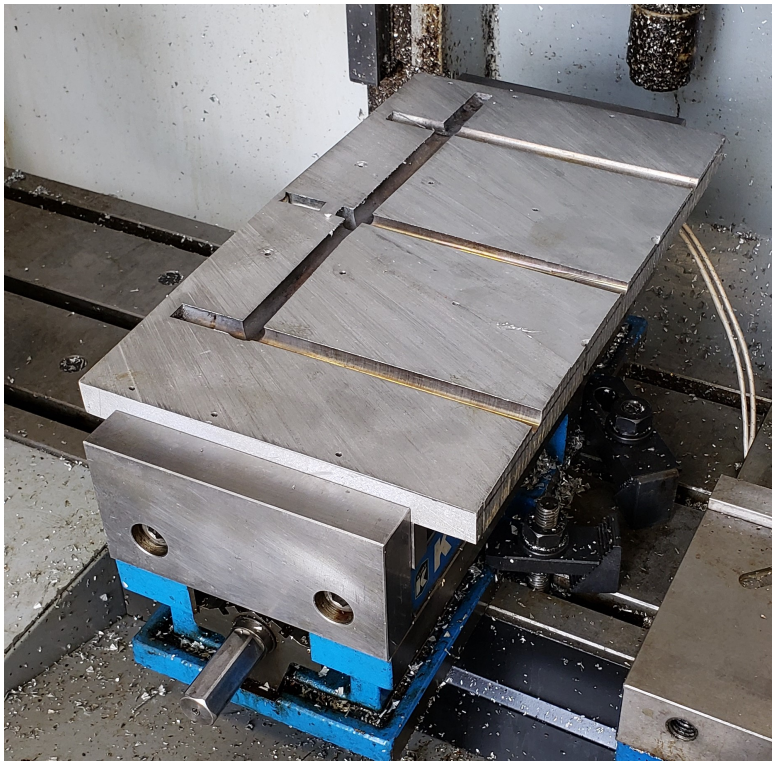

Figure 3.17: Heater plate section before final machining

Due to the long and thin nature of the heater plates, machining required careful fixturing to minimize chattering during machining, which would leave an undesirable surface finish. Additionally, because of the volume of material needing to be removed, many passes were needed to face the plates down on both sides. Figures 3.18 and 3.19 show one of three heater plates after final machining. The dimensions were mesured to ensure they met the required 0.14" throughout.

After the heater plates were machined, additional 10-32 threaded holes were added to the corners of the plates to aid in mounting them in the chamber. Additionally, two strips of aluminum were bolted to the back face of the heater plates to help retain the heater strips in the channel on the back of the heater plates.

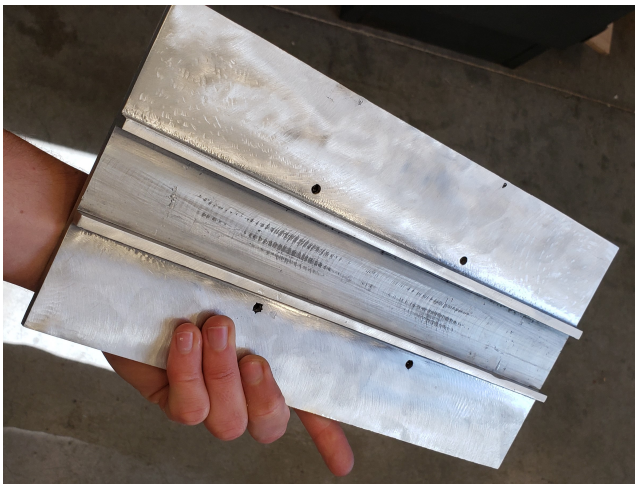

Figure 3.18: Heater plate back face after final machining

Figure 3.19: Heater plate front face after final machining

Finally, the heater plates were cleaned following the same cleaning process as the shroud, except citric acid cleaning was not needed since the heater plates did not have any brazing flux. The channel where the heater strip is installed, visible in Figure 3.18, was masked off using painters tape. Then, primer was applied using lint free wipes instead of the paint sprayer, because of the smaller area needed and to prevent possible contamination issues. After the primer dried, the Aeroglaze Z306 topcoat was applied using a paintbrush and allowed to dry before installing the heater strips. The heater plates can be seen in Figures 3.20 and 3.21.

Figure 3.20: Heater plates after primer application with additional mounting holes visible

3.3 Modular Platen Assembly

The platen is based on 304 stainless steel oven racks found in conventional home cooking applications. This was selected as the platen material because it has a large open area for radiative heat transfer from the upper and lower halves of the chamber, emissivity under 0.10, favorable out-gassing properties, and low cost compared to custom sized solutions. Two 10"x15" racks were brazed together along the 15" edge to form an approximately 20"x15" rack utilizing leftover brazing material from shroud

Figure 3.21: Heater plates integrated into the shroud after painting

brazing. Stainless steel tube sections were then brazed to the four corners of the rack so that it could be easily slid in and out of the chamber along the middle rails. The final assembly was cleaned using a wire brush, Scotchbrite, and IPA wiping to polish surfaces oxidized from brazing and to remove brazing flux residues. Figure 3.22 shows the platen integrated with the shroud. This platen can be easily removed from the chamber and larger test articles could be mounted using the existing mounting rails located at 90° intervals on the shroud.

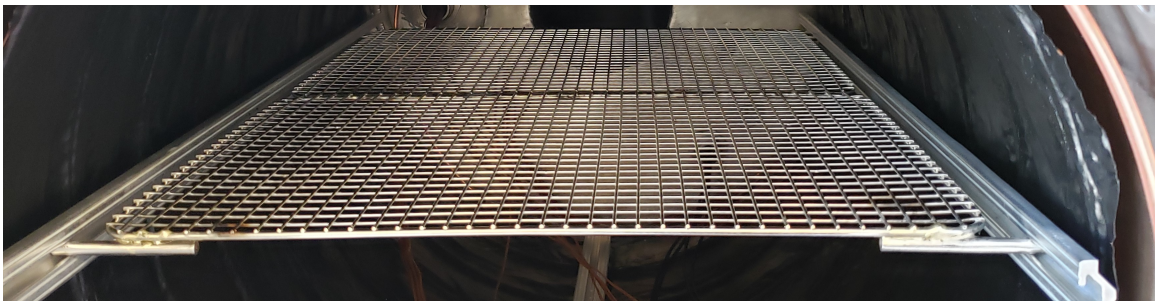

Figure 3.22: Modular platen assembly installed on mounting rails inside shroud

3.4 Outgassing Considerations

Every part going into a vacuum chamber must be capable of withstanding the vacuum environment without degrading and must not outgas significantly. Outgassing can cause test pressures higher than required, and condensation of outgassed materials on sensitive surfaces can cause a variety of issues, such as obscuring sensors, making non-conductive surfaces conductive, and contaminating thermal control surfaces like radiators, which could affect performance. For this project, efforts were made to ensure the new parts and materials going into the manufacturing process were adequately cleaned and consisted of vacuum compatible materials appropriate for achieving a vacuum on the order of $1.0e^{-6}$ Torr, with a desired vacuum level of $7.5e^{-6}$ Torr as required by ISO 19683 [9].

In general, vacuum compatible materials have an affinity to not adsorb volatile substances like water vapor, oils, etc. Additionally, every material has a vapor pressure, which can be thought as the pressure of a substance near a liquid or solid surface of a material in a closed system. In the case of a vacuum chamber where low pressures are desired, materials with higher vapor pressures will constantly evaporate into the chamber, increasing the pressure. This pressure can only be reduced by more pumping, a reduction in temperature, or coating or removing the material entirely.

NASA maintains an outgassing database with information on thousands of different samples [15]. This database contains information on various samples of the coating used for the shroud and heater plates, Aeroglaze Z306, and the data sheet for the coating cites a TML of 1.00% [19].

Fermi National Accelerator Laboratory published a technical memo outlining materials for ultra-high vacuum, which was utilized to help with material selection. Outgassing of materials is highly non-intuitive, as many metals outgas at significant

rates such that they should never be used in a vacuum chamber, like zinc, cadmium, and brass [13]. Even steels should be degassed since they can contain trapped hydrogen that is slowly released into a vacuum system [13]. The Fermi memo is specific to ultra-high vacuum, and some materials that are mentioned as "try to eliminate" like Kapton, Teflon, and zinc [13] alloys are used sparingly in this project by necessity. Additionally, existing wire insulation and plastic connectors are not screened for compatibility since many consist of unknown materials and have already been shown to allow the chamber to pump down to a reasonable level.

3.5 Integration

Integrating the new hardware with the chamber required modifications in order to fit the new shroud in the chamber. The chamber inner diameter is 18", and existing mounting rails and hangars protruded into this space, so to fit the 16.5" inner diameter shroud, these mounting rails and hangars had to be removed. They were tack welded to the chamber interior, and therefore could be removed by grinding the weld until they could be freed from the chamber walls. Before grinding, all ports and orifices were carefully masked off using tape and plastic sheeting so that no debris would enter where it could not be easily cleaned. This is especially important for the turbomolecular pump inlet at the back of the chamber, where cleaning would require extensive tear-down of the pump. After masking, additional material was placed in the bottom of the chamber to catch most of the grinding debris. After grinding, any sharp edges or indents in the chamber walls were ground smooth with sandpaper and Scotchbrite to reduce stress concentrations and prevent injury or damage when sliding the shroud in and out. The chamber was then vacuumed and thoroughly cleaned with IPA to remove grinding residue and other contaminants.

Before test fitting the shroud into the chamber, masking from painting was removed and the mounting rails were installed. Figure 3.23 shows the shroud with the mounting rails installed. After the mounting rails were installed, epoxy fiberglass blocks were mounted to the shroud to support it in the chamber and keep it thermally insulated from the chamber via direct contact. Two blocks were mounted underneath the shroud, and one block was mounted on each side, directly adjacent to the mounting rails and evenly spaced to support the weight of the shroud and test articles inside. Stainless steel lock wire was used to keep the insulating blocks attached to the shroud without significant clamping force such that contact resistance can be maximized to reduce thermal bridging. Each block is approximately 1" x 0.5" x 0.75" and has a hole drilled through it for the lock wire to pass through. Lock wire was also used to keep the inlet copper tube that runs from the front of the chamber to the back of the shroud from contacting the chamber inner walls, which would cause thermal bridging otherwise.

After the chamber and shroud was prepared for the new hardware, multiple test fits were made to ensure that the tubing for the coolant was correctly cut and installed. The tubing terminated with the slot cross section and had to be made circular using a punch and clamping tube rounding tool so that copper 90 degree fittings could be brazed on. After the 90 degree fittings, the tubing is brazed to Swagelok stainless steel caps for 3/8" tubing with a hole drilled in the top of them to allow the coolant to pass through. Figure 3.24 shows the tubing with the slot cross section cut to the correct length before bending and brazing.

Because the shroud is already painted and the brazing of the 90 degree fitting and Swagelok cap is adjacent to the painted surface and connected thermally by copper tubing, steps were taken to ensure the coating was not overheated during brazing. Aeroglaze Z306 has a maximum operating temperature of 250°F, a wetted paper towel stack was placed directly in contact with the shroud near the painted

Figure 3.23: Shroud after mounting rails were installed

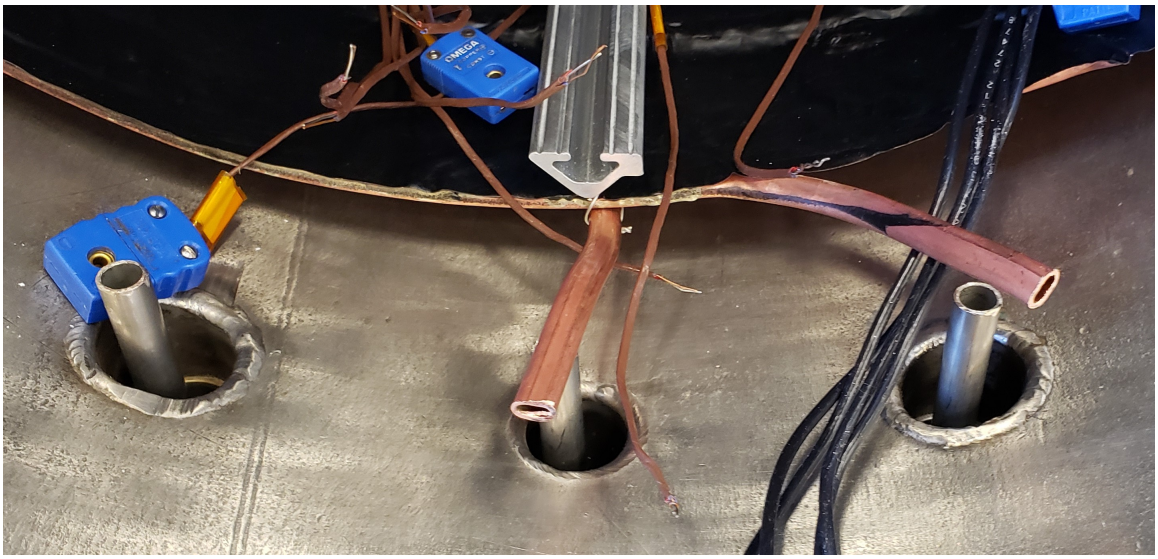

Figure 3.24: Trimmed shroud and chamber tubing after test fit

areas next to the tubing being brazed. This keeps the adjacent copper around 212°F through evaporative cooling. Figure 3.25 shows the brazing setup just before brazing began.

After brazing was complete for the final connections, the flux was removed using a wire brush, water, and IPA wiping. The shroud was given final IPA wiping before sliding into the chamber and tightening the Swagelok connectors. These connectors are designed to be opened and closed repeatedly while maintaining a gas tight seal, so the shroud can be easily removed if needed by loosening the connectors and sliding the entire shroud out of the chamber. Figure 3.26 shows the brazed connections, which must be gas tight to ensure air or nitrogen in the coolant lines does not leak into the chamber during operation.

After brazing was complete, the heater plates were wired into the existing wiring and the platen with heater plates on top were slid into the middle mounting rails. The thermocouple connector plate was mounted to the left middle mounting rail using stainless steel hardware. Figure 3.27 shows the fully integrated system in the chamber with thermocouples connected for initial testing.

Figure 3.25: Shroud connector brazing setup with wet cooling towels

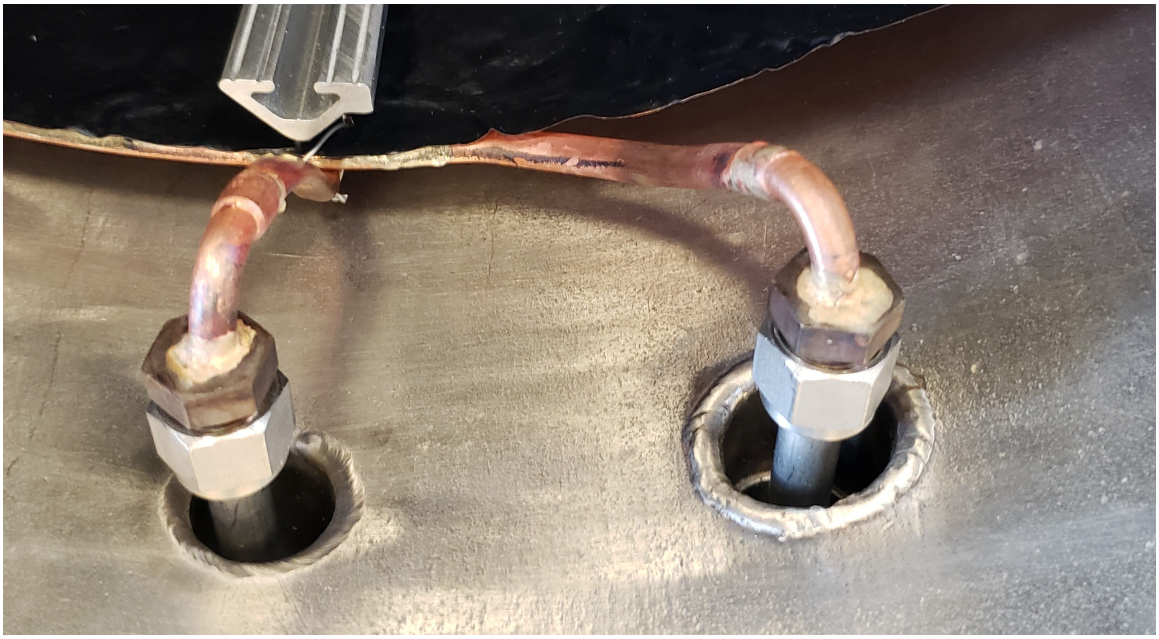

Figure 3.26: Shroud coolant tubing connections after brazing and fastening

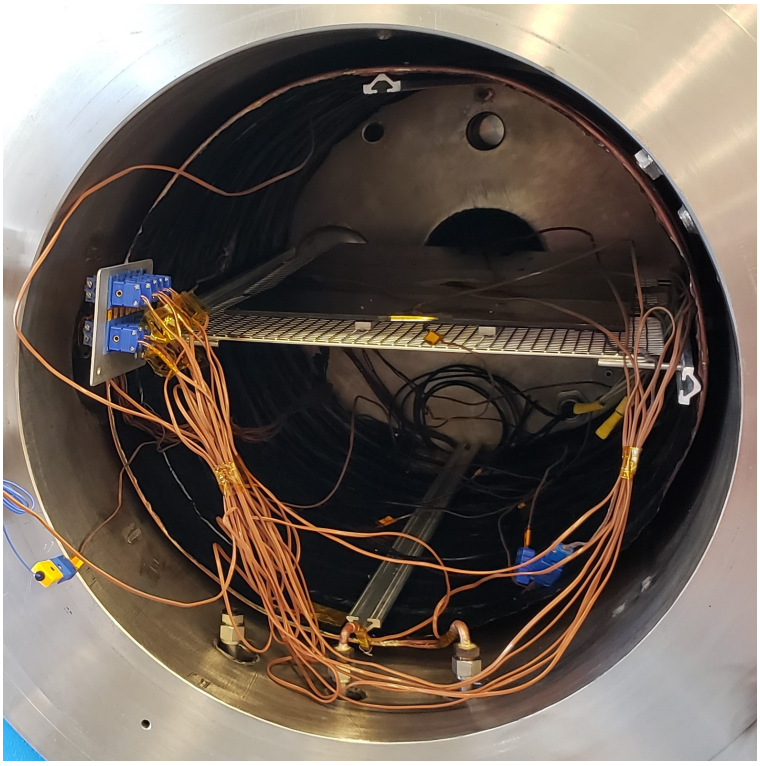

Figure 3.27: Shroud and heater plates integrated into the chamber

3.6 Cost and Schedule

The total budget for the modifications, not including liquid nitrogen refills, the upgraded liquid nitrogen tank and scale, and consumables like acetylene, nitrogen, oxygen, etc. was approximately $700, and was exceeded slightly as more brazing strip and miscellaneous fittings and screws were needed. For a similar project, the total modification cost could easily be under $1000 total for a well equipped shop with an HVLP paint sprayer, mill, bandsaws, ring roller, welding torch, and other hand tools.

The manufacturing portion for the project started with materials purchasing in early January 2021, and was completed by early May 2021. During this time, approximately 160 person-hours was spent on manufacturing, with the most time consuming parts being the shroud tubing brazing. This is likely to vary significantly depending

on the prior knowledge of the manufacturer as well as their experience with specific relevant tasks like HVLP spray painting, brazing, and machining.

Chapter 4

TESTING AND ANALYSIS METHODOLOGY

This chapter outlines the methodology for the thermal testing and analysis for this thesis. This includes chamber bakeout, controller configuration, data collection, thermocouple placement, and test configuration for each test as well as pre-test configuration changes to tune the control system. For the analysis methodology, the thermal model is discussed including validation requirements, model components, material and surface properties, and assumptions made along with their associated rationale. A mesh refinement study is presented to demonstrate the mesh size does not significantly affect the numerical simulation results.

Figure 4.1 shows the general outline of the methodology for this thesis. This chapter defines the configuration for the detailed thermal model and thermal vacuum tests as well as the validation process. Chapter 5 presents the results of these tests and numerical model correlations.

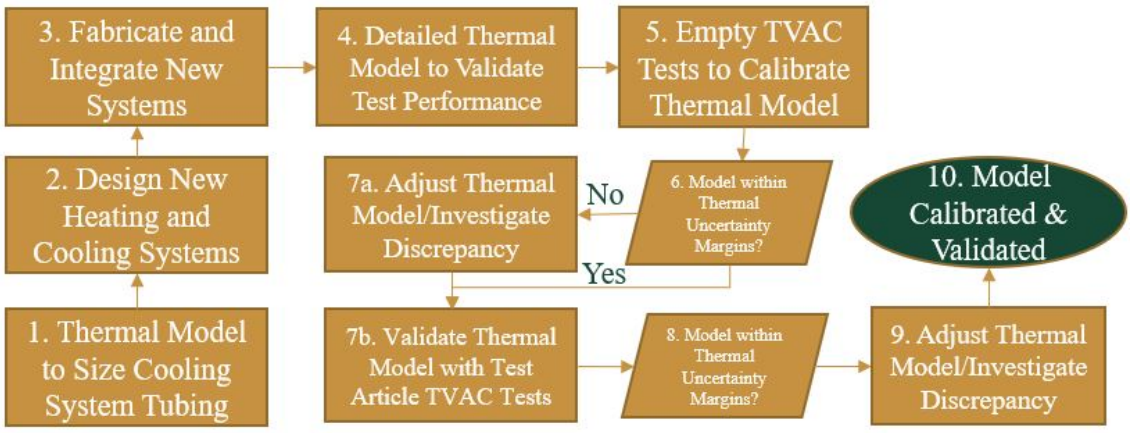

Figure 4.1: Methodology overview flowchart

4.1 Thermal Vacuum Chamber Testing Configuration

4.1.1 Chamber Bakeout

As discussed in the previous section on outgassing considerations, outgassing rates increase with temperature. This can be used to ones advantage using a chamber bakeout. A bakeout will reduce outgassing rates before initial testing and is useful because the Aeroglaze Z306 coating used requires cure time on the order of days to weeks depending on temperature, humidity, and airflow to reach the 1.0% TML specified on the data sheet [19]. Bakeouts were performed for this thesis primarily to accelerate the drying of the Aeroglaze Z306 coating used on the shroud and heater plates. The total bakeout time above 80°C was on the order of days but was not specifically recorded. Chamber specific bakeout procedures can be found in appendix A of this thesis.

4.1.2 Controller Configuration

The heating and cooling system is regulated by four Watlow brand controllers, each with their own specific functions and capabilities. The controller configuration focused on the Watlow F4DH-KKFK-01 dual channel ramping controller, which was used to control shroud and platen temperatures. Other controllers were not modified except to modify the chamber high and low limit alarm temperatures. When the previous shroud and platen were in use, the temperature was controlled only for the platen, and the shroud temperatures were correlated with the platen because they shared nitrogen plumbing lines [3, 11].

Initially, the controller was used as a single channel with the control thermocouple placed on the center heater plate directly on the heater element. This did not have the desired effect for chamber control and was modified to allow for independent

control. In the initial empty testing section 4.1.6, this is discussed in more detail. For this thesis and all test results presented the shroud and heater plates were configured to be independently controlled, with the heaters controlled on CH1 and the shroud controlled on CH2 of the main Watlow F4 controller.

4.1.3 PID Tuning

The Watlow F4DH-KKFK-01 dual channel ramping controller used to control heater plate and shroud temperatures is capable of automatically tuning the PID settings such that the system responds appropriately to a given input temperature and ramp rate or ramp time. It performs this tuning by ramping to a percentage of the set point (95% for this testing, based off how it was set previously), and uses on-off control to move the temperature above and below the tuning set point [21]. After crossing the set point four times, the controller uses the thermal response of the system to update the PID values automatically [21]. Figure 4.2 shows the auto-tune profile.

Auto-tuning was used for the heater plates (on CH1) and shroud (on CH2) before empty test 1. It is not required to re-tune the system between tests unless there is a significant change in the configuration that would affect the response of the heaters or shroud during heat-up or cool down. If the system is not responding appropriately, i.e, it is oscillating around a set point instead of maintaining the value within +/-1°C on the controller input thermocouple, re-calibration can be performed using the auto-tuning feature or manual tuning. It is recommended to set the auto tune set point below the maximum/minimum tolerable temperature, since the tuning process tends to overshoot the set point. It may overshoot if the previous PID values were tuned for a less responsive system, like the previous platen with larger thermal mass and greater separation between the strip heaters and the control thermocouple. Additionally, if the controller behavior is different in different temperature ranges,

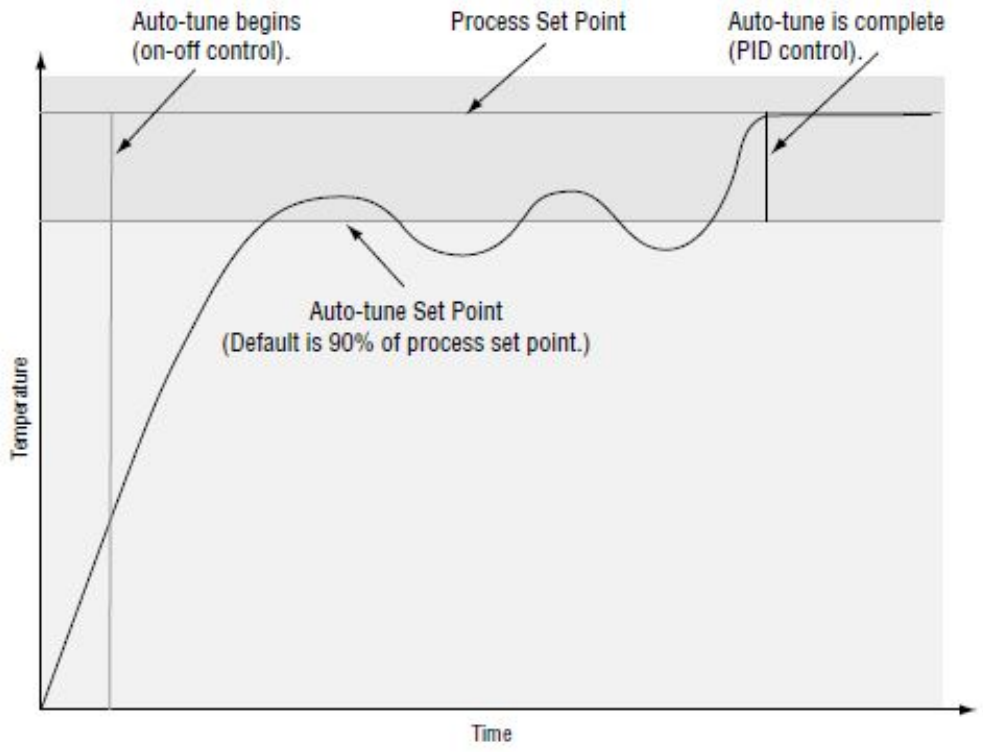

Figure 4.2: Auto-tuning process of the Watlow F4DH controller [21]

i.e, does not undershoot at 50°C but does at 90°C, then a separate set of PIDs can be stored for auto-tuning in different temperature ranges. The controller stores 12 PID sets for both channels, and any PID set can be selected to be used during any specified ramp or hold [21]. For this thesis testing, one set of PIDs was used for each channel, PID set 1 for CH1 and PID set 6 for CH2, which is the default or first option for each channel when setting a profile.

4.1.4 Data Collection

The data collection setup is shown in the annotated Figure 4.3. A tablet computer with webcam and time lapse software was used to monitor the status of the chamber and testing remotely as well as record parameters like liquid nitrogen scale weight, chamber pressure, and the control thermocouple temperatures as well as alarm status in the case the chamber exceeded the high or low limit alarms.

Figure 4.3: Labeled data collection experimental setup

4.1.5 Thermocouple Placement

Thermocouples were applied using procedure specified in Appendix B of Jensma's thesis [11]. Photos of installed thermocouples can be found in the photos of each test setup in the sections below along with a labeled diagram of their placement. T-type thermocouples were used for all data recording and control thermocouples, and have an error of +/- 1°C. Error bars are not included in any plots to improve readability.

4.1.6 Initial Testing

Before empty test 1 started, an initial empty test was performed to learn how the updated PID values affect the shroud response with the control thermocouples for the heater and the shroud both on the heating element of the center heater plate. In the initial testing, the heating and cooling system was controlled by a thermocouple located on the heater element outer surface of the middle heater plate. This location means that the temperature of the heater element is precisely controlled, but it does not correlate to the heater plate outer surface temperatures exactly, and during cooling cycles, the shroud will overshoot to much lower temperature in order to cool the heater element quickly. Because of these control issues, initial test data is not useful for analysis and is not presented.

4.1.6.1 Control Thermocouple Placement

Moving the control thermocouple for the heater plate to the top surface of the heater plate, which is the side exposed to the test article and shroud, allows for the surface to be maintained at a specific temperature by the heater on the other side of the heater plate. The second channel of the Watlow F4 controller is then used on the shroud, between thermocouple 8 and 10 in the empty test thermocouple placement

diagram. The PIDs were tuned as discussed in the previous section on PID tuning. The locations of the control thermocouples and the PID parameters were not changed between any tests after the initial modification discussed.

4.1.6.2 Coolant Leak Repair

During the initial testing, a leak in the nitrogen inlet line as the line enters the chamber enclosure was observed. The leak was due to thread tape being applied on a flared connector fitting, which should not have thread sealant tape since the flared mating surfaces is intended to provide the leak tight seal instead of the threads. After repairing the leak by removing the tape and re-fastening the joint, no significant leakage was visible.

4.1.6.3 Door Shroud Operation

The door shroud was operated during the initial testing and it was determined that the door shroud consumes significantly more nitrogen than the shroud and provides a marginal benefit during cold soaks. Additionally, because the door shroud is controlled separately, it cannot be easily turned on and off during the main controller cold and hot soaks. Similar conclusions were made by Jensma during their experiments, and they demonstrated the shroud had little effect on test article temperatures [11]. This makes sense because of the limited view factor for test articles with less surface area normal to the shroud cylinder axis. Despite this, the door shroud functions in that it is able to cool when nitrogen is flowed through it, and can be used if required, but was not used for any tests beyond initial testing discussed.

4.1.7 Empty Test 1

The purpose of the empty TVAC test is to ensure the chamber is functioning as expected with regard to following a specified thermal profile and to explore the capabilities of the modified system, as well as diagnose and adjust the system and thermal model based on the results. The test includes the cooling shroud, three modular heater plates, and the platen, as well as 12 logging thermocouples to record the temperatures across the systems.

4.1.7.1 Thermocouple Placement

Figure 4.4 shows the locations of the thermocouples for both empty test 1 and empty test 2. Note that shroud thermocouples have a blue outline and heater plate thermocouples have a red outline. All shroud thermocouples are located on the inside black faces of the shroud, and labels 6, 8, 9 and 11 are projected locations due to restrictions of the view.

The thermocouples were arranged such that the temperature distribution across the platen, heaters, and shroud is observable in key locations. The shroud thermocouples focus on the middle and front of the shroud since those locations had the greatest predicted temperature variation based on initial sizing models in Chapter 2. In addition, areas towards the front and back edges of the shroud and the heater plate middle and edges were monitored to evaluate the maximum and minimum locations to get an accurate picture of the temperature distribution across the shroud and heater plate surfaces.

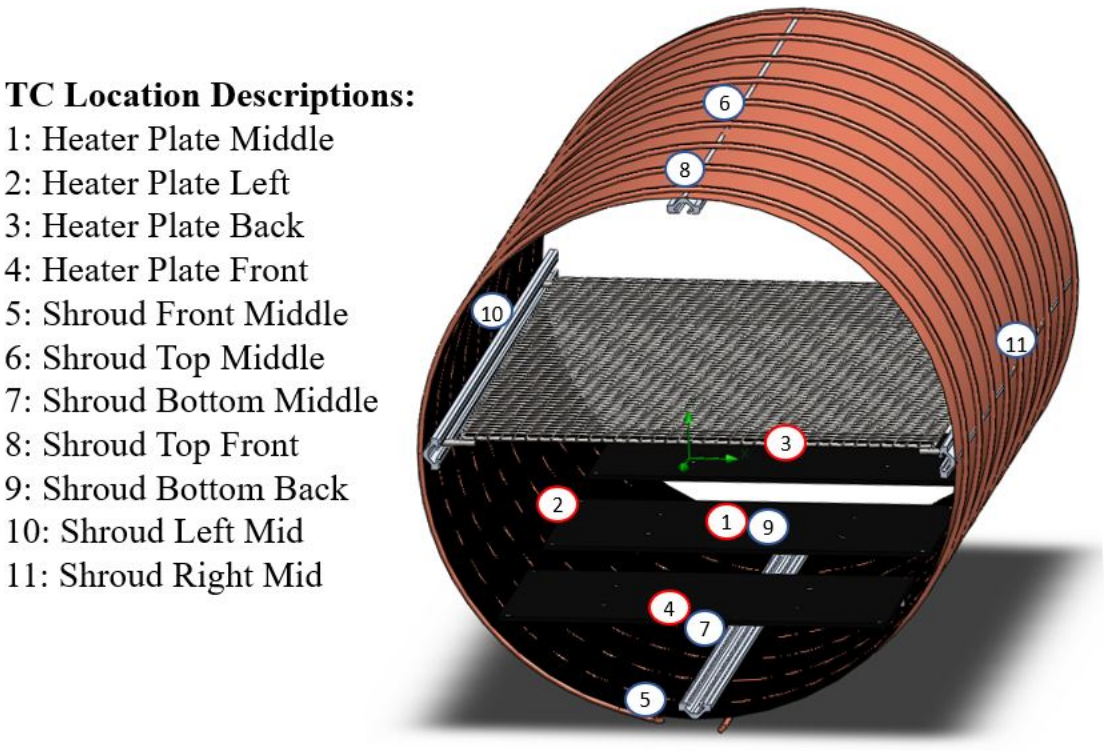

Figure 4.4: Empty test 1 & 2 thermocouple placement diagram

4.1.7.2 Experimental Configuration

Figure 4.5 shows the experimental setup for empty tests 1 and 2. It should be noted that for these tests and test article tests, aluminum foil reflectors were installed in the back of the chamber, over the door shroud, and over the front face of the shroud as shown in Figure 4.5 and Figure 4.6. As mentioned in Chapter 2, these allow for more even temperature distributions in the chamber and preserve cooling and heating power by reflecting the energy back into the shroud, heater plates, and test article.

4.1.7.3 Thermal Vacuum Test Profile

The thermal vacuum test profile for empty test 1 is intended to allow for two different temperature ranges to be tested with one cycle per set of hot and low temperatures. Soak times of two hours were set to allow the chamber to reach steady state. The

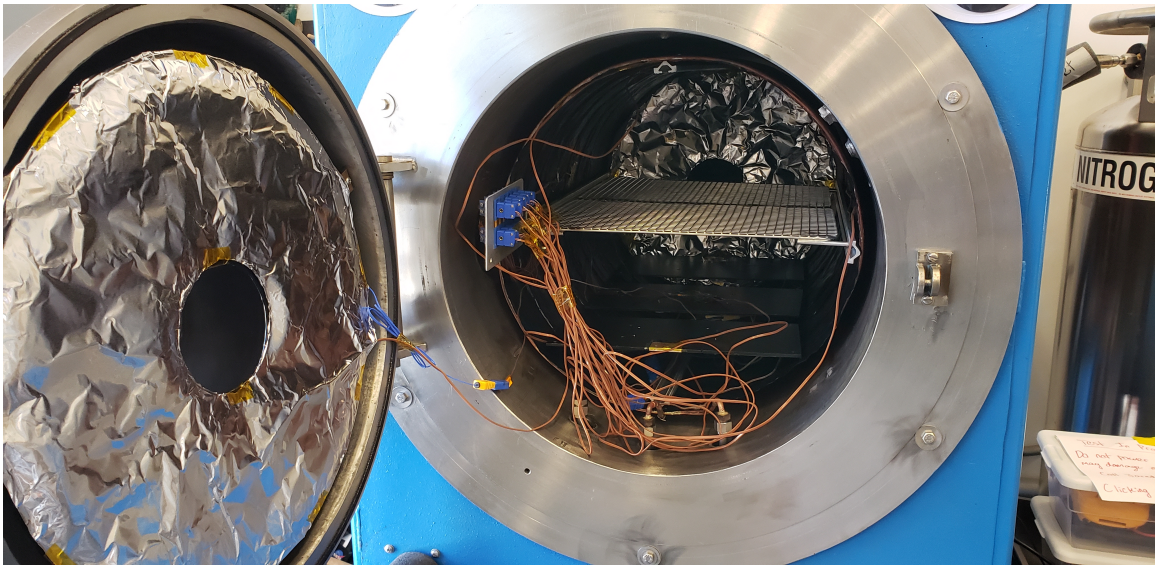

Figure 4.5: Empty test 1 & 2 configuration experimental setup

Figure 4.6: Empty test 1 & 2 configuration experimental setup with front foil reflector

profile in detail is shown in Table 4.1, including ramp rates and elapsed time. It should be noted that there is no soak after the first 55°C ramp due to user programming error when setting the profile. Because the test demonstrated control meeting the profile programmed and cycles between high and low temperature ranges with predicable response, the test results were used and the test was not repeated despite the programming error.

Table 4.1: Empty test 1 thermal vacuum test profile

Step Type	Temp [°C]	Step Time [min]	Ramp Rate [°C/min]	Elapsed Time [min]	Elapsed Time [hr]
Start	20	0	0	0	0.00
Ramp	-20	40	1.00	40	0.67
Soak	-20	240	0.00	280	4.67
Ramp	55	150	-0.50	430	7.17
Ramp	-40	190	0.50	620	10.33
Soak	-40	240	0.00	860	14.33
Ramp	80	240	-0.50	1100	18.33

4.1.8 Empty Test 2

Empty test 2 shared the same thermocouple placement and experimental configuration as empty test 1 except the thermal vacuum test profile, shown in Table 4.2, was modified to include more cycles using a low and high temperature range exceeding the requirement of ISO 19683 for thermal vacuum testing, , which were discussed previously in Chapter 1 Section 5, by 5°C. Soak times were reduced to 2 hours because empty test 1 demonstrated steady state for the chamber was achieved in less than 2 hours.

4.1.9 CubeSat Mass Model Test

The purpose of the CubeSat mass model test was intended to test the response of a large test article in the chamber over multiple thermal cycles.

Table 4.2: Empty test 2 thermal vacuum test profile

Step Type	Temp [°C]	Step Time [min]	Ramp Rate [°C/min]	Elapsed Time [min]	Elapsed Time [hr]
Start	20	0	0.00	0	0.00
Ramp	-20	40	1.00	40	0.67
Soak	-20	120	0.00	160	2.67
Ramp	55	75	-1.00	235	3.92
Soak	55	120	0.00	355	5.92
Ramp	-20	75	1.00	430	7.17
Soak	-20	120	0.00	550	9.17
Ramp	55	75	-1.00	625	10.42
Soak	55	120	0.00	745	12.42
Ramp	-20	75	1.00	820	13.67
Soak	-20	120	0.00	940	15.67
Ramp	55	75	-1.00	1015	16.92

4.1.9.1 Thermocouple Placement

Existing locations for shroud and heater plates were used for locations 1, 4, 6 and 8. The remaining thermocouples were used to measure the temperatures of the test article. Figure 4.7 shows the thermocouple locations across the test article surface, with a focus on the front of the test article since that is adjacent to the front of the chamber, which had more temperature variations than the back of the chamber in general.

4.1.9.2 Experimental Configuration

The test article used is a 3U CubeSat mass model. It is made of 6061 Aluminum with stainless steel fasteners. The surface is anodized and each 1U segment is colored differently. The test article is shown in Figure 4.8.

The test article was placed in the center of the platen, isolated by Teflon spacers as shown in Figure 4.9.

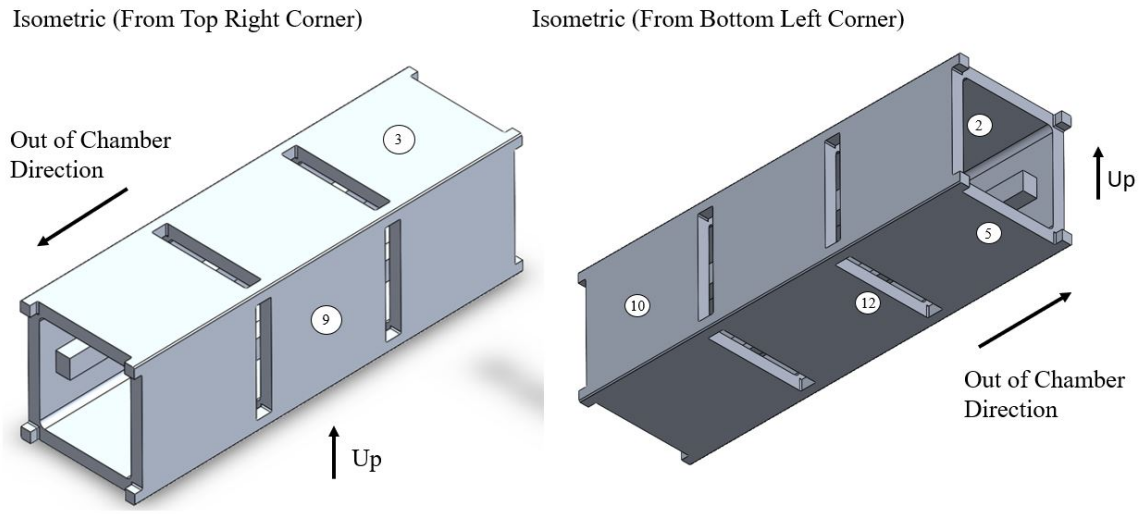

Figure 4.7: CubeSat mass model thermocouple placement diagram

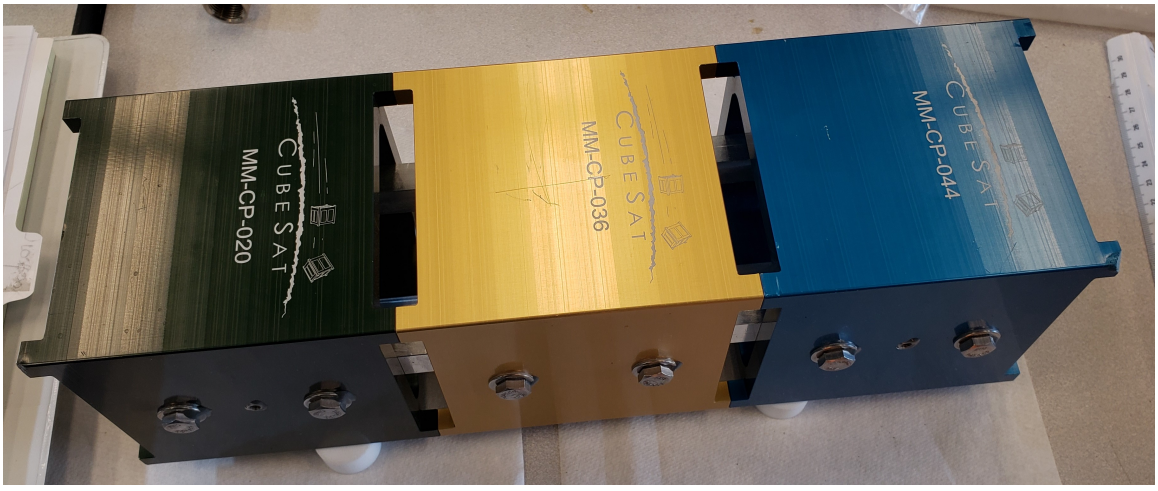

Figure 4.8: CubeSat mass model test article

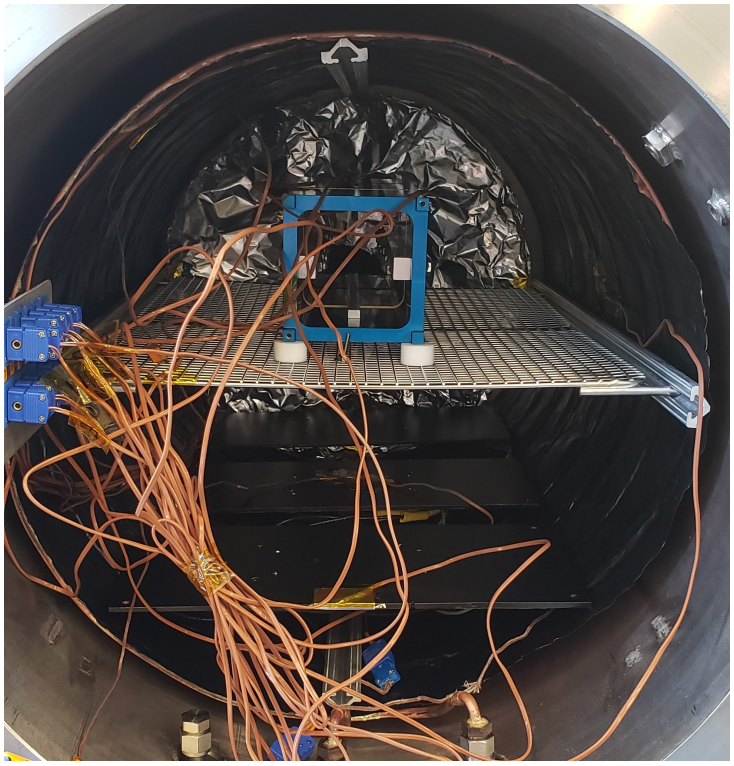

Figure 4.9: CubeSat mass model test article setup in the chamber

4.1.9.3 Thermal Vacuum Test Profile

Similar to empty test 2, multiple cycles using a low and high temperature range exceeding the requirement of ISO 19683 for thermal vacuum testing by 5°C were used. In addition, a hot soak at the beginning allowed for steady state temperatures for thermal model comparison, and the first cold cycle with a -45°C soak was used to test the response at lower temperatures. Table 4.3 shows the profile in detail. Note the ramp rate was increased from +/- 1°C per minute from the empty tests to +/- 2°C per minute to reduce ramp times and overall test time, with the ISO 19683 requirement of +/- 5°C per minute or less. Three hour soaks were used to allow for more time for the CubeSat mass model to reach steady state, however steady state was not achieved except for the initial 80°C soak.

Table 4.3: CubeSat mass model thermal vacuum test profile

Step Type	Temp [°C]	Step Time [min]	Ramp Rate [°C/min]	Elapsed Time [min]	Elapsed Time [hr]
Start	80	0	0.00	0	0.00
Soak	80	180	0.00	180	3.00
Ramp	-45	62.5	2.00	242.5	4.04
Soak	-45	180	0.00	422.5	7.04
Ramp	50	47.5	-2.00	470	7.83
Soak	50	180	0.00	650	10.83
Ramp	-15	32.5	2.00	682.5	11.38
Soak	-15	180	0.00	862.5	14.38
Ramp	50	32.5	-2.00	895	14.92
Soak	50	180	0.00	1075	17.92
Ramp	-15	32.5	2.00	1107.5	18.46
Soak	-15	180	0.00	1287.5	21.46
Ramp	50	32.5	-2.00	1320	22.00
Soak	50	180	0.00	1500	25.00
Ramp	-15	32.5	2.00	1532.5	25.54
Soak	-15	180	0.00	1712.5	28.54

4.1.9.4 Aluminum Plates Test

The purpose of the plates test was to further test the response of the chamber at greater temperature extremes than the CubeSat test to determine the response of a coated and bare aluminum test article. The test articles used are 145 mm x 102 mm x 6.5 mm 6061 aluminum plates and are shown in Figure 4.10. One plate was abraded with Scotchbrite to give it a consistent brushed appearance, and the other plate was primed and painted with Aeroglaze Z306 following similar procedures to those discussed for heater plate manufacturing in Chapter 3.

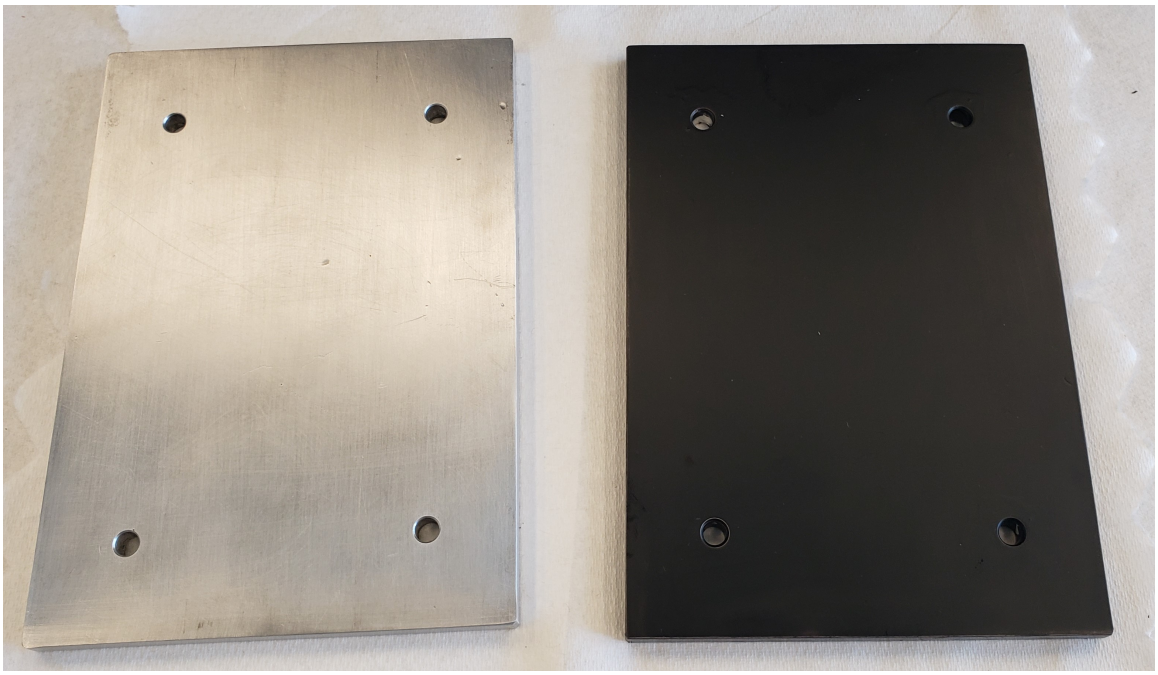

Figure 4.10: Plates used for testing, one bare aluminum, one painted black

4.1.9.5 Thermocouple Placement

Existing locations for shroud and heater plates were used for locations 1, 4, 6 and 8. The remaining thermocouples were used to measure the temperature of the test articles. Figure 4.11 shows the thermocouple locations across the test article surface. The placement of thermocouples for this test is intended to measure in the middle and edges since the distribution is not expected to be significantly different on any one side or face. Measuring in the middle allows for more of an average temperature, and temperatures at the edges typically represent more extremes, based on similar results with test articles in Chapter 2.

4.1.9.6 Experimental Configuration

The setup with the plates in the chamber is shown in Figure 4.12. Note that the plates are placed in the back of the chamber since this part of the chamber has more consistent temperatures for the surrounding shroud during cold soaks.

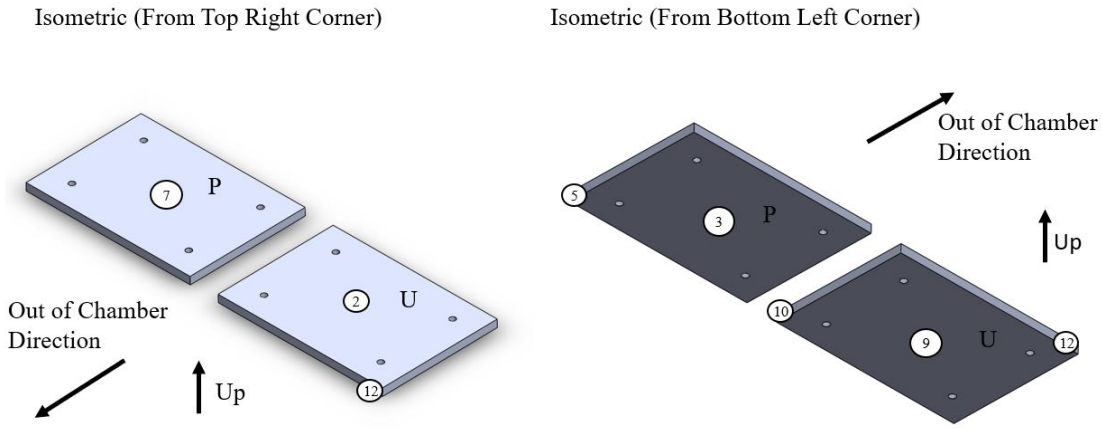

Figure 4.11: Plates thermocouple placement diagram

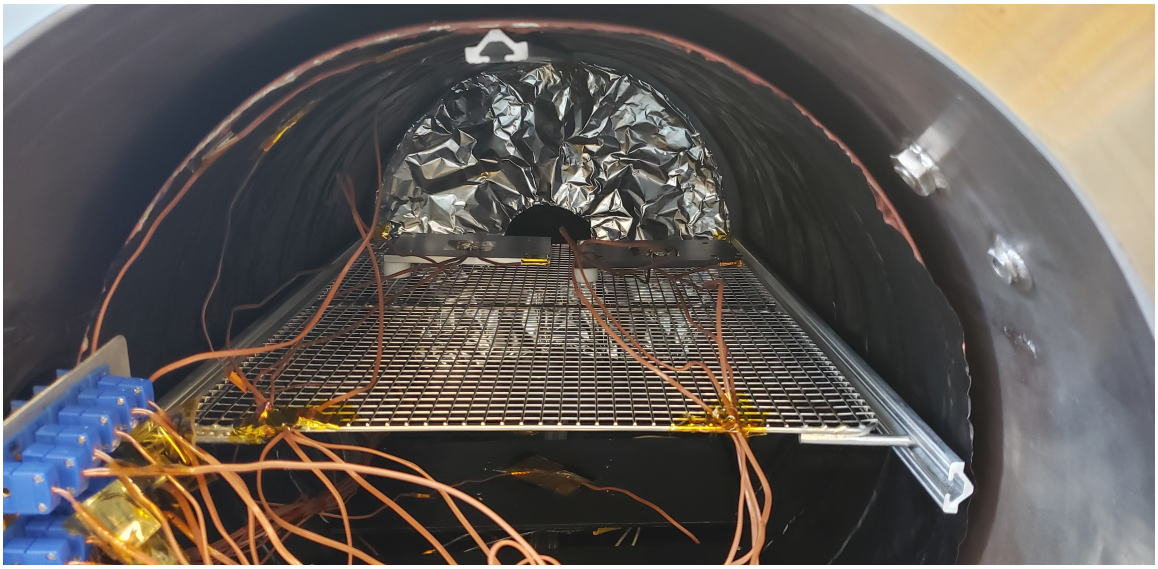

Figure 4.12: Plate test articles setup in the chamber

4.1.9.7 Thermal Vacuum Test Profile

The profile includes increasingly colder minimum soak temperatures to test the limits of the cooling system, with the maximum soak temperatures that the chamber is capable of at 95°C. This represents a final cycle temperature difference of 175°C over a period of 87.5 minutes, thermally stressing the test article and chamber to the maximum.

Table 4.4: Plates thermal vacuum test profile

Step Type	Temp [°C]	Step Time [min]	Ramp Rate [°C/min]	Elapsed Time [min]	Elapsed Time [hr]
Start	25	0	0.00	0	0.00
Ramp	-60	42.5	2.00	42.5	0.71
Soak	-60	120	0.00	162.5	2.71
Ramp	95	77.5	-2.00	240	4.00
Soak	95	120	0.00	360	6.00
Ramp	-70	82.5	2.00	442.5	7.38
Soak	-70	120	0.00	562.5	9.38
Ramp	95	82.5	-2.00	645	10.75
Soak	95	120	0.00	765	12.75
Ramp	-80	87.5	2.00	852.5	14.21
Soak	-80	120	0.00	972.5	16.21
Ramp	95	87.5	-2.00	1060	17.67
Soak	95	120	0.00	1180	19.67

4.2 Minimum Temperature Testing

After the plates test was completed, the controller was set to -145°C to determine the lowest temperatures the chamber was capable of achieving. The same setup and configuration as the plates test was used. The intent of this test was to use residual nitrogen after testing and allow the chamber to soak at the lowest temperature possible. The shroud temperature is limited by the coating lower temperature operating

limit, which is -150°C. There is no profile or additional setup diagrams since the temperature was held constant with an uncontrolled ramp at -145°C, and temperatures were manually recorded.

4.3 Thermal Model Setup

4.3.1 Assumptions and Simplifications

The solid model for this analysis was built up during the modification design and manufacturing process, which means that the dimensions and materials are generally well known. However, simplifications and assumptions are still made in the geometry and boundary conditions where necessary. A list of simplifications and their associated rationale for the thermal model is as follows:

- The chamber exterior is modeled as a cylinder with flat caps on either end with constant thickness throughout and does not include ports or pass-throughs. Modeling these accurately would require knowledge of the materials and interfaces of the caps, connectors, o-rings, etc. and is not likely to have a impact on the overall results because the pass throughs are similar in geometry to the overall cylinder and represent a fraction of the total area of the pressure vessel.

- The shroud supports between the shroud exterior face and chamber interior face are not included in the thermal model due to their small size and low thermal conductivity. The total contact area is less than 4 in^2 and the material is an unknown fiberglass reinforced polymer. Similar materials have thermal conductivity hundreds of times lower than copper, therefore minimizing thermal bridging.

- The shroud tubing is isolated from the chamber and terminates at the front of the shroud in the model, where in reality it passes through the chamber

walls to the outside. There is likely thermal bridging where the tubing contacts the chamber to seal the chamber, but the exact geometry is unknown and not easily accessible, and the tubing is stainless steel after the front of the shroud, which greatly limits conduction compared to copper. This should have a minimal impact on the results because the tubing is thermally isolated as much as possible with foam insulation outside the chamber and seals and low conductivity materials inside the chamber.

- The shroud wrinkles are not modeled, and the shroud is assumed to be a cylinder. This is because modeling the wrinkles accurately would be highly complex and will not significantly affect the overall results.

- The Aeroglaze coating thickness and material properties are not included in the model - the surfaces are assigned an emissivity based on the coating emissivity. This is because the thermal conductivity and thickness of the paint coating is unknown, but the thickness is on the order of 0.001", such that the impact on surface temperatures is expected to be negligible.

- Wires, brackets, and connectors for thermocouples and heater power are not included in the model. These can act as thermal bridges and can block radiative heat transfer, but are expected to have minimal impact on the overall model because most wires and connectors are in spaces where they do not significantly block radiative heat transfer between the shroud or heater plates and test articles.

- All contact resistances are assumed to be bonded, i.e, zero thermal contact resistance. This is because it is difficult to correctly characterize the contact resistance because of unknown clamping forces and surface qualities. Additionally,the amount of contact between components that are different temperatures is intentionally limited by design, like contact between the shroud and chamber

walls. Assuming bonded contact for components inside the shroud is reasonable since they are expected to be at similar temperatures during steady state.

- The outer chamber and insulation is assumed to be at a constant 20°C boundary condition to simulate ambient conditions. This is not exact but is intended to approximate the average temperature as it changes due to day/night cycles since the chamber is in a non-climate controlled lab. It is possible this should be changed depending on the season to best approximate average ambient conditions. Testing took place in May and June 2021 for this thesis.

- For the CubeSat mass model, simplifications to the geometry were made including assuming no bolts or small holes, but major features are maintained including the outer shell and interior rails. This is acceptable for this type since emissivity and conductivity largely determines steady state temperatures.

- For simulating hot cases, heater top surface temperature boundary condition is set based on hot soak set temperature. This is acceptable because the temperature distribution on the heater plate surfaces was measured to be within 1-2 degrees at steady state.

- For simulating cold cases, either a shroud tubing temperature boundary condition is set based on cold soak set temperature, or flow of nitrogen is simulated through the shroud tubing using SolidWorks Flow Simulation.

- Material properties and surface properties for some components are assumed due to lack of verifiable documentation. This is acceptable because the materials are classifiable by eye and exact alloy details do not greatly affect thermal conductivity in this case.

If the results vary from the thermal model predictions, it may indicate one or more of these assumptions are not valid and the model will be tuned or detail will be added until the required predictive capability is met.

4.3.2 Material and Surface Properties

Table 4.5 outlines the material properties used for components in the chamber. Note that constant properties are not assumed and for materials like aluminum and copper the conductivity changes significantly with temperature. This is important since the chamber experiences large temperature swings during cycling.

Table 4.5: Chamber material properties for thermal model

Component	Material	Thermal Conductivity [W/(m*K)]	Heat Capacity** [J/(Kg*K)]	Density** [kg/m^3]
Shroud	Copper	401 @ 300 K*	384 @ 298 K*	8960
Mounting Rails, CubeSat Mass Model, Test Article Plates	6061 Aluminum	156 @ 300 K*	954 @ 300 K*	2700
Platen, Outer Chamber Walls	302 Stainless Steel	16.3	500	7900
Chamber Insulation	Glass Fiber Quilt	0.040	840	12
Test Article Spacers	Teflon	0.273 @ 300 K*	104 @ 300 K*	2160

*SolidWorks built in variable properties curve used, value shown only for specified temperature

**Specific heat and density are not relevant for steady-state analysis

Table 4.6 outlines the surface properties used for components in the chamber along with the source of that value. Note that the chamber interior walls and shroud outer surface were user defined based on model tuning that took place after empty test 1. The thermal model results shown all include the modified emissivities and remain constant for all simulations shown.

Before the final results for empty test 1, the thermal model was manually tuned to best match the experimental results. The tuning involved iterating a hot case soak

for empty test 1, where the heater plate top surface is set to a constant temperature boundary condition. The simulation is then run while changing the two user defined emissivities in Table 4.6 until the modeled temperatures most closely correlated to the experimental results for empty test 1. This tuning process was manually performed by changing the user defined emissivities by 0.01 for each run of the model and was only performed after empty test 1 to tune the thermal model to match the experimental results, because the exact surface properties for the chamber inner walls and shroud outer surface is not known as precisely compared to other surfaces. These surface properties in particular are not known precisely because the inner chamber is not perfectly rough or polished and the shroud outer surface is not perfectly polished, compared to a surface like the Aeroglaze coated surfaces where the emissivity is well characterized by the supplier.

Table 4.6: Chamber surface properties for thermal model

Surface Descriptions	Surface	Emissivity	Source
Shroud Inner Surface, Painted Heater Plate Surfaces, Painted Test Article Plate	Aeroglaze Z306	0.910	Socomore TDS
Mounting Rails, Unpainted Door Shroud Face	Bare aluminum, rough	0.070	SolidWorks Flow Simulation 2020 Pre-defined
Platen	Polished stainless steel	0.074	SolidWorks Flow Simulation 2020 Pre-defined
Chamber Interior Walls	Bare stainless steel	0.110	User defined, based on empty model tuning
Shroud Outer Surface	Roughly polished copper	0.060	User defined, based on empty model tuning
Unpainted Heater Plate Surfaces, Aluminum Foil Reflectors (Polished Side)	Polished aluminum	0.040	SolidWorks Flow Simulation 2020 Pre-defined
Aluminum Foil Reflectors (Dull Side), CubeSat Interior Rails	Commercial sheet aluminum	0.090	SolidWorks Flow Simulation 2020 Pre-defined
Anodized CubeSat Mass Model Surfaces	Anodized Aluminum	0.770	Engineeringtoolbox.com
Teflon Spacer Blocks	Polytetrafluoroethylene, Teflon, PTFE	0.920	Engineeringtoolbox.com

4.3.3 Mesh & Mesh Refinement Study

A mesh refinement study was performed to verify heater and shroud average, minimum, and maximum temperatures did not change by more than 1°C with mesh size. The empty model was used for mesh comparisons, and the smallest mesh size was used for the analysis correlations because all measured temperatures did not change by more than 1°C with mesh size. The larger meshes were approximately three times larger by total cell count compared to their smaller counterparts. Because there are experimental results for additional comparison, mesh refinement consisted of only 2 levels for a high level comparison. Simulations with test articles have larger meshes to include test articles, mesh size is similar in appearance to heater plates depending on geometry, and always has more total cells because of the addition of the test article. Additional mesh refinement was considered unnecessary for all configurations. Table 4.7 shows the results for the flow simulation and conduction + radiation only simulations.

Table 4.7: Mesh refinement study results

Mesh Description	Total Cells	Shroud Avg. Temp. [°C]	Shroud Max. Temp. [°C]	Shroud Min. Temp. [°C]
With flow Simulation: Large Mesh	7,638,811	-179.38	-175.73	-190.31
With flow Simulation: Small Mesh	2,596,994	-178.38	-175.57	-190.34
Conduction + Radiation only: Small Mesh	86,504	47.96	49.27	46.55
Conduction + Radiation only: Large Mesh	276,246	47.89	49.40	46.38

SolidWorks' meshing algorithm allows the user to specify a level of detail based on locations in the model and detail in that region, as well as levels of detail for the entire model, based on a minimum mesh size and other parameters or based on a sliding scale. Based on these details, the software calculates the mesh and shows key parameters like total number of cells.

Figure 4.13 and 4.14 show the meshes used for the empty test comparisons. Note that the mesh is focused around smaller features, especially the shroud tubing for flow simulation, and is less refined in less critical areas like the outer chamber. Closeups outlined in red show the region near the shroud tubing and heater plates in more detail.

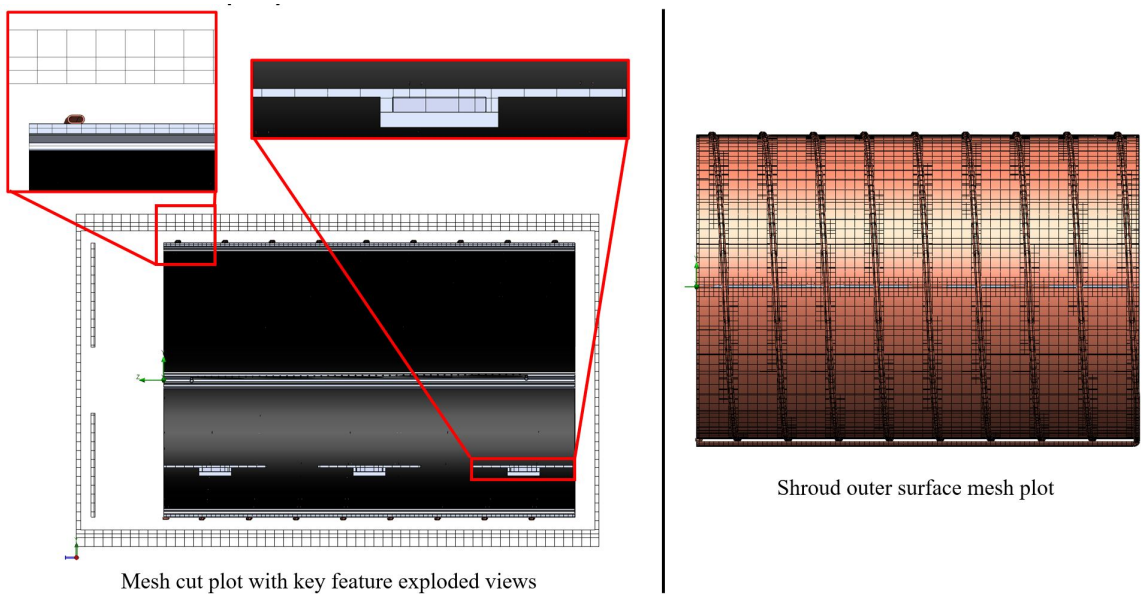

Figure 4.13: Small mesh used for numerical simulations with conduction and radiation only

4.3.4 Thermal Model Validation

In order to demonstrate that the computational thermal model accurately predicts temperatures in the chamber, experiments using the modified chamber were performed and compared to the model. The experimental data is considered to be the

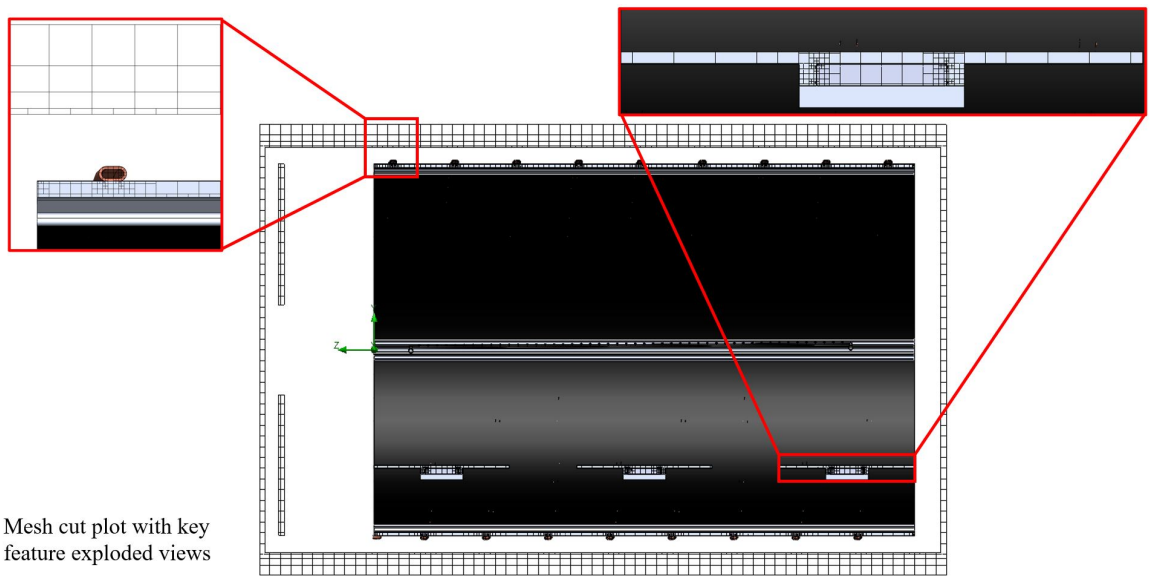

Figure 4.14: Small mesh used for numerical simulations with conduction, convection (flow simulation), and radiation

true solution, and the goal is for the computational model to be able to predict the response of the chamber and test articles accurately before tests are performed. Whenever a model is referred to, it is referencing the computational models used to predict the temperature distribution using SolidWorks and SolidWorks Flow Simulation tools as configured and described in this chapter.

For this thesis, two empty tests are performed first with the chamber operating a specified profile. During these tests, the temperatures at various points of interest are logged and used to fine tune the thermal model. Fine tuning involves ensuring that the simplifications and assumptions made to the model are reasonable and result in accurate predictions of the response of the chamber under the test conditions. After the model is tuned such that the model accurately predicts the temperatures of the chamber empty, tests with test articles are conducted and temperatures of the test article and points of interest in the chamber are recorded. These results are compared to the numerical model with the test article included.

For numerical model comparisons to test results, temperatures are compared at the same locations as tested on the corresponding computer model, and the absolute difference in temperature is calculated for each location and reported to the nearest 1°C. The maximum absolute difference for each test is reported for all locations or for a particular component like the shroud or test article. These maximum absolute differences are used to check against thermal uncertainty margin requirement of 15°C, which is based on the European Cooperation for Space Standardization (ECSS) margin and is the same margin used in previous thermal model comparisons in Jensma's thesis for model vs experimental comparisons [11]. This means that the numerical model must predict the temperatures at measured locations to within 15°C of the experimental value in all cases to be considered validated.

Chapter 5

RESULTS AND ANALYSIS

This chapter discusses the outcomes of leak testing and repair as well as the thermal vacuum testing results compared to the numerical model results at steady state soak temperatures where appropriate. Different methods of simulating the cold soaks are presented, one using only conduction and radiation, and the other simulating nitrogen coolant flow. The thermal cycle consistency is compared for the CubeSat mass model testing.

5.1 Leak Testing and Repair

Before modifications were made to the existing heating and cooling system, leak testing was performed using a vacuum technologies Model 979 Series Helium Mass Spectrometer Leak detector. This device connects to the chamber in place of the roughing pump and uses its own pump as well as an inline mass spectrometer to perform leak detection. Helium from an external tank is manually sprayed on the outside of the chamber in areas of interest, and if a leak is present, the helium atoms will enter the chamber and eventually pass through the mass spectrometer in the leak detector. The leak detector displays the calculated leak rate and creates an audible tone proportional to the leak rate.

Using the leak detector, one relatively large leak source was identified, which was the threaded connection where the vent valve connects to the chamber in the back of the chamber wall on the top left looking from the front of the chamber and is outlined in red in Figure 5.1.

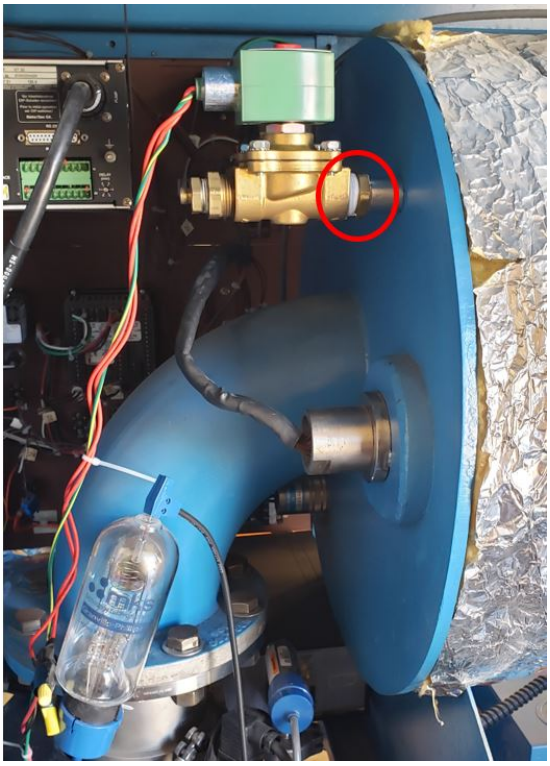

Figure 5.1: Vent valve leak source outlined in red

After it was identified, the valve was removed, cleaned and reinstalled tightly with teflon tape on the threads. An additional relatively large leak source was identified as the existing nitrogen plumbing, specifically in the lines running to the platen and shroud. This leak was not able to be corrected at the time and because the hardware would be replaced it was ignored. After these leaks as well as other small leaks were identified and corrected, except for the leak in the existing nitrogen plumbing, the chamber was pumped down using the roughing and turbomolecular pump to determine the new baseline pressure. After approximately 23 hours, a vacuum of $3.5e^{-4}$ Torr was achieved, which compared to the previous baseline pressure of $5.0e^{-4}$ Torr represents a 35% improvement. After the old heating and cooling system was removed in preparation for the new system installation, an additional pump down test was performed to determine the effect of removing the old hardware. During this test, a pressure of $1.5e^{-5}$ Torr was achieved, which represents an 80% improvement over

the baseline before any leak testing. It was determined that any further leak testing would likely offer little improvement, so leak testing was considered complete, despite not meeting the ISO 19683 standard requirement of $7.5e^{-6}$ Torr. This is because the remaining leaks were likely numerous and small, so chasing them all down would require additional effort that may not be needed after new hardware is installed and the system is allowed to bakeout. In addition, the new baseline at $1.5e^{-5}$ Torr was achieved in less time than the previous baseline at a higher pressure.

After hardware installation and multiple bakeouts and empty thermal vacuum tests, the CubeSat mass model test pressure was measured. The control panel with the ion gauge visible was recorded using a time lapse webcam. Figure 5.2 shows the pressure recorded during the testing. After approximately 11 hours with the turbomolecular pump on, chamber pressures were below $7.5e^{-6}$ Torr for at least 2.5 cycles between -15°C and 50°C. The base pressure after the thermal cycling was complete and after more than 48 hours baking out with the heater plates set to 95°C, the base pressure achieved was $4.4e^{-6}$ Torr. Minimum temperature capability testing, pressures as low as $1.7e^{-7}$ Torr were observed.

5.2 Empty Test 1

5.2.1 Experimental Results

The minimum temperatures at the end of the -20°C cold case at 9.5 hours was used to represent steady state for thermal model comparisons. Average temperatures for hours 25-26 were used for the 80°C hot case thermal model comparisons.

The empty test 1 data seen in Figure 5.3 shows the temperature response of the chamber. Note that the heater plates take longer to reach equilibrium temperatures in cold cases compared to hot cases. This makes sense because the cooling power

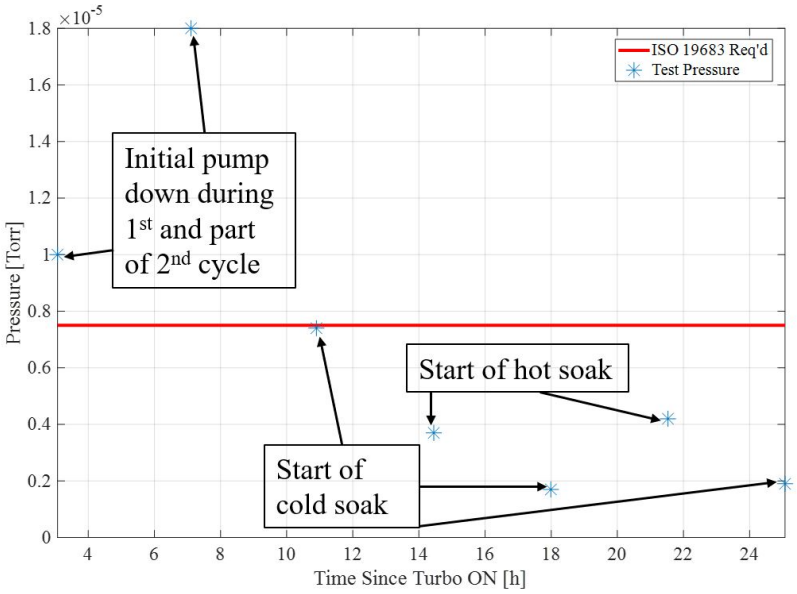

Figure 5.2: Annotated chamber pressure during CubeSat mass model testing

comes from the shroud, and has to transfer to the heater plates through radiation only because there is limited contact between them. The shroud is more responsive, even in hot cases, because the thin copper sheeting and tubing have low thermal mass as noted Chapter 2. The response of the heater plates in hot cases lag behind the profile set temperature, possibly due to worse thermal contact due to the different thermocouple sizes for the control vs logging thermocouples. Time to reach steady state in this test, which is time after the soak starts that it takes for the temperatures to remain constant to within +/- 3°C, was less than an hour for the hot cases and less than 3 hours for the cold case. It is expected to take less time for the hot case since the shroud coolant takes time to cool down the tubing throughout the shroud before the entire shroud reaches steady state, whereas the heaters reach steady state quickly and warm the surrounding shroud quickly.

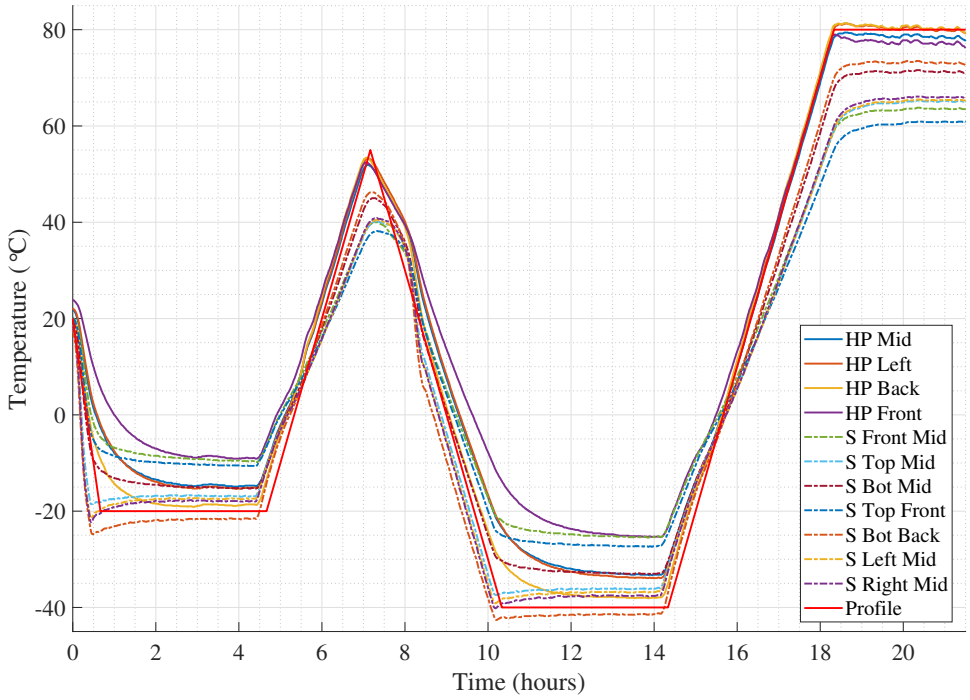

Figure 5.3: Logged temperature data during empty test 1

5.2.2 Numerical Model Results

The numerical model results for the empty 1 hot case with flow simulation is shown in Figure 5.4. The heater plate top surface temperatures are set to 80°C based on the profile set temperature. Note that the heater plate temperatures are not shown since they reduce the resolution of the legend.

The numerical model results for the empty 1 cold case with flow simulation is shown in Figure 5.5. As mentioned in the methodology, the blue outlined labels correspond to shroud temperatures and red outlined temperatures correspond to heater plate temperatures. The shroud tubing is set to a constant temperature boundary condition of -20°C to simulate the coolant through the tubing without requiring the flow to be simulated.

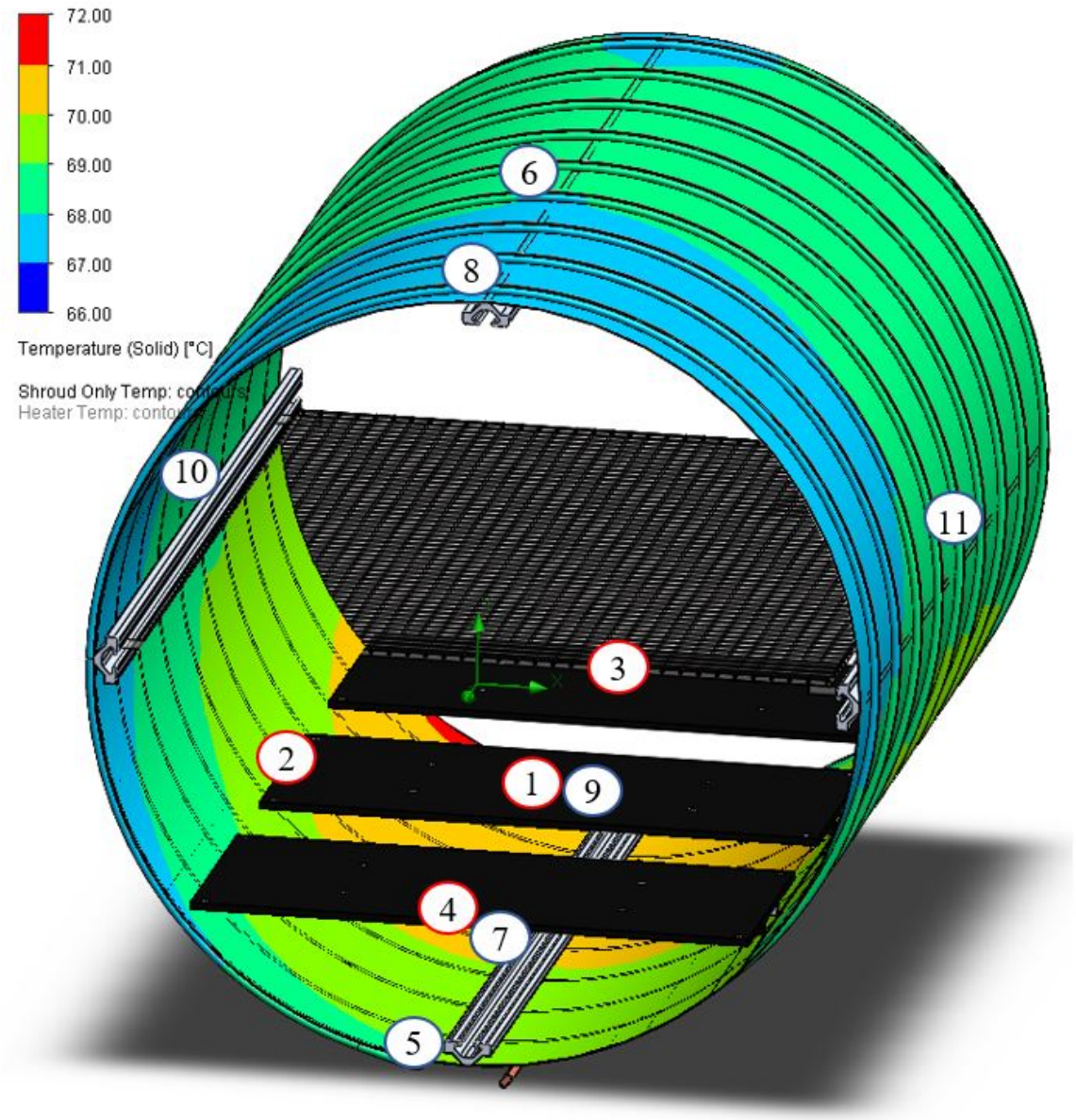

Figure 5.4: Numerical model results for empty test 1, 80°C case

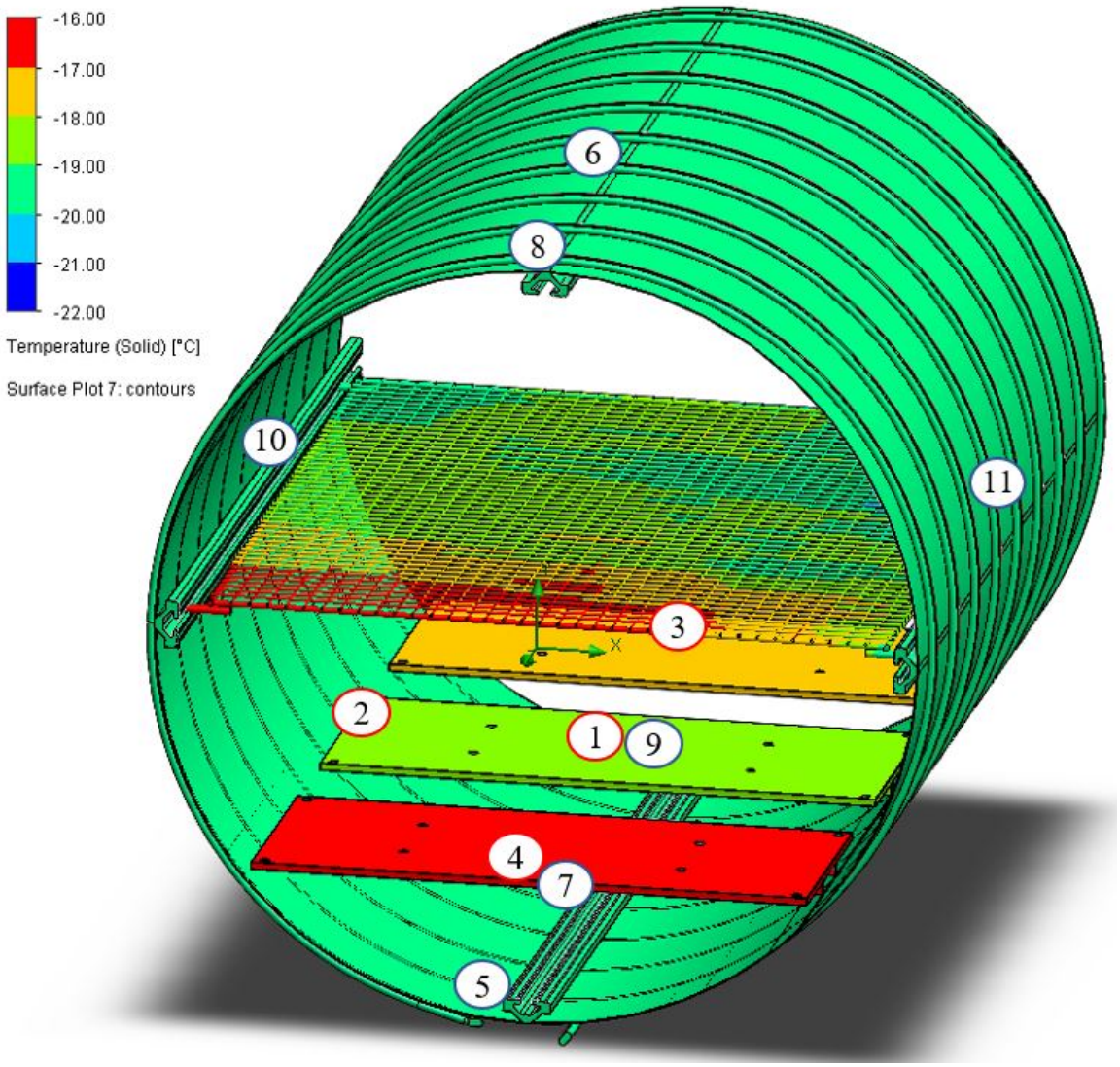

Figure 5.5: Numerical model results for empty test 2, -20°C case without flow simulation

5.2.2.1 Simulating Shroud Coolant Flow

It is possible but impractical to use flow simulation to simulate nitrogen coolant through the shroud in order to predict the temperatures in the chamber. It is possible to perform an iterative approach, by iterating different nitrogen flow rates in the thermal model and running the model until the average temperature corresponds to the desired controller profile temperature. This method was used to correlate empty 2 test cold soak temperatures with the thermal model, however it takes orders of magnitude greater time because multiple calculations must be run with a much larger mesh for the flow simulation cases. This process can be sped up by ensuring you are using the results of the previous calculation as an initial condition for the new simulation. For the empty 2 correlation at -20°C, the following conditions were assumed:

- A flow rate of nitrogen of 1.000 g/s at an inlet temperature of -150°C and a pressure of 21 psi
- A back pressure at the outlet of 5 inches of water with a temperature of -9.5°C (based on measured outlet temperatures during the soak)
- A chamber outer wall temperature boundary condition of 20°C
- The coolant flow is assumed to be fully developed, dry gaseous nitrogen
- Gravity is turned on

The numerical model results for empty test 1 cold case with flow simulation is shown in Figure 5.6. There is a difference in temperature in the shroud temperatures from front to back, with the shroud minimum and maximum temperatures being 28°C in the worst case. This difference is due to the lower flow rate used compared to the sizing model and because of the single spiral geometry, and is not unexpected.

Despite this difference, the average shroud temperature is -20°C with the majority of the shroud area being between -16°C and 26°C.

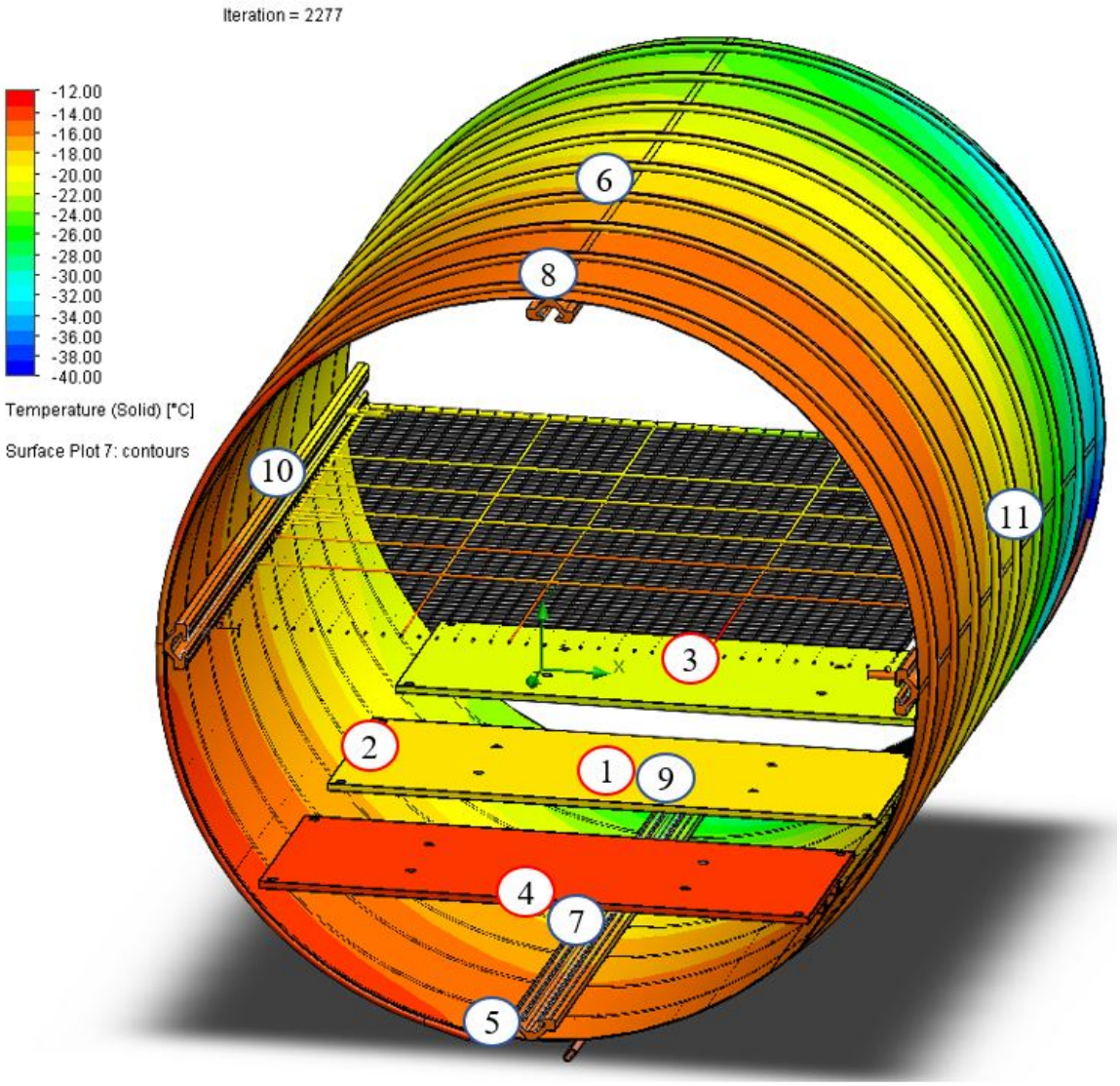

Figure 5.6: Numerical model results for empty test 2, -20°C case without flow simulation

5.2.3 Model vs. Experimental Results Comparison

Table 5.1 shows the comparison between experimental and numerical model temperatures for the hot case. Note that the shroud front middle and shroud top front, thermocouples 5 and 8 respectively, have the greatest absolute difference in tempera-

tures with consistently higher temperatures in the model vs the experimental results. This makes sense because front of the chamber has more uncertainty in the geometry due to the more details like the door shroud, gaps between the shroud, door shroud, and chamber walls, and effects from the inlet and outlet tubing, foil, and thermocouple wires which are concentrated at the front of the chamber.

Location Index	**Location Name**	**Exp. Temp. [°C]**	**Model Temp. [°C]**	**Absolute Diff. [°C]**
1	**HP Mid.**	**79**	**80**	**1**
2	**HP Left**	**80**	**80**	**0**
3	**HP Back**	**80**	**80**	**0**
4	**HP Front**	**77**	**80**	**3**
5	**S Front Mid.**	**64**	**69**	**5**
6	**S Top Mid.**	**65**	**68**	**3**
7	**S Bot. Mid.**	**71**	**70**	**1**
8	**S Top Front**	**61**	**67**	**6**
9	**S Bot. Back**	**73**	**71**	**2**
10	**S Left Mid.**	**65**	**69**	**4**
11	**S Right Mid.**	**66**	**68**	**2**

Table 5.1: Comparison of numerical model and experimental results for empty test 1, 80°C hot case

Table 5.2 shows the results when flow simulation is not used for the cold case. The cold case with flow simulation is later compared to this cold case without flow simulation. Similarly to the hot case, the front of the shroud is least correlated with the model, but this time the temperatures are consistently lower in the model compared to the experimental results. This suggests some aspect of the front of the chamber is not being precisely modeled enough to produce similar differences as other locations, or experimental setup error. This could be due to a difference in shroud or platen surface temperatures, or the reflectors performing worse than expected, among other possible reasons like the geometry differences discussed in the previous paragraph.

Location Index	Location Name	Exp. Temp. [°C]	Model Temp. [°C]	Absolute Diff. [°C]
1	HP Mid.	-15	-19	4
2	HP Left	-15	-19	4
3	HP Back	-19	-17	2
4	HP Front	-9	-16	7
5	S Front Mid.	-10	-20	10
6	S Top Mid.	-17	-20	3
7	S Bot. Mid.	-15	-20	5
8	S Top Front	-11	-20	9
9	S Bot. Back	-22	-20	2
10	S Left Mid.	-18	-20	3
11	S Right Mid.	-18	-20	2

Table 5.2: Comparison of numerical model and experimental results for empty test 1, -20°C cold case without flow simulation

Table 5.3 shows the same cold case experimental results compared to the model with flow simulation results. This simulation has a 50% decrease in maximum absolute difference compared to the model without flow simulation. This indicates that the flow simulation improves the predictability for cold cases, at the cost of more effort computationally. As an example, iterating the flow simulation model and solving it many times takes on the order of days whereas the model without flow simulation takes minutes to run on the same computer. The shroud front middle and shroud top front continue to be sources of greater difference compared to the average, however this is less of the case when flow simulation is included since two additional locations have 5°C absolute differences. This greater difference is likely due to the same reasons as mentioned in Section 5.2.3.

Location Index	Location Name	Exp. Temp. [°C]	Model Temp. [°C]	Absolute Diff. [°C]
1	HP Mid.	-15	-18	3
2	HP Left	-15	-18	3
3	HP Back	-19	-22	3
4	HP Front	-9	-14	5
5	S Front Mid.	-10	-15	5
6	S Top Mid.	-17	-18	1
7	S Bot. Mid.	-15	-18	3
8	S Top Front	-11	-16	5
9	S Bot. Back	-22	-27	5
10	S Left Mid.	-18	-18	1
11	S Right Mid.	-18	-20	2

Table 5.3: Comparison of numerical model and experimental results for empty test 1, -20°C cold case with flow simulation

5.3 Empty Test 2

5.3.1 Experimental Results

Figure 5.7 shows the experimental results for empty test 2. Note the consistency between the thermal cycles, with similar, repeatable response when comparing identical cycles. Some variation is seen during the hot soaks and is most visible in the heater plate temperatures. This is likely variation due to the heater PID controller as it attempts to reach equilibrium without over or undershooting the target value significantly. For cold soaks, the front of the shroud tends to be warmer than the middle and back of the shroud.

5.3.2 Numerical Model Results

Empty 2 numerical model results at -20°C are the same as the results presented in empty test 1 Figure 5.5 without flow simulation because they share cold soak temperatures. The results for the 55°C hot case are shown in Figure 5.8. Similarly to

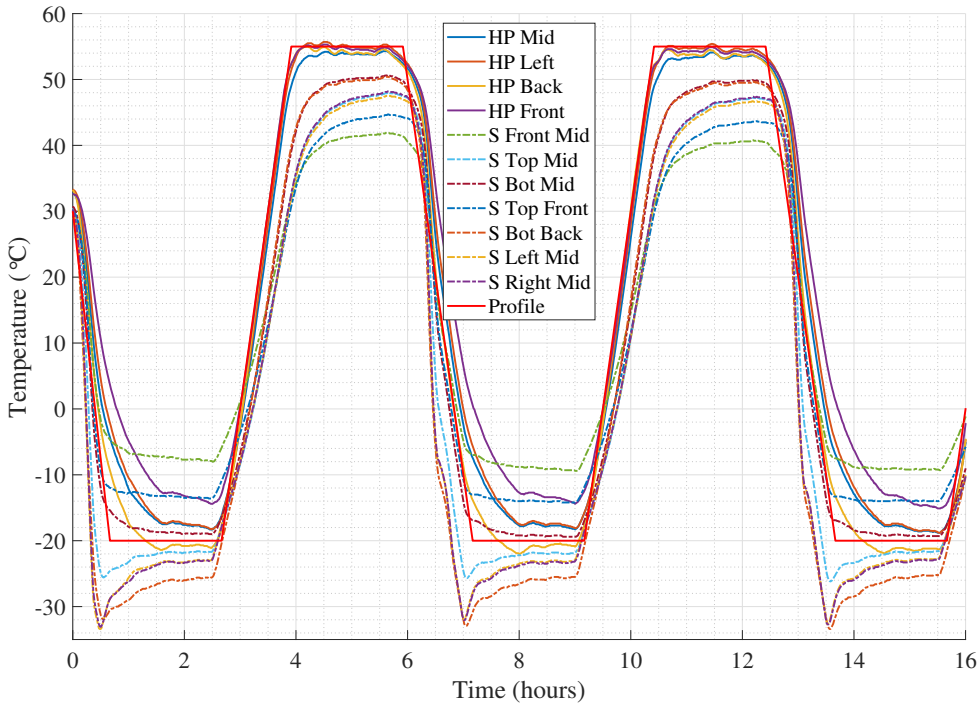

Figure 5.7: Logged temperature data during empty test 2

empty test 1 hot cases, the heater plate top surfaces are set with a constant surface temperature equal to the profile set temperature, with the difference being empty test 1 compared at 80°C instead of 55°C because it had a longer dwell at 80°C in empty test 1.

5.3.3 Model vs. Experimental Results Comparison

The empty 2 experimental results compared for the -20°C case uses average of the lowest temperatures at the end of each cold soak, and the hot case uses an average temperatures at hours 12.5-12.7 during the last hot soak for the steady state comparisons. Comparisons for the hot case are shown in Table 5.4 with a similar maximum absolute difference to the empty 1 hot case results with similar higher temperatures than predicted in the model vs the experimental case.

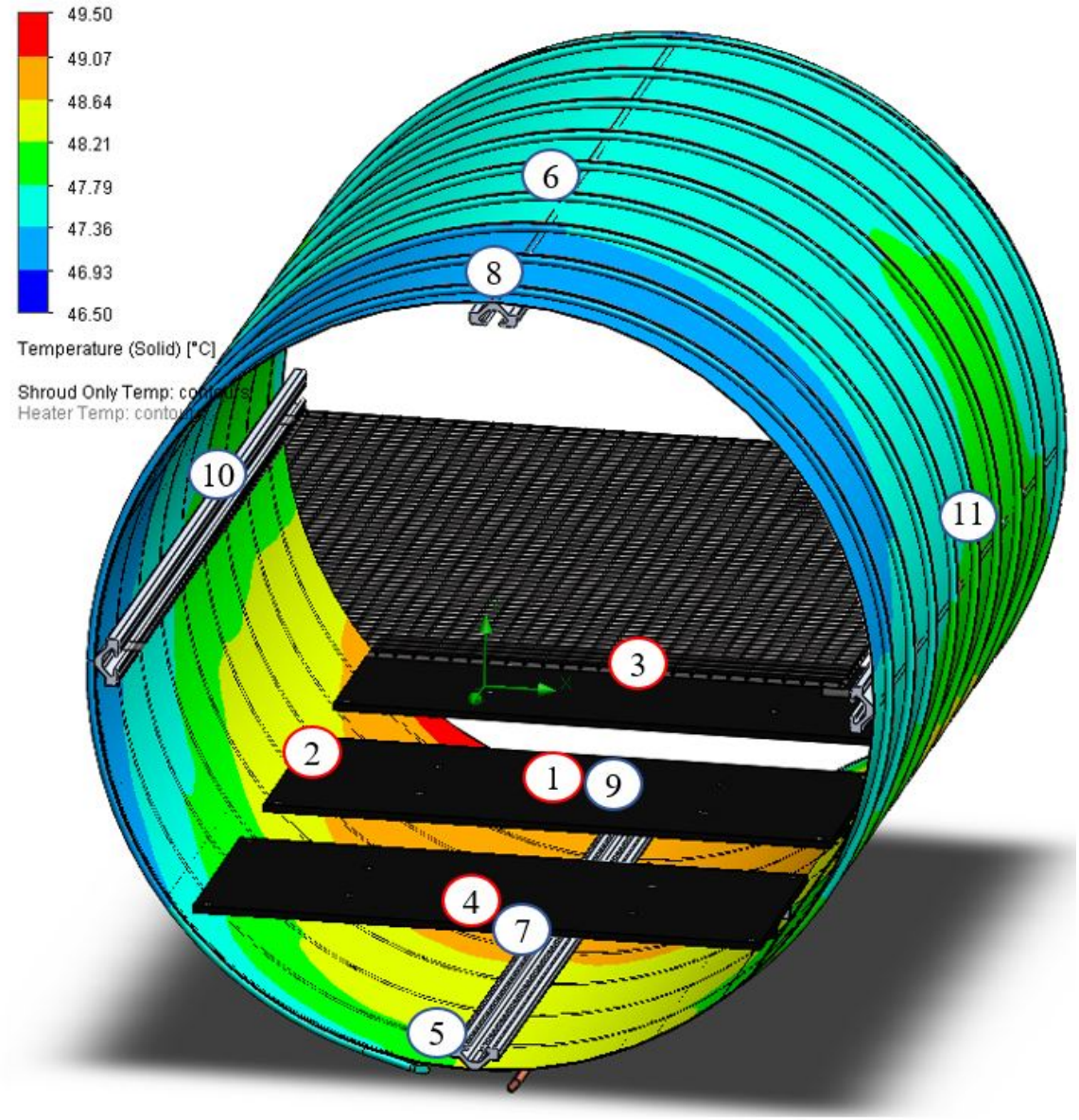

Figure 5.8: Numerical model results for empty test 2, 55°C case

Location Index	Location Name	Exp. Temp. [°C]	Model Temp. [°C]	Absolute Diff. [°C]
1	HP Mid.	54	55	1
2	HP Left	55	55	0
3	HP Back	54	55	1
4	HP Front	55	55	0
5	S Front Mid.	41	48	7
6	S Top Mid.	48	48	0
7	S Bot. Mid.	50	49	1
8	S Top Front	44	47	3
9	S Bot. Back	50	49	1
10	S Left Mid.	47	48	1
11	S Right Mid.	48	48	0

Table 5.4: Comparison of numerical model and experimental results for empty test 2, 55°C hot case

Similarly to empty test 1, the results for the -20°C cold case are compared with and without flow simulation in Tables 5.6 and 5.5 respectively. Similar trends to empty test 1 in locations and magnitudes of absolute temperature difference are seen comparing the model and experimental results.

5.4 CubeSat Mass Model Test

After the empty tests were completed and the results demonstrated that the chamber was capable of consistent control to a specified thermal profile for multiple cycles, test article testing was performed to compare the thermal response of the test article for various test profiles. The empty test results demonstrated a maximum absolute difference of 11°C between the predicted and measured temperatures at all measured locations, indicating that the chamber is consistently predicable within the required 15°C thermal uncertainty margin.

Location Index	Location Name	Exp. Temp. [°C]	Model Temp. [°C]	Absolute Diff. [°C]
1	HP Mid.	-19	-19	1
2	HP Left	-18	-19	1
3	HP Back	-21	-17	4
4	HP Front	-15	-16	1
5	S Front Mid.	-9	-20	11
6	S Top Mid.	-22	-20	2
7	S Bot. Mid.	-19	-20	1
8	S Top Front	-14	-20	6
9	S Bot. Back	-26	-20	6
10	S Left Mid.	-23	-20	3
11	S Right Mid.	-23	-20	3

Table 5.5: Comparison of numerical model and experimental results for empty test 2, -20°C cold case without flow simulation

The CubeSat mass model subjected to the previously specified thermal vacuum test profile in the chamber and the experimental results are compared to the thermal model results. Additionally, the consistency of identical cycles is compared for the CubeSat mass model test to compare the response of the chamber and test article after identical thermal cycling.

5.4.1 Experimental Results

The CubeSat mass model test results are shown in Figure 5.10. Note that the test starts from a high temperature soak which was the end of a pre-test bakeout. It was included in the results because the initial 80°C hot soak is compared to numerical model results. The remaining soaks and dwells never achieved steady state for the test article temperatures, as indicated by the slope of the temperatures before each soak ends, therefore no numerical model correlations are made for the cold case.

Location Index	Location Name	Exp. Temp. [°C]	Model Temp. [°C]	Absolute Diff. [°C]
1	HP Mid.	-19	-18	1
2	HP Left	-18	-18	0
3	HP Back	-21	-22	1
4	HP Front	-15	-14	1
5	S Front Mid.	-9	-15	6
6	S Top Mid.	-22	-18	4
7	S Bot. Mid.	-19	-18	1
8	S Top Front	-14	-16	2
9	S Bot. Back	-26	-27	1
10	S Left Mid.	-23	-18	5
11	S Right Mid.	-23	-20	3

Table 5.6: Comparison of numerical model and experimental results for empty test 2, -20°C cold case with flow simulation

5.4.2 Numerical Model Results

CubeSat mass model results for the 50°C hot case are shown in Figure 5.10. Similarly to empty tests hot cases, the heater plate top surfaces are set with a constant surface temperature equal to the profile set temperature. Note that the CubeSat surface temperature does not vary by more than +/- 1°C at steady state in this case.

5.4.3 Model vs. Experimental Results Comparison

Comparing the absolute differences for the CubeSat mass model hot case, Table 5.7 demonstrates a maximum absolute difference of 3°C for all locations and a maximum difference of only 2°C for the CubeSat at the measured locations. This indicates that the thermal model is capable of accurately predicting the CubeSat surface temperatures in the hot case. It makes sense that the CubeSat surface temperatures have a lower absolute difference than the shroud because the CubeSat is more isolated thermally since it can primarily only be affected by radiation from the shroud, heater

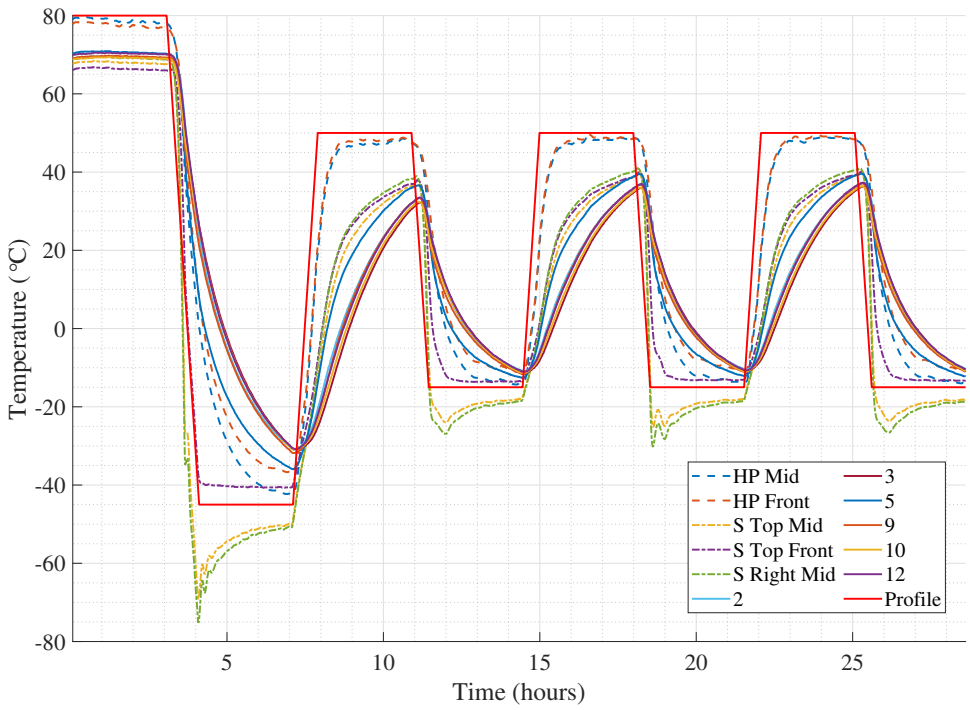

Figure 5.9: Logged temperature data during CubeSat mass model test

plates, and reflectors, and it sees more of an average environment temperature than the shroud or heater plates alone.

5.5 Aluminum Plates Test

5.5.1 Experimental Results

The experimental results for the aluminium plates test are shown in Figure 5.11. Note that the thermocouple numbers with a P refer to the painted plate and thermocouple numbers with a U refer to the unpainted plate. This test went to the limits of the chamber's temperature capability. Despite the dwell times being 2 hours, the plates did not reach steady state, which is especially true for the hot cases with the unpainted plate as indicated by the greater slope of the unpainted plate temperature response at the end of each soak.

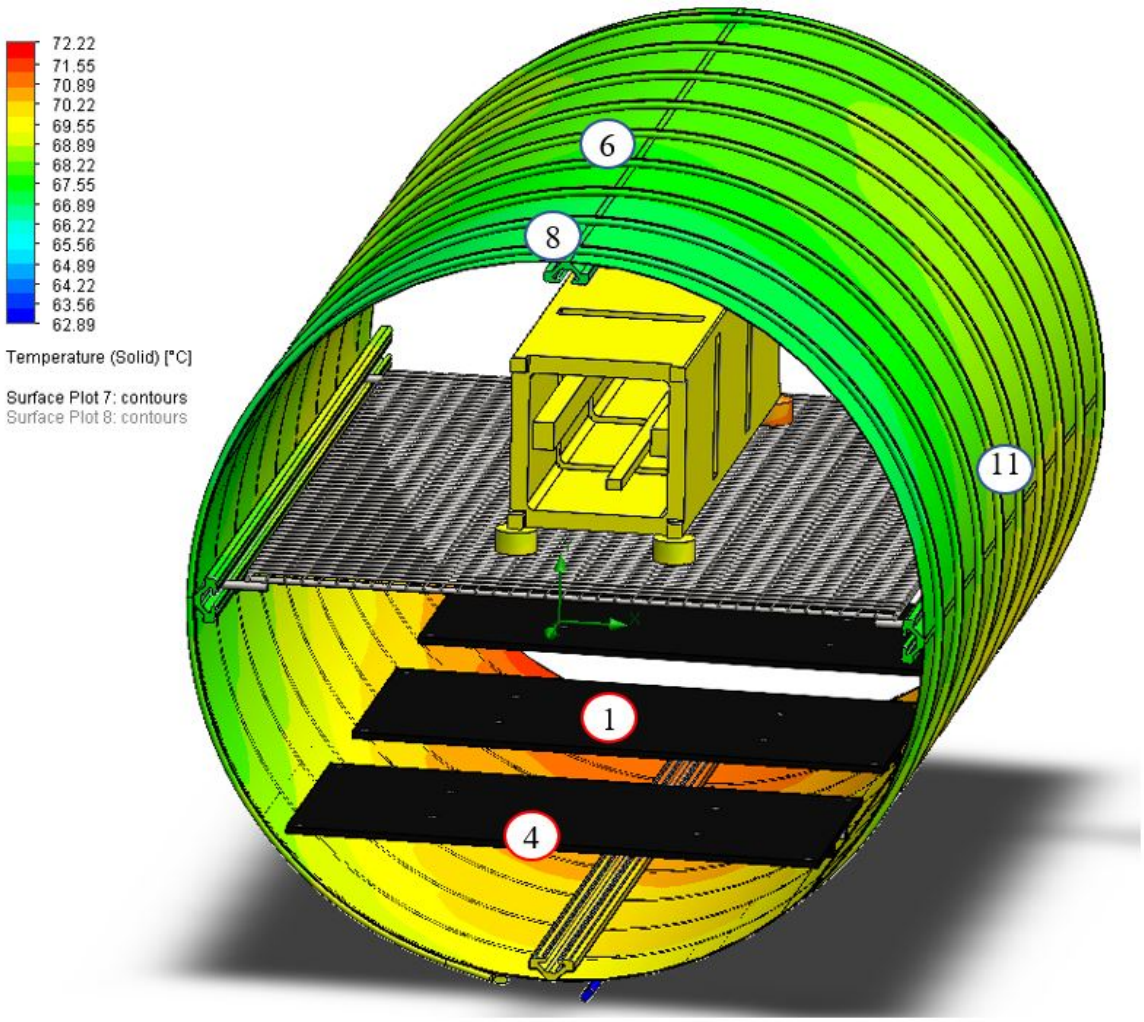

Figure 5.10: Numerical model results for CubeSat mass model test, 80°C case

Location Index	Location Name	Exp. Temp. [°C]	Model Temp. [°C]	Absolute Diff. [°C]
1	HP Mid.	79	80	1
4	HP Front.	77	80	3
6	S Top Mid.	68	68	0
8	S Top Front	66	67	1
11	S Right Mid	69	69	0
2	See Dia.	69	69	0
3	See Dia.	69	70	1
5	See Dia.	71	69	2
9	See Dia.	70	70	0
10	See Dia.	69	70	1
12	See Dia.	70	70	0

Table 5.7: Comparison of numerical model and experimental results for CubeSat mass model, 80°C hot case

Steady state was not achieved for the CubeSat mass model during the test because the dwell period was too short. As a result, the thermal model results could not be compared for any soaks during the test. To allow for a thermal model comparison, after the test was completed the chamber was set to dwell at 90°C. Results for hours 9-10 of the soak which were used for the comparison and are shown in Figure 5.12

5.5.2 Numerical Model Results

Aluminum plate model results for the 90°C hot case are shown in Figure 5.13. Similarly to empty tests hot cases, the heater plate top surfaces are set with a constant surface temperature equal to the profile set temperature. Note that the plate surface temperatures does not vary by more than +/- 1°C for each plate at steady state in this case.

5.5.3 Model vs. Experimental Results Comparison

Comparing the absolute differences for the aluminum plates hot case, Table 5.8 demonstrates a maximum absolute difference of 3°C for all locations and a maxi-

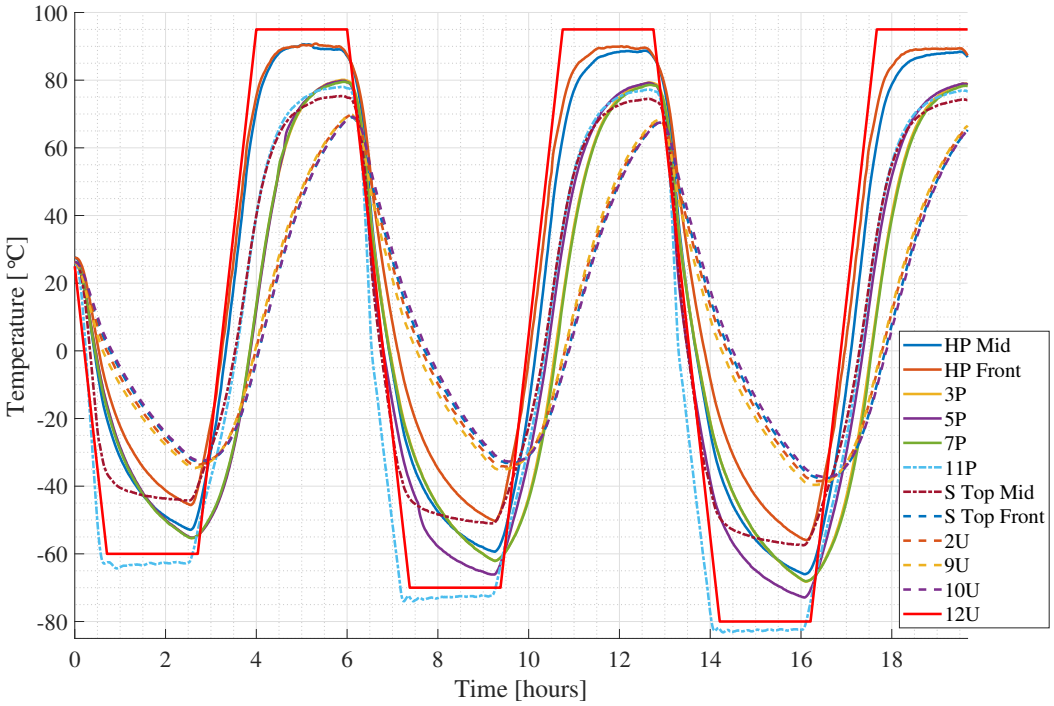

Figure 5.11: Logged temperature data during aluminum plates test

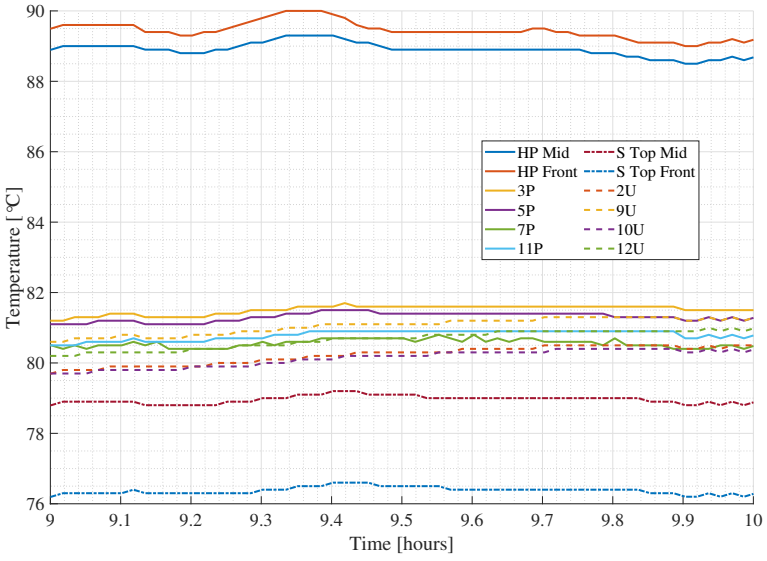

Figure 5.12: Logged temperature data during hot soak after aluminum plates test

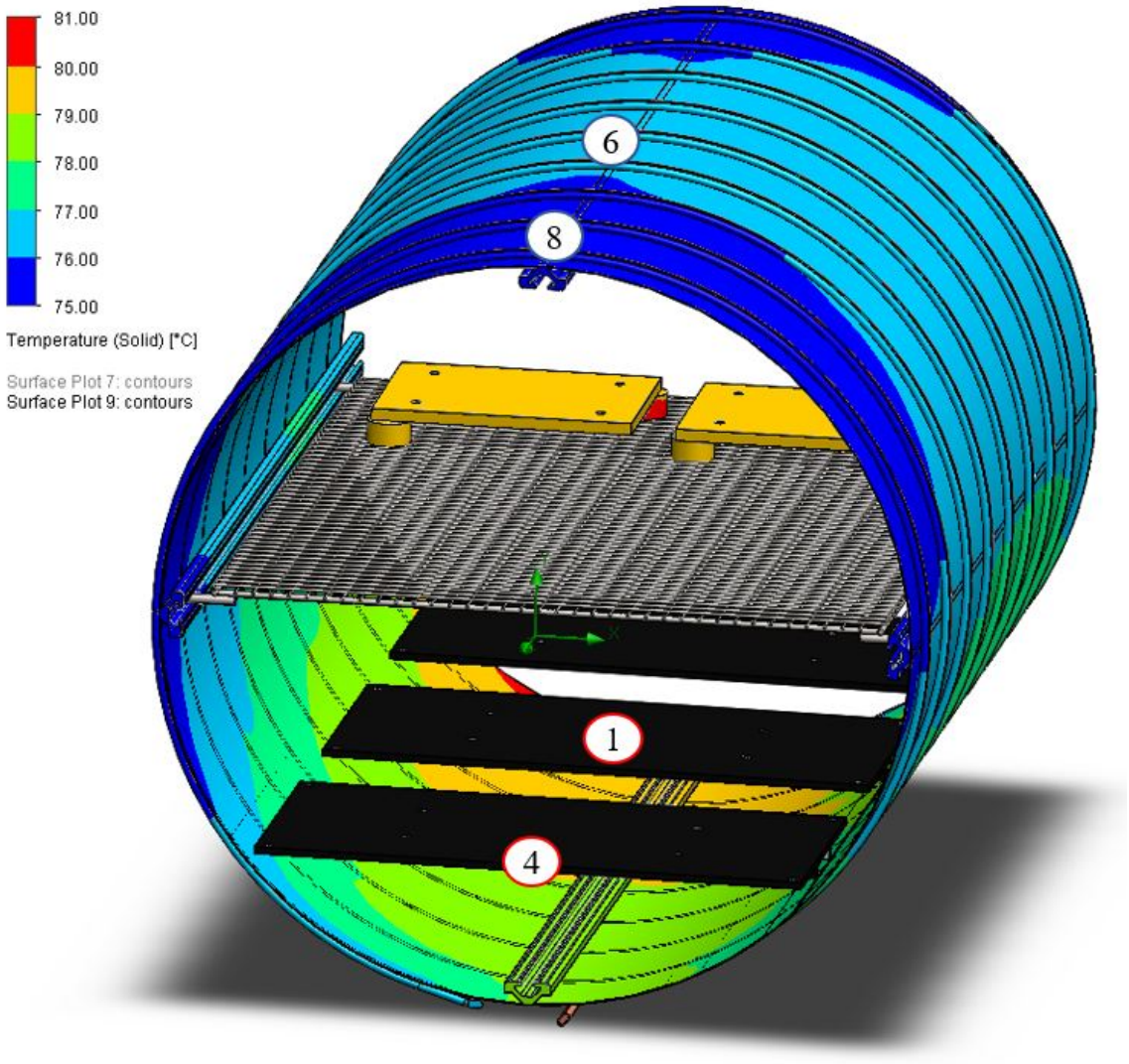

Figure 5.13: Numerical model results for plates test, 90°C case

mum difference of 3°C for the plates at the measured locations. This indicates that the thermal model is capable of accurately predicting the plate surface temperatures in the hot case with the maximum difference well within the required 15°C thermal uncertainty margin.

Location Index	Location Name	Exp. Temp. [°C]	Model Temp. [°C]	Absolute Diff. [°C]
1	HP Mid.	89	90	1
4	HP Front.	89	90	1
6	S Top Mid.	79	76	3
8	S Top Front	76	75	1
3	Painted	82	79	3
5	Painted	81	79	2
7	Painted	81	79	2
11	Painted	81	79	2
2	Unpainted	80	80	0
9	Unpainted	81	80	1
10	Unpainted	80	80	0
12	Unpainted	81	80	1

Table 5.8: Comparison of numerical model and experimental results for the plates test 90°C hot case

5.6 Thermal Cycling Consistency

The consistency of identical thermal cycles is compared by calculating the absolute difference in temperature for the last two thermal cycles of the CubeSat mass model test. The temperature response for each cycle is overlayed and subtracted from each other and the absolute difference is plotted vs time and shown in Figure 5.14. The cycles compared take place approximately from hours 10.0 to 24.5 and hours 11.0 to 17.5. Note that there is a greater absolute difference during cold transients than hot transients. This makes sense because the heaters are simply controlled with consistent power per time on, while the cooling power for the nitrogen system depends on more variables including external tank pressure, inlet line temperatures, variation in fluid flow, etc. This comparison demonstrates that from hours 19 to 24, for steady state

dwells where no cold transients take place, that the chamber systems can maintain CubeSat mass model surface temperatures to within 1.5°C between each cycle at all times.

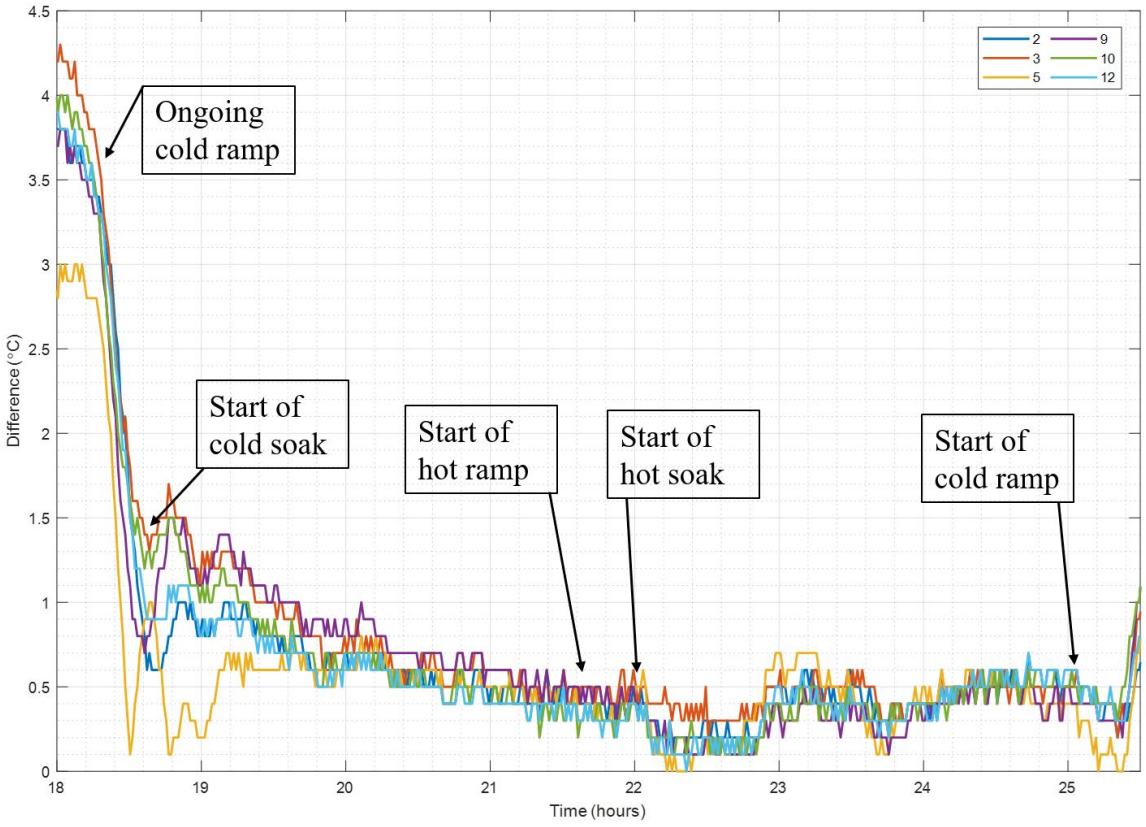

Figure 5.14: Annotated plot of absolute difference in CubeSat temperature response for last 2 cycles of test

5.7 Thermal Model Correlation Summary

Table 5.9 shows the maximum absolute difference between the numerical model results and experimental results. The worst case for all cases is a difference of 11°C. The difference not including cold soaks without flow simulation drops to 7°C and the difference for test article temperatures only is 3°C. Hot cases are more predictable than cold cases with or without flow simulation included. This makes sense because the cold cases have to simulate the nitrogen through the shroud tubing in order to

precisely determine the temperature distribution or otherwise approximate it with a constant temperature boundary condition on the tubes whereas the hot cases just assume a constant surface temperature boundary condition for the top of the heater plates.

Test Name	**Case**	**Max. Abs. Diff.[°C]**
Empty 1	**80°C hot**	**6**
Empty 1	**-20°C cold w/o flow simulation**	**10**
Empty 1	**-20°C cold w/ flow simulation**	**5**
Empty 2	**55°C hot**	**7**
Empty 2	**-20°C cold w/o flow simulation**	**11**
Empty 2	**-20°C cold w/ flow simulation**	**6**
CubeSat	**80°C hot**	**3**
Plates	**90°C hot**	**3**

Table 5.9: Comparison of maximum absolute difference between numerical model and experimental results for all tests

Chapter 6

CONCLUSION AND FUTURE WORK

6.1 Conclusion

The goals of the modifications and testing were to improve and document the capabilities of the Blue Thermal Vacuum Chamber, the conclusion section will outline the effects of the modification as it relates to ISO 19683 and other requirements, referencing the testing and analysis as evidence for each capability. Then, the accuracy and practicality of the thermal model will be discussed. Figure 6.1 shows the state of the chamber in its previous configuration compared to the chamber with the modifications from this thesis. This figure shows the increase in available test volume and highlights the differences between the configurations, including the addition of coatings, less thermally massive materials, and improved modularity.

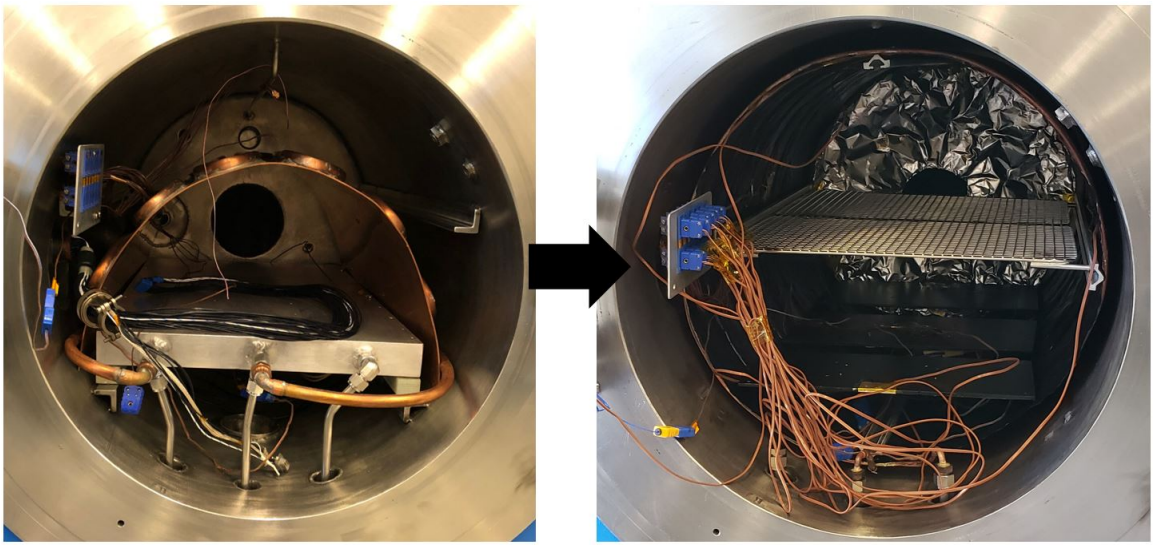

Figure 6.1: Chamber modifications (right) shown with previous configuration (left) [11]

6.1.1 Temperature Range

Testing for this thesis demonstrated the chamber was capable of heater plate temperatures of 95°C and corresponding shroud temperatures >75°C and aluminum plate temperatures of >75°C at the hottest case. Temperatures as low as -145°C were measured at the shroud control thermocouple location during extended cooling testing, and temperatures of approximately <-55°C for the entire shroud and <-70°C for the aluminum plates during aluminum plate testing. Previous testing by Jensma was performed with controller temperatures set between -15°C to 50°C. Therefore, the testing in this thesis demonstrates capability well beyond the -15°C to 50°C requirement of ISO 19683.

6.1.2 Chamber Pressure

Based on the leak testing and repair in chapter 4 demonstrated that after significant chamber baking out and a low-outgassing test article are used, pressures exceeding the ISO 19683 requirement can be met after a pump down time of approximately 11 hours. Additionally, pressures as high as $10e^{-4}$ are allowed by MIL-HDBK-340A, TR-2004(8583)-1 Rev.A., and NASA LSP-REQ-317.01 Rev.B. [4]. These higher base pressures were achieved within minutes after the turbomolecular pump is powered on and was maintained throughout all tests. Compared to the lowest pressure from previous testing by Jensma of $2.0e^{-4}$ this represents an improvement of 2 orders of magnitude [11]. Therefore, this thesis demonstrates the system is capable of meeting and exceeding ISO 19683 chamber pressure requirements for thermal vacuum testing and the pressure is sufficiently low to assume that convection is negligible.

6.1.3 Number of Cycles

The maximum number of cycles for any given test was four during the CubeSat mass model test, which exceeds the ISO 19863 minimum requirement of 2. The chamber is capable of more cycles than that per tank of liquid nitrogen. For example, all of the testing for this thesis required 2 refills of the 180 L tank including time running extended cooling testing to determine minimum temperatures, as well as calibration testing that consumed significant amounts of nitrogen at the beginning of testing. Based on the tests performed, it is estimated that more than 10 cycles between -15°C and 55°C could be performed with 2-3 hour dwells using a single tank of liquid nitrogen. Consumption during the test can be estimated by recording the scale with a time lapse camera or webcam and calculating the average mass decrease of the tank during ramps and soaks. These values can be used to estimate the number of cycles that the chamber will be capable of performing for any given test setup and test profile. For comparison in previous testing by Jensma, only one complete thermal cycle was able to be completed due to the limitations of the previous hardware and 35 L liquid nitrogen dewar [11].

6.1.4 Tolerance Limits and Temperature Variation

During test article testing, it was demonstrated that the test articles were able to maintain surface temperature at the measured locations within a 3°C band at steady state. This means that the chamber cooling and heating systems, on average, are able to maintain the surface temperatures of these test articles with consistent material and surface properties. Additionally, cycles were compared with each other for the CubeSat mass model test and demonstrated less than 1.5°C difference in CubeSat surface temperatures from one cycle to another. However, the chamber is not capable of achieving test article temperatures within a 3°C band of the set temperature in the

steady state. The disagreement between the controller set temperature and the test articles could be due to different thermocouple setups for the control vs data logging thermocouples. As is mentioned in the future work section, the control thermocouples are smaller and more flexible and therefore able to be in better contact with surfaces compared to the thicker thermocouples.

6.1.5 Thermal Dwell

The chamber is capable of dwells of 1 hour or greater as required by ISO 19683 as demonstrated in all tests. It is expected that extended dwells beyond the 0-3 hour range tested can be performed as desired with multiple cycles at each dwell. For this testing, shorter dwells were used in general to conserve liquid nitrogen to minimize refills needed. The previous system as tested by Jensma could only dwell for an hour at -15°C due to a combination of the limitations of available liquid nitrogen, uncoated surfaces, and high thermal mass [11].

6.1.6 Temperature Ramp Rate

The ramp rate used during all testing for this thesis varied from +/- 1 to 2°C, which meets the ISO 19683 requirement of +/- 5°C or slower. It is possible that faster ramp rates are achievable and are desirable when the test article is capable of such ramp rates. This is because faster ramp rates save heating and cooling power by reducing the total test time. The reason they were not tested up to +/- 5°C for this test was to minimize overshoot. Minimizing overshoot is important because it can damage the test article or chamber if the maximum or minimum temperatures for the materials are exceeded, and because the high limit alarm may trigger, which shuts off the relevant heating or cooling system, interrupting the test.

In previous testing by Jensma, programmed ramp rates of -5°C/min were measured at approximately -0.2°C/min, and a maximum of -0.9°C/min when manually stepped in temperature, whereas in this thesis the programmed rates of -1°C/min and -2°C/min were maintained [11]. This demonstrates an increase in control precision with the new configuration, however in both the ISO 19683 requirement of +/-5°C/min or slower.

6.1.7 Test Article Volume

With a shroud inner diameter of 16.5" not including mounting rails, the available test volume increased, and the current system is capable of fitting CubeSats 6U or larger with the existing modular platen without modifications. The system in its previous configuration had approximately half the usable test volume [11].

6.1.8 Thermal Model Correlation

The thermal model and experimental correlations demonstrate that the thermal model is validated with a thermal uncertainty margin requirement with less than the maximum of 15°C in all cases, and as low as 3°C in the best case, keeping in mind thermocouple measurement error alone is +/- 1°C.

While the previous experimental setup and analysis conducted by Jensma is not directly comparable due to geometry and setup differences as well as differences in how the the thermal uncertainty margin is calculated, the values can be roughly compared for the cold and hot soaks. The platen temperature thermal uncertainty margin from Jensma during cold soaks and hot soaks was 9.5°C and 7.2°C respectively, and the CubeSat mass model temperature thermal uncertainty margin during cold and hot soaks was 1°C and 11°C respectively [11]. In this thesis, the worst case thermal uncertainty margin for the shroud and heater plates during cold soaks and hot soaks

was 11°C and 7°C respectively, and the CubeSat mass model thermal uncertainty margin during hot soaks was 2°C.

6.2 Lessons Learned

There were a variety of lessons learned throughout this thesis, and they are noted below and organized by chapter, including modification design, manufacturing processes, thermal vacuum testing, and results and analysis.

6.2.1 Modification Design

The main lessons learned during the modification design process is to be sure to add margin to the design, and to try as much as possible to design to the right conditions. Specifically, during the modification design the liquid nitrogen flow rates used to check the temperature distributions were estimated based on previous testing observations. These estimated flow rates on the surface seemed acceptable, but if other conditions with less or more flow was modeled and evaluated, a different shroud design may have been more suitable for this application. Specifically, the flow used for checking the temperature distribution was higher than what ultimately occurred during testing, which meant that the temperature distribution was greater than expected during cold soaks.

Another major lesson was to make sure to keep track of geometry and how all the parts fit together carefully. Initially the shroud sheet was sized with a 16.5" diameter to fit in the chamber with barely enough clearance for the L-shaped bars welded inside the chamber that held up the old hardware. However, with the addition of the tubing during the brazing process and due to workmanship, the final diameter was not exactly 16.5" and was barely too large to fit in the chamber with the L-shaped bars. The bars had to be removed, which added to the manufacturing time, and

required masking and cleaning the chamber before and after removing the bars to prevent contamination of the inside of the chamber and the turbo molecular pump.

6.2.2 Manufacturing Processes

The manufacturing process for this thesis ended up being a significant time commitment, with manufacturing starting in mid-January 2021 and finishing by early May. From the authors personal experience, manufacturing always takes longer than one expects, but this ended up significantly exceeding that. A major lesson learned from this is to plan as detailed as possible, each process and step that is required to complete something in order to properly assess how long it will take, and add margin to that.

Unfamiliar processes like brazing over 40 feet of tubing to the copper sheet added significant troubleshooting time spent determining the most efficient methods to complete the work. Coupon level testing is critical for unfamiliar process, and generally should be used for any process as practice for making the final part if small volumes are needed and mistakes that could scrap the entire part are possible. The coupon testing performed for this thesis was extremely valuable, especially for troubleshooting painting issues and practicing brazing techniques.

6.2.3 Thermal Vacuum Testing

The most important parts of testing are to ensure that the conditions are consistent and the user completely understands all the systems and how they operate together. One issue when initially setting up the data-logger is that when it powers on it does not default to T type thermocouple input, and the default produces similar but slightly incorrect temperature readings. This is easy to miss before a test and one

can change it during the test, but it invalidates the data up to that point unless it can be corrected for.

Understanding the system completely is critical, especially when it comes to control systems. Significant time was needed reading through the manual for the PID controller so that the control system could be setup as desired.

6.3 Future Work

Future work includes potential changes that could be made to further improve the capabilities or functionality of the chamber, as well as potential test types that could be performed to further demonstrate the capabilities of the chamber.

6.3.1 Powered Test Article

There are various feed-throughs and connectors with the chamber that could be used to feed power or data to a test article during thermal vacuum testing. For high power test articles, black wires labeled 3 and 4 in the back right of the chamber are spare heater power wires and are currently not connected on either end. These could be used to feed power or data through to a test article easily with an external power supply or other equipment. A powered test article test would allow for capabilities like thermal balance tests with active spacecraft systems, where thermal control systems on the spacecraft are used to maintain operational limits. Alternatively, powered subsystems could be tested using a similar experimental setup.

6.3.2 Independent Heater and Shroud Control Tests

As configured, the shroud is capable of being independently controlled from the heaters. This allows the shorud to act as a radiative sink similar to the cold dark-

ness of deep space. The heater plates can then be mounted as desired to simulate heat input from one or multiple directions depending on how they are arranged. The plates can be moved as needed and not all plates are required to be in the chamber at once, and are sized to be slightly larger than the largest face of a 3U CubeSat. This configuration is expected to consume more liquid nitrogen because the heat input from the heaters will require more shroud cooling. One way to mitigate this is to wrap the bottom face of heater plate, the side not facing the test article, in high vacuum compatible aluminum foil to reflect heat away from the shroud and back to the heater face.

6.3.3 Leak Testing

Ongoing work is needed to correct remaining smaller sources of leakage as well as perform maintenance if required. The door gasket, as mentioned in Jensma's thesis [11], remains a likely source of leakage and will require regular maintenance as it degrades over time and with usage. Feed-throughs should be checked in more detail using the helium leak detector. This can be accomplished by using an enclosure like a plastic bag or other container that focuses the helium injected to specific parts of the chamber in order to more precisely locate remaining leak sources. This was done only to a limited extent during the leak testing for this thesis.

6.3.4 Heater Modifications

Currently, the heater plates act as the only source of heat for the chamber, and because of the limited size and number, are not able to provide a perfectly even temperature distribution across the entire shroud. Generally, the heater plate temperatures on average were 10-15°C hotter than the rest of the shroud. Depending on the requirements and needs of a specific test, this may be acceptable. However,

if it was desired to have an even temperature distribution across the entire shroud for a test, strip heaters can be installed on the shroud exterior faces. Thin, flexible polyimide strip heaters are available from suppliers like Watlow for high vacuum applications that could be bonded to the exterior faces of the shroud to heat the entire shroud during hot soaks. This system could utilize the existing power feed-through for the heaters without modification if they are 240V compatible and would not require permanently removing the heater plates, since they can be unplugged and removed from the chamber without any tools. This would allow the chamber to be heated and cooled entirely by the shroud, increasing the available test volume and allowing for more consistent environmental temperatures for test articles during hot soaks.

6.3.5 Cooling System Improvements

While the upgraded cooling system improved the chamber capabilities, there is always room for improvement, especially with regard to the temperature distribution across the shroud during cold soaks. Temperatures across the shroud varied by approximately 16°C in the worst case at steady state during empty test 2. This is not surprising because the model with flow simulation predicted similar variation, but could affect the temperature distribution of test articles depending on the test requirements. In order to improve the temperature distribution across the shroud, a variety of solutions could be tested, either experimentally or through the model, to improve the distribution. Possible changes include but are not limited to:

- Limiting the maximum flow rate from the liquid nitrogen tank to allow the chamber valves to spend less time cycling on and off and act more as continuous flow
- Modify the inlet and outlet conditions by changing the inlet pressure and/or outlet backpressure

- Modifying the outlet geometry by adding orifices to modulate maximum mass flow rates
- Installing a sensor to measure flow rate

Many of these modifications can be simulated using the model with flow simulation, and then the changes could be implemented on the physical system.

6.3.6 Data Acquisition System

The existing T type thermocouples and DT4208SD 12 channel thermocouple logger are adequate for testing, however the logger is currently battery operated and requires replacement after about few days of continuously logging data. The logger has a 9V input for powering from a standard 120V outlet, and this could be acquired so that batteries are not needed and there is no risk of loss of battery power causing loss of data.

The T-type thermocouples used inside the chamber for data logging have thick, difficult to bend wires compared to the T-type control thermocouple thermocouples. The thickness and lack of compliance means that when applying the thermocouples, it is difficult to ensure good thermal contact between the thermocouple and surface, and there is a greater risk of thermocouples lifting from the surface and not providing good contact. It was noted during testing that the control thermocouples tended to report temperatures closer to the set point compared to thicker thermocouples directly adjacent to the control thermocouples, and tended to more quickly reach steady temperatures due to their smaller thermal mass and better contact. It is recommended that new thermocouples be purchased that are compliant and have thinner wires.

6.3.7 Cooling System Insulation

Before testing for this thesis, the cooling system inlet tubing from the tank to the chamber was improved using standard polyethylene pipe insulation available at hardware stores. This insulation was wrapped around existing degraded tubing where it was present, and was added along the hose that runs from the liquid nitrogen tank to the chamber. Despite these additions, there are more locations where insulation would help reduce liquid nitrogen consumption and are shown in Figures 6.2 and 6.3. In Figure 6.2, multiple locations around the liquid nitrogen tank top show icing, in addition to the valve stem and exposed tubing for the liquid withdraw lines. Insulated covers could be made for these exposed parts using a soft and flexible type of insulation material rated for cryogenic temperatures which will improve cooling system efficiency.

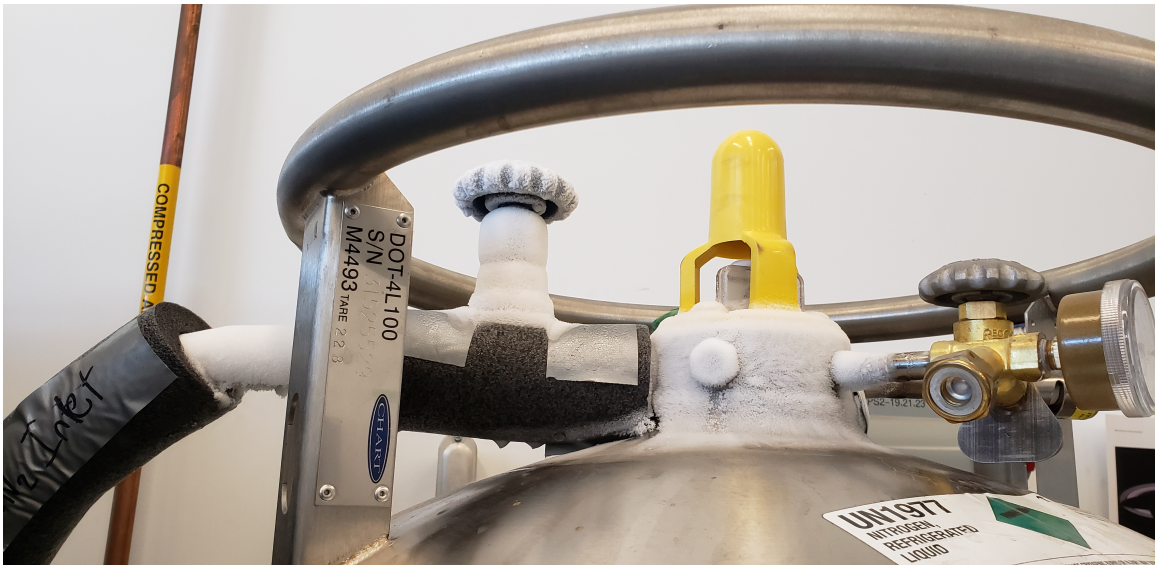

Figure 6.2: Insulation around the liquid nitrogen tank inlet and uninsulated areas with ice buildup

Figure 6.3 shows the cryogenic valves uninsulated with significant ice buildup. These could similarly be covered with a soft and flexible insulation material rated for cryogenic temperatures.

Figure 6.3: Insulation around chamber cryogenic valves and uninsulated areas with ice buildup

6.3.8 Webcam

It would be useful to be able to view the control panel of the chamber as well as the liquid nitrogen tank scale and thermocouple logger for the purpose of data logging and monitoring. For example, using a webcam with a time lapse allowed for chamber pressure to be logged during overnight tests. For this thesis, a personal tablet computer with a camera was used and directed at the instruments. Installing a permanent webcam using a computer or similar setup would allow any students to access it easily for their testing and would not require personal resources.

BIBLIOGRAPHY

[1] General Environment Verification Standards (GEVS) for GSFC Flight Programs and Projects. Technical Report GSFC-STD-7000A, NASA Goddard Space Flight Center, Greenbelt, Maryland, Apr. 2019.

[2] BasicCopper. 24 X 6'/ 5 Mil (36 ga.) Copper Sheet. `https://basiccopper.com/24x65micofo1.html`, 2021.

[3] M. Caudill and B. Diamond. Cal poly tvac chamber: Cryogenics. 2019.

[4] C. D. O. L. Chisabas R. S. S., Loureiro G. and C. D. F. Method for cubesat thermal-vacuum cycling test specification. In *47th International Conference on Environmental Systems*, Charleston, South Carolina, 2017.

[5] Copper Development Association, Inc. Cryogenic properties of copper. `https://www.copper.org/resources/properties/cryogenic/`, 2021.

[6] N. A. Fishwick, K. A. Smith, and J. A. Romera Perez. Lessons learned from thermal vacuum testing of lisa pathfinder over three system level thermal tests. In *45th International Conference on Environmental Systems*, Bellevue, Washington, 2015.

[7] D. G. Gilmore. *Spacecraft Thermal Control Handbook*. American Institute of Aeronautics and Astronautics, 2002.

[8] J. L. Golden. Results of the examination of ldef polyurethane thermal control coatings. Technical Report NASA Contractor Report 4617, Boeing Defense & Space Group, Seattle, WA, July 1994.

[9] International Organization for Standardization, Geneva, Switzerland. *ISO 19863: Space systems — Design qualification and acceptance tests of small spacecraft and units*, 2017.

[10] S. Jayaram and E. Gonzalez. Design and construction of a low-cost economical thermal vacuum chamber for spacecraft environmental testing. *Journal of Engineering, Design and Technology*, 9:47–62, 2009.

[11] M. R. Jensma. Thermal modeling and testing of the blue thermal vacuum chamber. Master's thesis, California Polytechnic State University, San Luis Obispo, San Luis Obispo, CA, June 2020.

[12] R. D. Karam. *Satellite Thermal Control for Systems Engineers*. American Institute of Aeronautics and Astronautics, 1998.

[13] G. Lee. Materials for ultra-high vacuum. Technical Report TM-1615, Fermi National Accelerator Laboratory, P.O. Box 500, Batavia, Illinois, Aug. 1989.

[14] McMaster-Carr. Cleaned and capped copper tubing. `https://www.mcmaster.com/5174K21/`, 2021.

[15] NASA. Outgassing data for selecting spacecraft materials. `outgassing.nasa.gov`, 2021.

[16] Paul Fredericks, Aerospace Metals LLC. How to remove anodized aluminum? `https://aerospacemetalsllc.com/how-to-remove-anodized-aluminum`, 2021.

[17] V. L. Pisacane. *The Space Environment and Its Effects on Space Systems*. American Institute of Aeronautics and Astronautics, 2008.

[18] Socomore. *Aeroglaze 9947 Wash Primer Technical Data Sheet*. Socomore by Lord Corporation, Saegertown, PA, 2021.

[19] Socomore. *Aeroglaze Z306 Polyurethane Coating Technical Data Sheet.* Socomore by Lord Corporation, Saegertown, PA, 2021.

[20] S. Team. *SolidWorks Flow Simulation Manual.* Dassault Systèmes SolidWorks Corporation, Waltham, MA, USA, 2020.

[21] Watlow Inc. *Watlow Series F4S/D User's Manual.* Watlow Winona, Winona, Minnesota, 2011.

[22] A. Williams. Thermal vacuum chamber refurbishment and analysis. Master's thesis, California Polytechnic State University, San Luis Obispo, San Luis Obispo, CA, June 2018.

APPENDICES

Appendix A

BAKEOUT PROCEDURE

This bakeout procedure is intended for the Blue TVAC located in at Cal Poly's Space Environments Lab 41-137. The purpose of a bakeout is to remove contaminants like water vapor or other volatiles that were not removed with standard cleaning process like IPA wiping. A bakeout is required when it is desired to reach the lowest vacuum pressures possible. With a bakeout, ambient pressures in the chamber under $4.0e^{-6}$ Torr can be achieved at ambient temperatures.

1. Configure chamber for bakeout:
    - Include all heater plates to maximize effectiveness
    - Remove aluminum foil cover from door shroud and front of shroud, if present
    - Thoroughly clean all exposed chamber surfaces with IPA (Do not use paint thinner or acetone on painted surfaces!)
    - Include the cleaned test article for bakeout, if applicable, ensuring that the maximum survival temperature of the article and melting points, vapor pressures, and outgassing rates of the materials are known and not exceeded.
    - Verify the hot limit TC (23) is installed directly on the middle of one of the exposed heater elements (this is extremely important!)

- Install the heater control TC (26) on the location where the set temperature is desired (usually the middle face of the middle heater plate, opposite side as the element)
- Prepare LN_2 if an extensive bakeout is desired

2. Rough pump to $5.0e^{-2}$ Torr and turn on the turbomolecular pump and then ion gauge when the convectron gauge reads 0 per standard chamber procedures

3. After $1.0e^{-4}$ Torr is achieved, set a profile to ramp and soak at the desired bakeout temperature at a slow ramp rate (¡0.5°C/min) on the F4 controller to the, based on the test article maximum temperature. 90°C is the maximum recommended control temperature to keep the hot limit from tripping. Switch on the hot switch to activate the heater.

    - Monitor the control temperatures and ion gauge pressure. If the pressure climbs above $1.0e^{-3}$ Torr, turn down the heat until it stabilizes. If it is approaching $1.0e^{-2}$ Torr with the heaters off, turn off the turbomolecular pump and ion gauge to protect them from damage.

4. Hold at the bakeout temperature, noting the pressure change over time. Proceed to the next step after 24 hours or if the pressure is below $7.5e^{-6}$ Torr while at the bakeout temperature.

5. Switch off the heaters. If LN_2 is available, flood the door shroud with LN_2 by setting set point 2 to -150°C on the F4 controller.

6. After the door shroud has achieved steady state temperatures and the pressure has stabilized in the chamber, turn off the cooling and turn off the turbomolecular and ion gauge.

7. After 40 minutes with the turbomolecular off, turn off the roughing pump and vent the chamber.

8. After the chamber is vented, turn off the main breaker and open the chamber door.

9. Using clean gloves and lint free wipes, use IPA to wipe down the door shroud on the front face and back face with as much as possible by reaching through the viewing port.

10. After the chamber is dry, close the door and proceed with regular testing. The bakeout process can be repeated periodically as desired to remove adsorbed water vapor or other contaminants.

Appendix B

UPDATED CHAMBER OPERATING PROCEDURE

The operating procedures are largely unchanged from their current state as documented in the manual, which was last updated on December 12th, 2019. This appendix will discuss the relevant changes to each section as applicable.

B.1 Safety

No change. Note that the liquid nitrogen stored capacity, not mentioned in this section, has increased from 35 liters to 180 liters. Nitrogen can displace oxygen in the atmosphere, leading to hypoxia and death depending on the remaining oxygen concentration. The existing oxygen sensor was unreliable when used in May 2021, and likely needs re-calibration or replacement periodically, likely every year or sooner.

B.2 Chamber Overview

The interior image of the chamber is outdated and should be replaced with 6.1 from this thesis.

B.3 Vacuum System

The system is now capable of pressures below $7.5e^{-6}$ Torr with bakeout of the chamber and test article.

B.4 Heating System

The same except the platen is replaced by the three heater plates and the maximum tested set temperature is 95°C, which is driven by a maximum coating temperature of 120°C near the heater strips, which is where the high limit TC is currently installed.

B.5 Cryogenic Cooling System

The same except the platen no longer part of the cooling system and the liquid nitrogen tank has a relief pressure of approximately 22 psig instead of 7.25 psig.

The system was tested to -145°C in uncontrolled ramp testing, and to -80°C in the plates thermal vacuum testing.

B.6 Operating Procedures

There are no changes to the operating procedures. Only the times to reach ¡50 mTorr and times for the pressure to zero out, which are for information only, are changed from 2 hours to 30 mins for ¡50mTorr and from 10 minutes to about 2 minutes for the chamber pressure to zero out.

B.6.1 Starting The Cooling System

There are no changes to the procedures except for the ideal dewar pressure. The ideal dewar pressure of between 4-7 psig is now 21-22 psig for the new liquid nitrogen tank.

B.6.2 During Normal Operation

As mentioned in the last subsection, the dewar pressure is now liquid nitrogen tank pressure and the ideal range is 21-22 psig. There is unlikely to be a need to reduce liquid nitrogen flow rates because of the larger tank and higher operating pressures.

B.6.3 Shutdown

These procedures are unchanged.

B.6.4 Opening the Dewar and Ordering LN2

The dewar is replaced by the liquid nitrogen tank and does not need to be opened or vented by students at any time to fill. The filling is done by Praxair and they can be called to come and refill the tank. Coordinate with them and Cody to ensure they come to the right place to fill, use the same code or get the code from Cody. Delivery and pickup is usually between 9:30am - 11:00am.

B.7 Contingencies

B.7.1 O_2 Sensor Alarm (Evacuation Procedure)

These procedures are the same.

B.7.2 Increased Chamber Pressure

These procedures are the same.

B.7.3 Low Dewar Pressure (<3 PSIG)

This procedure is irrelevant because of the larger liquid nitrogen tank.

Appendix C

SOLIDWORKS FLOW SIMULATION THERMAL MODEL GUIDE

This guide is intended to be a basic demonstration of the various options and parameters relevant to the thermal model in this thesis that uses SolidWorks Flow Simulation.

C.1 Adding a Test Article

Figure C.1 shows how to add a solid model to the existing thermal model assembly.

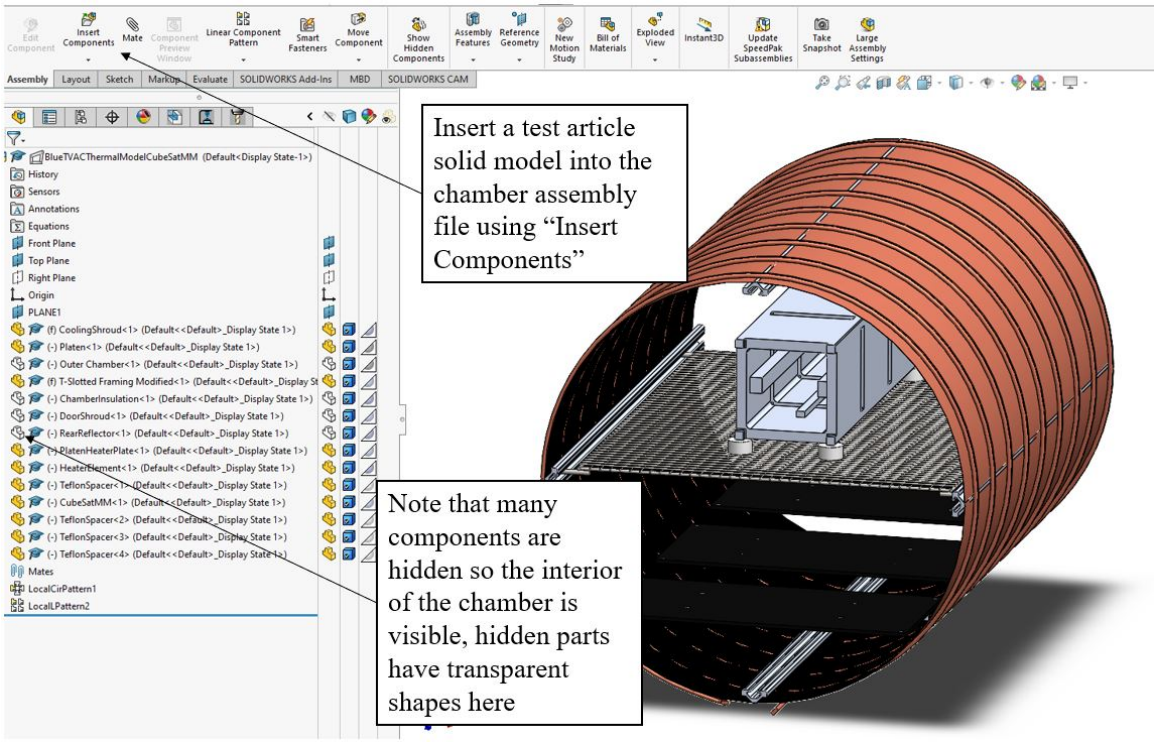

Figure C.1: Adding an test article part or assembly to the thermal model

Figure C.2 shows the options for moving the test article around in the assembly as well as mating it to other parts like the platen or mounting rails.

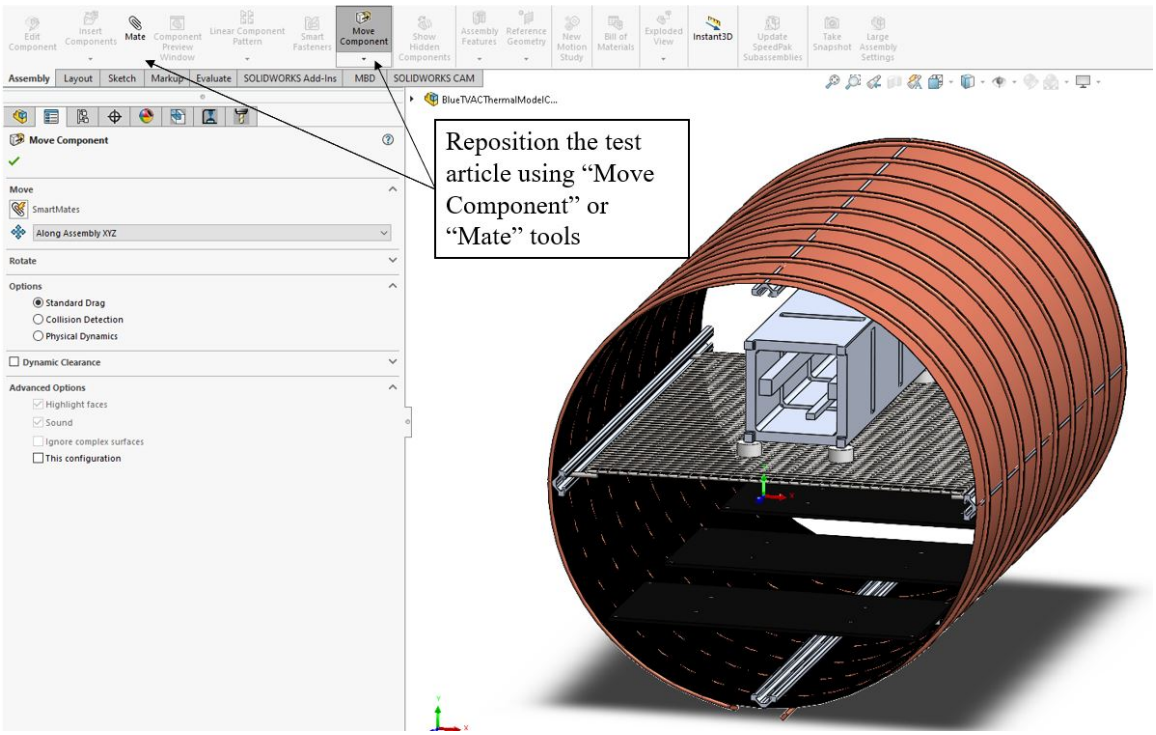

Figure C.2: Moving and mating the test article in the assembly

C.2 Setting Up A Simulation

Figure C.3 shows how to load the SolidWorks Flow Simulation add on, as well as view relevant fields in the flow simulation tab including different simulation cases as well as material and surface properties, boundary conditions, and mesh setup.

Figure C.4 shows how to view parameters and how they apply.

Figure C.5 shows how change the heater plate temperature boundary condition. This is what is changed to match the set point on the thermal vacuum chamber controller. Other than defining the test article material and surface properties, this is all that needs to be changed for hot case simulations with a new test article.

Figure C.6 shows how to change cases to the cold case and modify the temperature boundary conditions for the cold case without flow simulation. For cold case

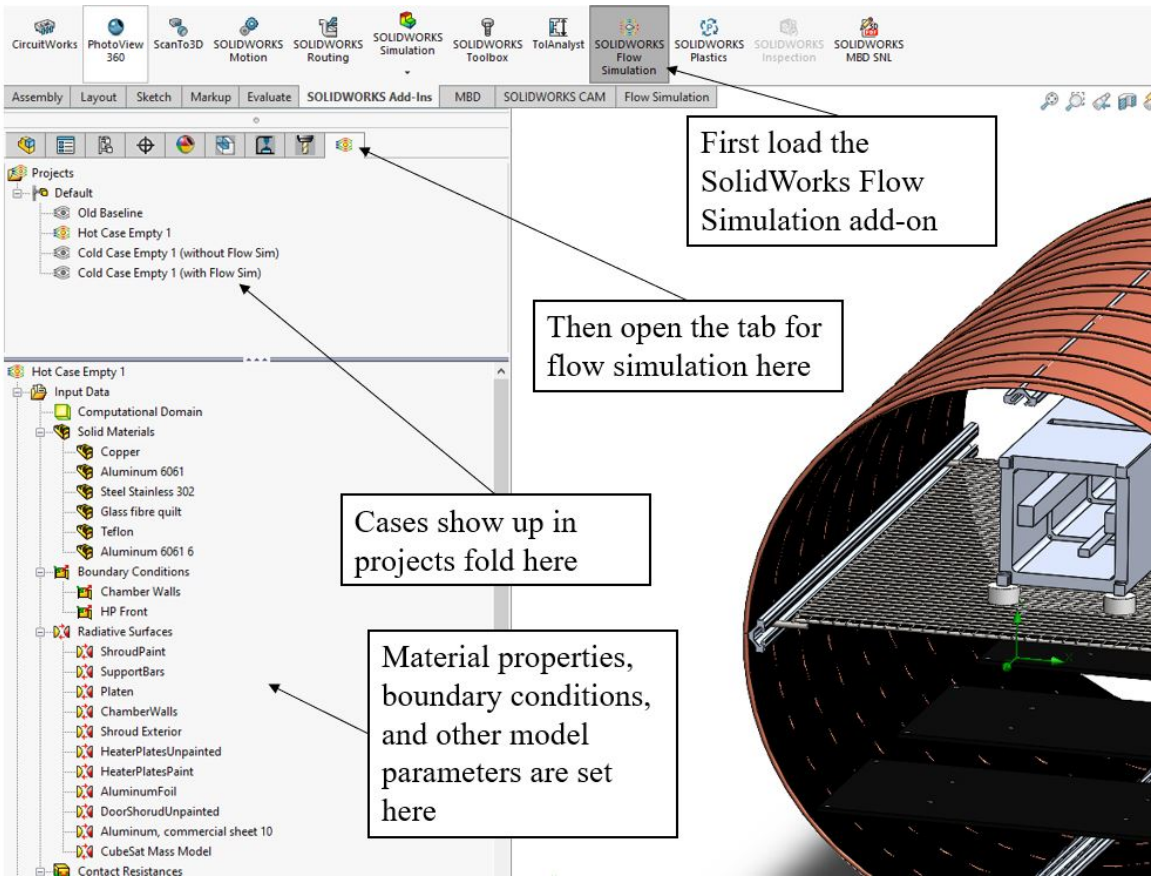

Figure C.3: Loading flow simulation and viewing cases and details

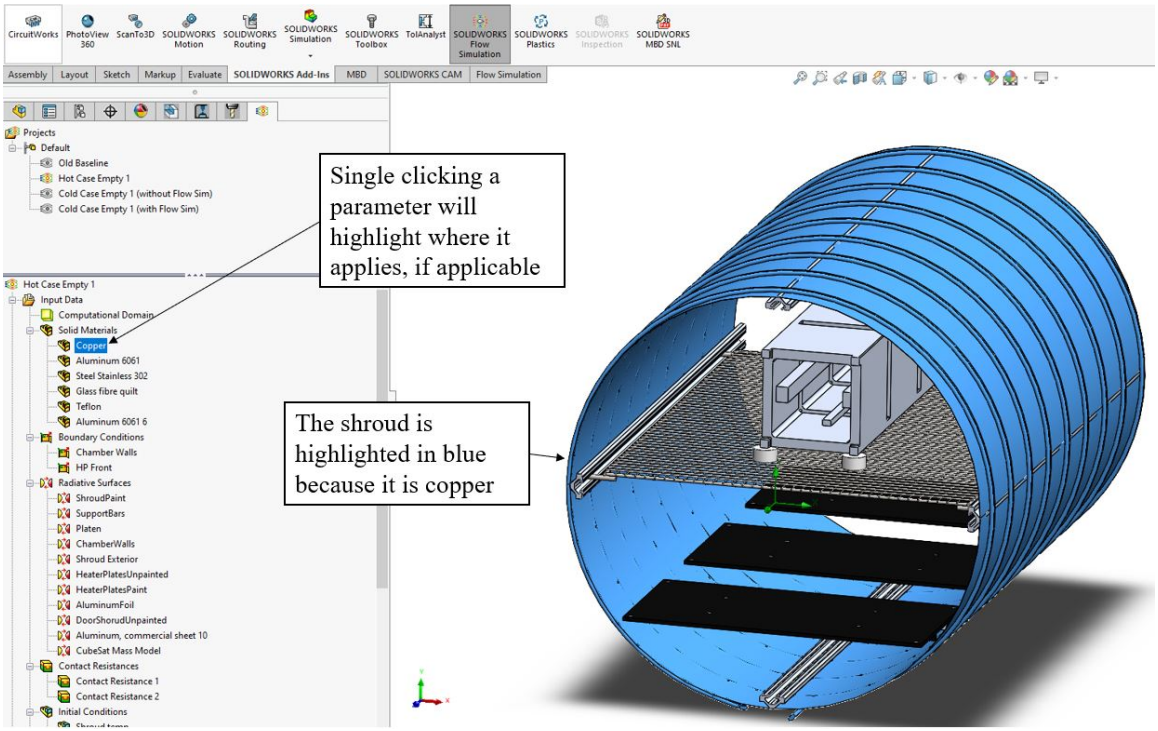

Figure C.4: Specific parameter selection

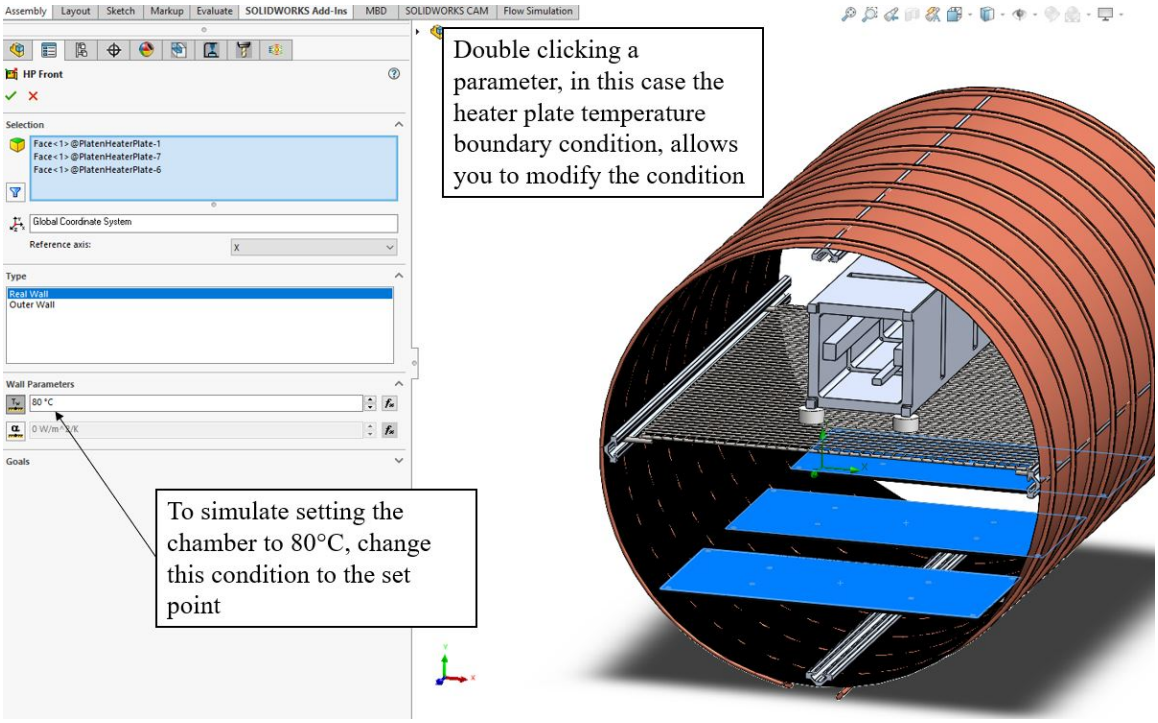

Figure C.5: Defining temperature boundary conditions for the hot case

simulations with flow, instead of temperature boundary conditions the user defines flow boundary conditions in the same boundary conditions section.

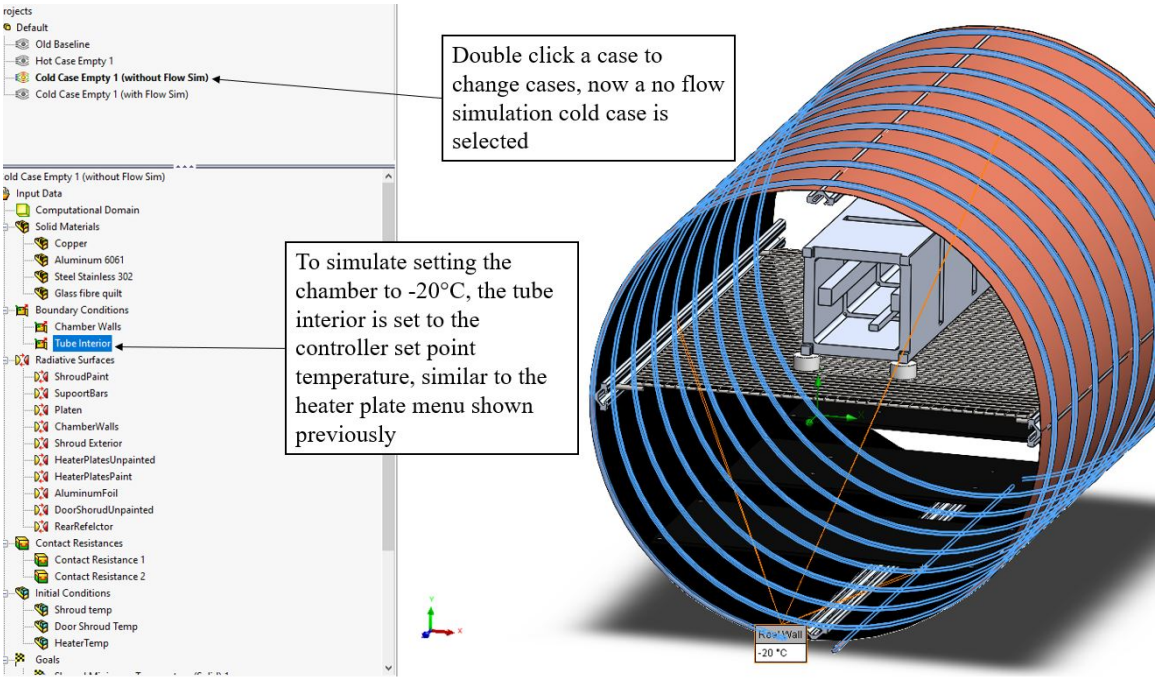

Figure C.6: Defining temperature boundary conditions for the cold case, without flow simulation

Figure C.7 shows how to add a radiative surface, and C.7 shows the process for setting surface properties for individual surfaces of a test article. This process is similar for defining material properties, initial conditions, and other boundary conditions.

Figure C.9 shows how to define goals, which can be used to monitor parameters during iteration as well as control convergence. Temperature goals for various surfaces are particularly insightful for these thermal simulations.

C.3 Meshing, Solving, and Visualizing Results

Figure C.10 shows how to set up local and global meshes. The existing settings for the meshes should be adequate however the level of detail can be easily adjusted.

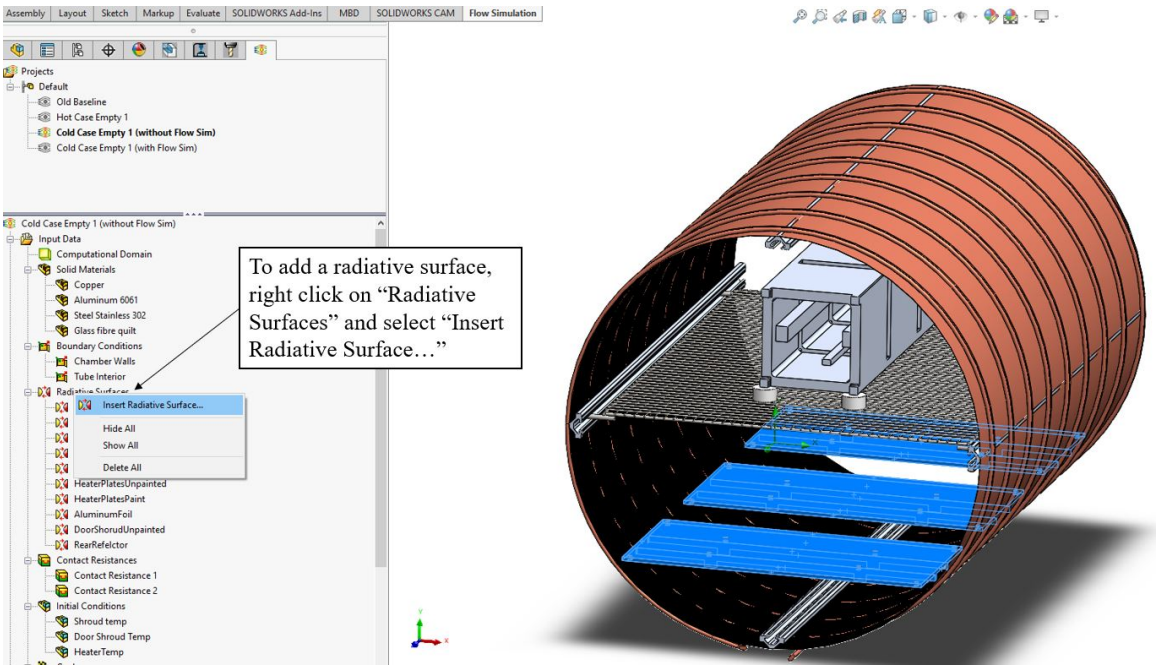

Figure C.7: Adding a radiative surface

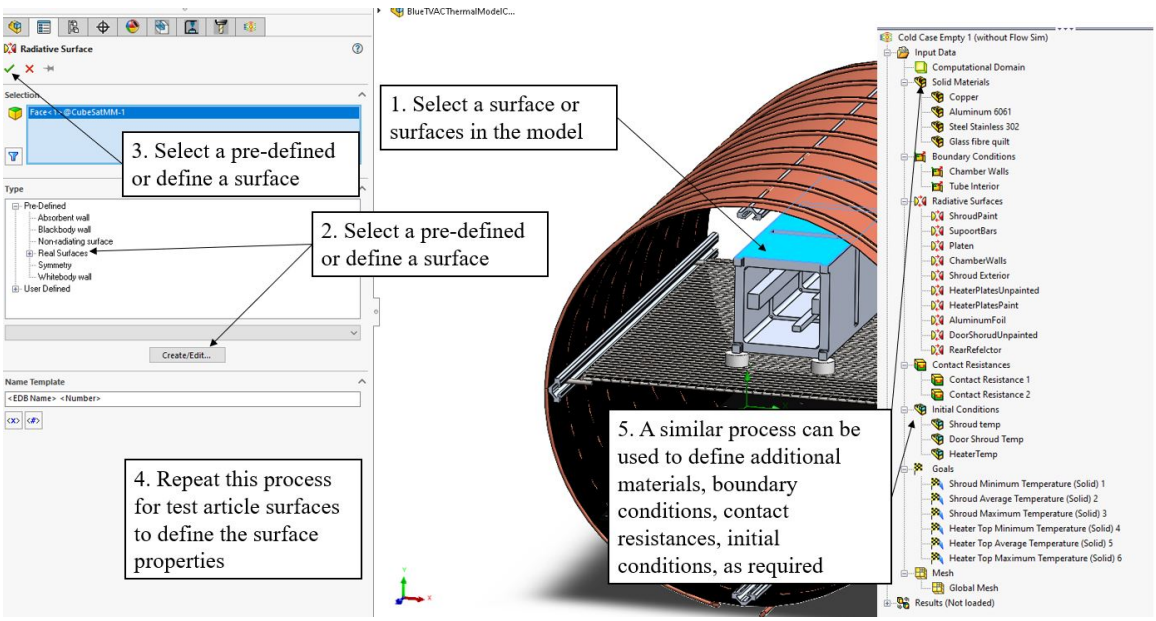

Figure C.8: Adding a radiative surface in detail

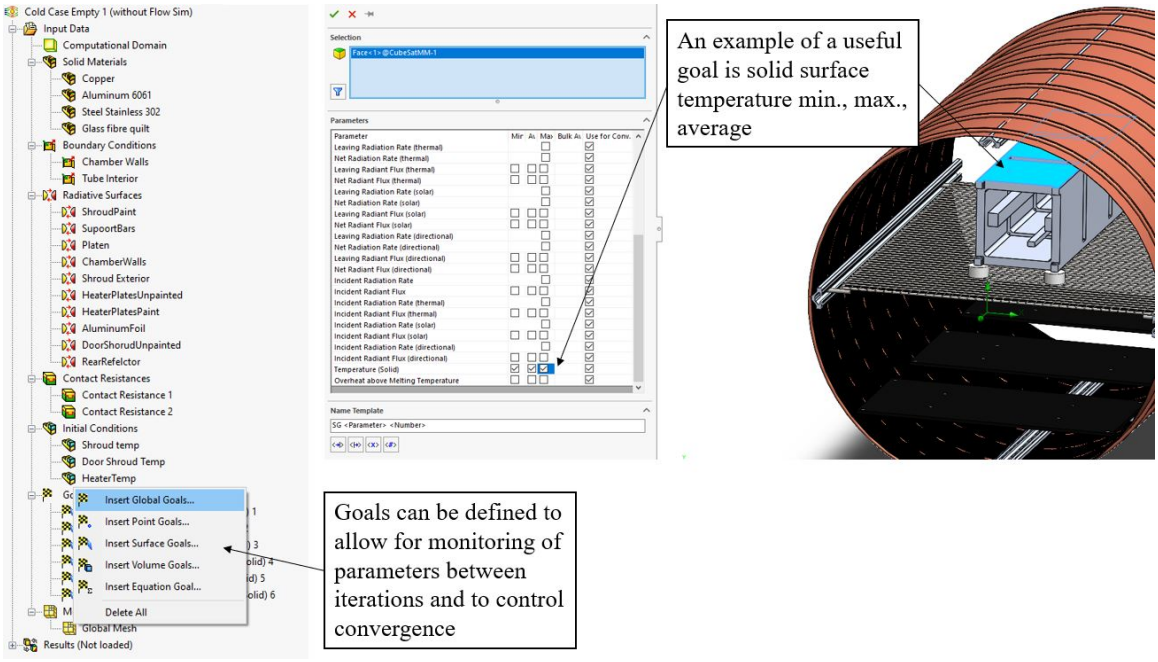

Figure C.9: Defining goals

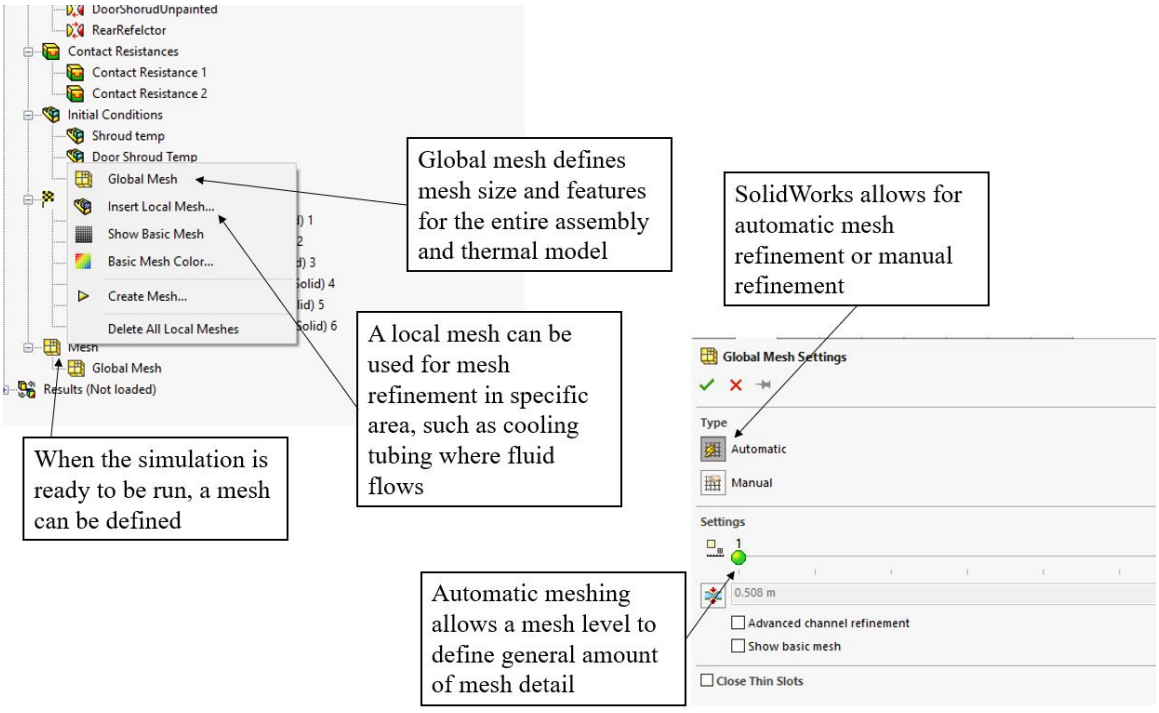

Figure C.10: Basic meshing using global and local meshes

Figure C.11 shows how to run the mesher and solve the simulation.

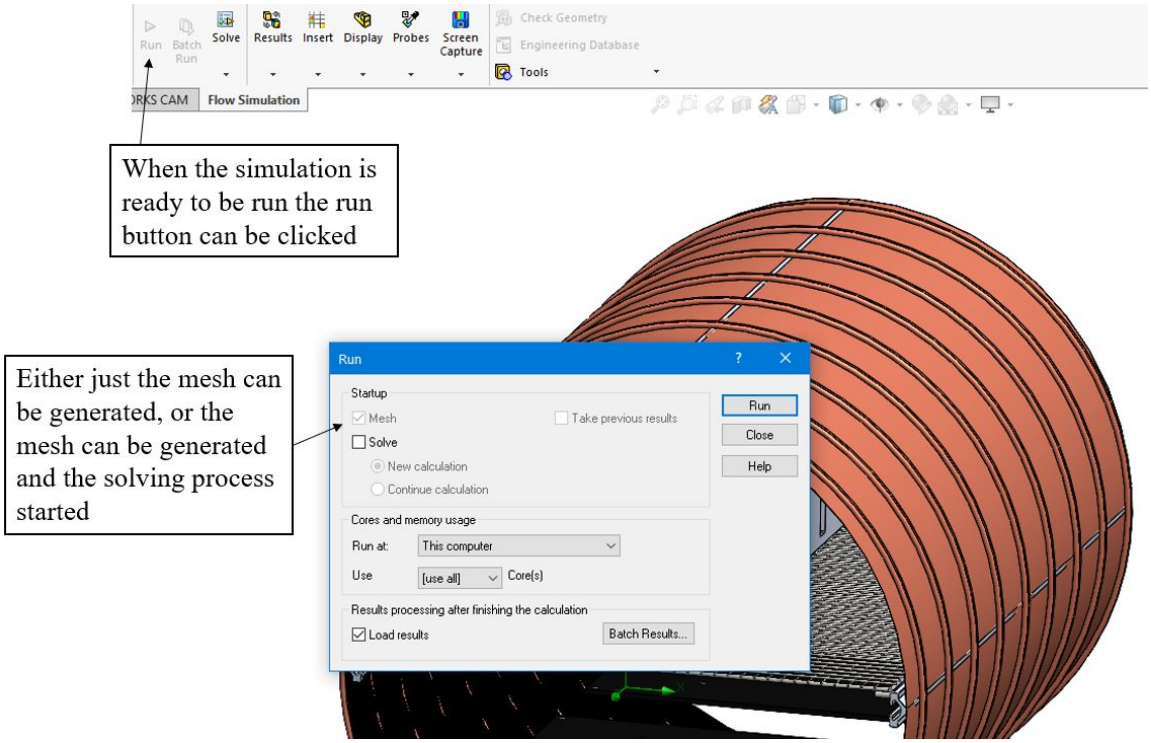

Figure C.11: Running the mesher and solving the simulation

Figure C.12 shows how to view the mesh cut plot.

Figure C.13 shows how to visualize results relevant to this thermal model, including probing locations for point temperatures and visualizing temperature distributions across surfaces.

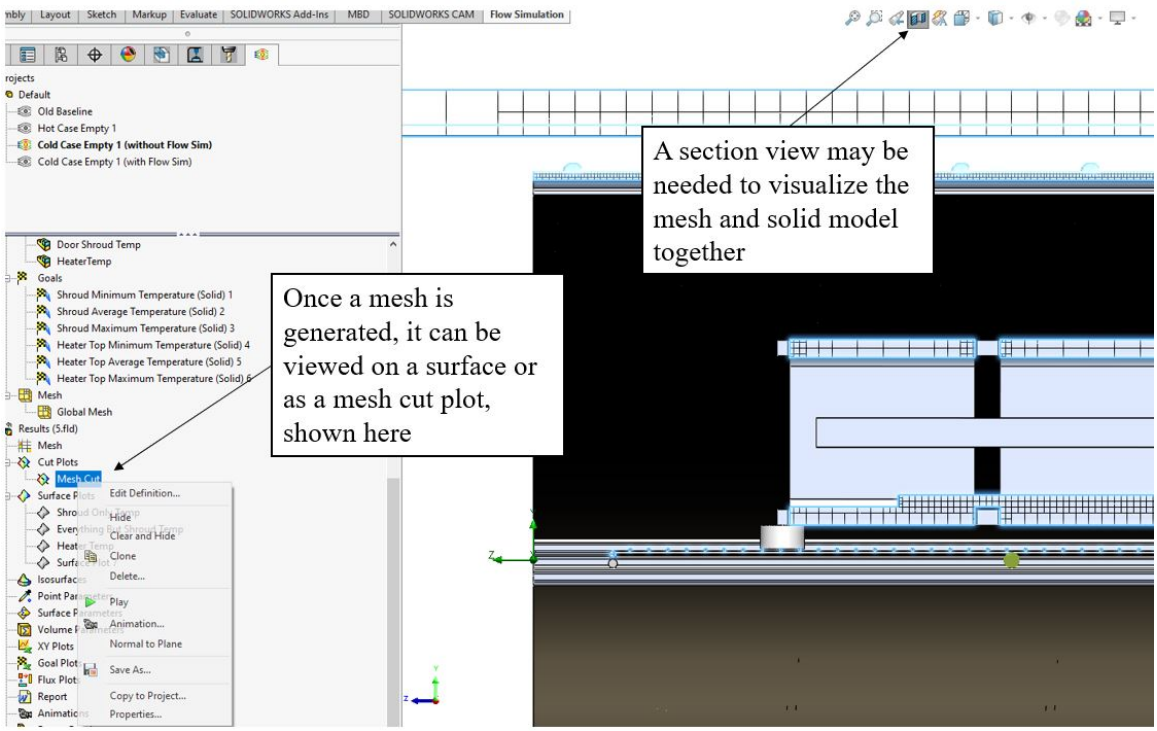

Figure C.12: Viewing the mesh

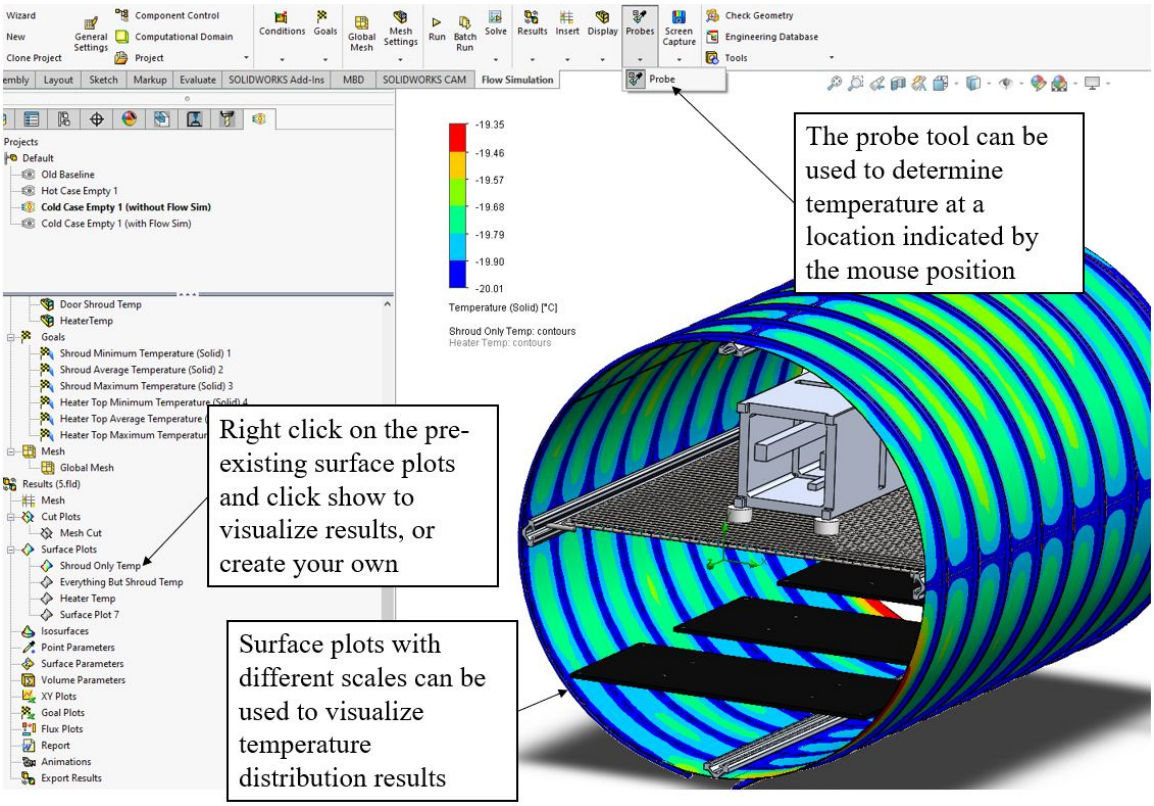

Figure C.13: Viewing temperature surface plots and probing results